Computational Systems Biology Analysis of Cell Reprogramming and Activation Dynamics

Yan Fu

Dissertation submitted to the faculty of the Virginia Polytechnic Institute and State University in partial fulfillment of the requirements for the degree of

Doctor of Philosophy

In

Genetics, Bioinformatics and Computational Biology

Jianhua Xing, Chair

John J. Tyson, Co-Chair

Liwu Li

Lu Chang

July 17, 2012

Blacksburg, VA

Keywords: computational modeling, network motifs,
LPS priming and tolerance, bacterial phenotypic transition

Computational Systems Biology Analysis of Cell Reprogramming and Activation Dynamics

Yan Fu

Abstract

In the past two decades, molecular cell biology has transitioned from a traditional descriptive science into a quantitative science that systematically measures cellular dynamics on different levels of genome, transcriptome and proteome. Along with this transition emerges the interdisciplinary field of systems biology, which aims to unravel complex interactions in biological systems through integrating experimental data into qualitative or quantitative models and computer simulations. In this dissertation, we applied various systems biology tools to investigate two important problems with respect to cellular activation dynamics and reprograming.

Specifically, in the first section of the dissertation, we focused on lipopolysaccharide (LPS)-mediated priming and tolerance: a reprogramming in cytokine production in macrophages pretreated with specific doses of LPS. Though both priming and tolerance are important in the immune system's response to pathogens, the molecular mechanisms still remain unclear. We computationally investigated all network topologies and dynamics that are able to generate priming or tolerance in a generic three-node model.

Accordingly, we found three basic priming mechanisms and one tolerance mechanism. Existing experimental evidence support these *in silico* found mechanisms.

In the second part of the dissertation, we applied stochastic modeling and simulations to investigate the phenotypic transition of bacteria *E.coli* between normally-growing cells and persister cells (growth-arrested phenotype), and how this process can contribute to drug resistance. We built up a complex computational model capturing the molecular mechanism on both single cell level and population level. The paper also proposed a novel way to accelerate the phenotypic transition from persister cells to normally growing cell under resonance activation. The general picture of phenotypic transitions should be applicable to a broader context of biological systems, such as T cell differentiation and stem cell reprogramming.

Dedication

This dissertation is dedicated in memory of my dearly loved mother Lan (Linda) Zhou, who used her life and true love to support me, to help me, through each step of my way. The memory will never fade, that at the last moment of her life when she suffered great pain of cancer, she still asked me whether I have finished the data analysis of my project, and what my future career plan would be. She taught me that women should be independent, be wise, and be brave in pursuing dreams. She encouraged me to stand in front of difficulties and never run away. She showed me the true meaning of happiness. Without her, nothing I did or could ever accomplish has any importance.

Acknowledgements

I would like to express my sincere gratitude to my advisor Prof. Jianhua Xing, who offered me tremendous mentoring, continuous support and exemplary guidance throughout my PhD study, turning me from basically a blank page into a confident computational and systems biologist. I will always be so grateful to him.

I would like to thank my co-advisor Prof. John J Tyson, who offered me great support throughout these years, inspired me with immense knowledge, and encouraged me through difficulties. He showed me that a great scientist with such high achievement could also be humble, earnest, broad-minded and down-to-earth.

I would also like to thank the rest of my committee: Prof. Liwu Li and Prof. Chang Lu, for their constant support, great encouragement, and insightful comments. Thanks to Prof. Li, who let me go into his lab and see how experiments are done. For a student working on computational side, this experience means a great deal. Thanks to Prof. Chang Lu, who spent a lot of his valuable time giving me great suggestions for career development.

Lastly, I need to thank all the members of Prof. Xing's lab, Prof. Tyson's lab, my husband Meng Zhu and all my best friends at Virginia Tech and in China, who helped me, encouraged me, and inspired me throughout these years. I give my greatest appreciation to each one of you.

Attribution

Several colleges aided in the research and writing of the papers presented as Chapter 2 and Chapter 3 in this dissertation. Their contributions are included as follows.

Chapter 2 included my work "Network Topologies and Dynamics Leading to Endotoxin Tolerance and Priming in Innate Immune Cells". This paper was published in 2012 in PLoS Computational Biology 8(5): e1002526.

Trevor Glaros, PhD from Dr. Liwu Li's lab in the Department of Biological Sciences at Virginia Tech, co-authored on this paper. He performed experiments on endotoxin-induced priming and tolerance in macrophage cells. Meng Zhu, a PhD student in Dr. House's lab in the Department of Computing Science at Clemson University, was a co-author on this paper for his contribution to implement fast simulation in C++. Dr. Ping Wang and Dr. Zhanghan Wu, post-doctoral researchers from Dr. Jianhua Xing's lab in the Department of Biological Sciences at Virginia Tech, made intensive and very helpful discussions over our novel Monte-Carlo algorithm. They also helped me on my data analysis. Dr. John J Tyson, University Distinguished Professor in the Department of Biological Sciences at Virginia Tech, co-authored on the paper for his great guidance and contribution throughout the research and writing. Dr. Liwu Li and Dr. Jianhua Xing, professor and assistant professor in the Department Biological Sciences at Virginia Tech, were co-corresponding authors on this paper.

Chapter 3 presented my work “Resonant activation: a strategy against bacterial persistence”, which was published in 2010 on Physical Biology 10.7(1):16013.

Meng Zhu, a PhD student from Dr. House’s lab in the Department of Computing Science at Clemson University, helped on fast implement of the algorithm and co-authored on the paper. Dr. Jianhua Xing, assistant professor in the Department of Biological Science at Virginia Tech, gave me great guidance and helps on this work. He was the corresponding author of this paper.

Table of Contents

List of Figures

List of Tables

Chapter 1. Introduction and Overview of the Research

1.1 Introduction

Recent two decades have witnessed great achievement in the development of quantitative and high-throughput experimental techniques (e.g. microarrays, RNA-seq, ChIP-seq, Q-PCR etc) which greatly deepened our understanding of the complex biological systems. For example, with the help of the technique of chromatin immunoprecipitation sequencing (ChIP-seq), one can accurately pin-point all DNA-binding events of a specific protein across entire genomes (Johnson et al, 2007), thereby, revealing new mechanisms of transcriptional regulations, histone modifications, and nucleosome architecture (Heintzman et al, 2009; Schmid & Bucher, 2007). By virtue of these new techniques, biologists are now able to track genome-wide cellular dynamics on multiple levels of genome, transcriptome and proteome. Our understanding of biological systems has thereby jumped from a bunch of static black-boxes with simple input-output relationships, into quantitative and dynamic models of molecular interaction networks that are controlled by multi-scale spatial and temporal regulations (Chen et al, 2004; Oda & Kitano, 2006).

However, as the "wiring diagram" of molecular interactions expands, understanding system behaviors out of complex interactions and large-scale experimental datasets is beyond just eyeballing and intuition. For a signaling pathway involving dozens of molecular species connected in several feedback and feedforward loops, which is typical, attempts to track the dynamics of each molecular species through intuition must face failure in the end. This is where systems biology comes into the arena. Systems biology aims to unravel complex biological

systems by integrating multi-scale experimental data into qualitative or quantitative computational models that, by virtue of theoretical analysis and numerical simulations, can reproduce the experimental observations and reveal new insights of the system for further experimental tests (Alon, 2007; Cheong et al, 2008; Gardy et al, 2009; Gilchrist et al, 2006).

From a system biologist's point of view, a cell works as an information processing unit that senses subtle changes in the micro-environment, processes the information and makes appropriate responses. This information processing unit is composed of a number of signaling and regulatory pathways that are connected in a way to elicit specific and robust response to different stimulating conditions. In vitro, signal-response relationships could be studied under different external perturbations to wild-type or genetically-altered cells. For example, we can stimulate cells with different kinds of signals, different doses or durations, or sequential stimulations. In this respect, numerous experimental and theoretical studies have demonstrated that both combinatorial and dynamical characteristics of signaling networks are indispensable for coordinating specific gene expression programs to different stimulating conditions (Huang et al, 2009).

As one example, macrophages are one kind of tissue-resident innate immune cells that can exert anti-microbial and inflammatory responses against infections. There are at least ten Toll-like receptors (TLRs) expressed on cellular membrane or on endosome membrane of macrophages. These receptors are responsible for recognizing a wide range of microbes through pathogen associated molecular patterns (PAMPs) and for initiating an effective innate immune response (Akira & Takeda, 2004). Challenging macrophages with different PAMPs selectively activates a

specific TLR signaling pathway and corresponding gene expression program. For example, TLR2 recognizes bacterial lipoproteins and peptidoglycan, while TLR4 is responsive to lipopolysaccharide (LPS, product of gram-negative bacteria) and fibrinogen (Huang et al, 2009). Activation of TLR2 and TLR4 both lead to the activation of MyD88-dependent pathway and subsequent NFκB activation, giving rise to a profound inflammatory response. At the same time, TLR4, but not TLR2, also activates MyD88-independent pathway, which is essential for transcribing Interferon-responsible factors (IRFs) and many anti-microbial genes (e.g. *Ifn-β*).

It is extremely fascinating but also challenging for systems biologists to study how signaling and regulatory networks function based on complex pathway cross-talks and great variation of time-scales (Behar et al, 2007; Hoffmann et al, 2002; Hu & Ivashkiv, 2009; Litvak et al, 2009; Natarajan et al, 2006). For example, according to various studies, transcription factors NFκB and Interferon-beta (IFN-β) could demonstrate either positive or negative cooperation on target genes with both κB site and Interferon-Response-Element (IRE). Based on current research, there are 15 homo-dimers and hetero-dimers of NFκB being assembled and disassembled in macrophages in context dependent manners (Hoffmann et al, 2006). While transcriptionally active dimers of NFκB can positively cooperate with IFN to initiate gene expression, transcriptionally inactive dimers (such as p50:p50) send IFN away through competitively binding to guanine-rich IRE sequence on the enhancers of the target genes (Cheng et al, 2011).

For pathway signaling and cross-talks, timing is everything. First, each pathway operates with specific kinetics. Co-stimulation or sequential stimulation of two pathways with different activation kinetics could lead to synergy, priming or tolerance effect on the co-regulated target

genes, as observed between different TLRs in macrophages (Bagchi et al, 2007; Foster et al, 2007; Zhang & Morrison, 1993). Second, separation of time scale also exists on different levels of transcriptional regulations. Take mammalian cells as an example, binding of transcription factors to DNA (~ 1 sec) is typically 3-orders of magnitude faster than transcription and translation (~ 30 min) (Alon, 2007). As for chromatin modification, different histone modifications (e.g. phosphorylation, acetylation, methylation and ubiquitylation) could also exhibit a great variance in kinetics during signaling processes and histone markings (Barth & Imhof, 2010).

In order to interpret complex signaling networks, systems biologists have made tremendous effort in building up a map of "functional motifs" of signaling networks in various model systems (Alon, 2007; Alon & Mangan, 2003; Gilchrist et al, 2006; Ma et al, 2009; Tyson et al, 2003; Tyson & Novak, 2010; Yao et al, 2011). Functional motif refers to a small network of molecular species (e.g. kinase, transcription factors etc.) interacting in a way that enables the system to generate a specific information-processing function. For example, with appropriate parameter settings, a negative feedback loop can generate homeostasis or oscillation (Hoffmann et al, 2002; Ma et al, 2009; Tyson et al, 2003). A coherent-feedforward loop, on the other hand, generates an "AND" gate logic on transcriptional regulation between two cooperating transcription factors, thereby enables the system to induce signal-specific or duration-specific responses (Alon & Mangan, 2003; Litvak et al, 2009). A complex biochemical interaction map is therefore considered as a circuit of functional motifs operating under multiple spatial-temporal controls (Alon, 2007; Tyson & Novak, 2010).

In this dissertation, we have investigated into fundamental questions about functional motifs and dynamics in the signaling or regulatory network for specific gene expression response, under two important contexts: cellular reprogramming and polarized activation dynamics.

1.2 Research Overview

In Chapter 2, we adopted and developed several computational systems biology methods to study network motifs and dynamics that lead to adapted cytokine production in macrophages upon sequential challenge of LPS (Shnyra et al, 1998; West & Koons, 2008; Zhang & Morrison, 1993). Since macrophage responses are governed by a complex signaling network, it remains unknown what molecular mechanisms enable a cell to calculate its cytokine level precisely based on a pathogen exposure history.

The motivation led us to study all possible network motifs and dynamics that could possibly generate priming or tolerance in a generic three-node network. A mathematical model based on Ordinary Differential Equations was build up to simulate the dynamical behavior of each network motif. A novel two-stage Monte-Carlo sampling of parameters was developed to achieve an efficient search in the high-dimensional parameter space for all possible priming/tolerance motifs. All the motifs were further clustered according to their time courses.

As a result, we found three basic priming mechanisms and one tolerance mechanism. Each priming/tolerance mechanism was found to meet a unique minimum requirement on network topology and dynamics. Using information from databases and literatures, we have identified molecules that may contribute to priming and tolerance effects. This paper has been published in

PLoS Computational Biology in 2012 (Fu et al, 2012). The method should be applicable to other types of cellular responses.

In Chapter 3, we use computational modeling and statistical physics to investigate potential ways to reprogram bacterial cells between phenotypes. The killing time of a bacterial colony usually follows a two-phase killing curve where the majority of bacteria die quickly within several hours (*h*) of antibiotic treatment, a small fraction of cells (typically 0.01% ~ 1% depending on the bacteria strains), however, could survive even after 50 *h* of antibiotic treatment (Balaban et al, 2004). These persister cells are genetically identical to normally growing cells. However, as they are in a growth-arrest phenotype, they are insensitive to antibiotics (Balaban et al, 2004). In this chapter, we demonstrated a way to accelerate the "killing" of persister cells through triggering a series of synchronized phenotypic transitions from persister cells into normally growing cells. In statistical physics, a noise-assisted barrier-crossing event can be accelerated under a weak perturbing signal with resonance frequency. This theory is called Resonance Activation. Because phenotypic transition of a bacterium can be mapped into a barrier-crossing event on energy landscape, we introduced Resonance Activation into this context and demonstrated, *in silico*, that resonance activation could occur under the perturbation of a weak external signal with resonance frequency.

Based on stochastic simulations on both single cell level and population level, we showed that with resonance activation, persister cells could quickly transform into the normally growing phenotype and get killed by antibiotics, thereby greatly reducing antibiotic usage and corresponding side-effects. The method shown in this chapter should be applicable to other

systems, such as stem cell reprogramming or cancer therapies that can be mapped to barrier-crossing events in physics. The paper in Chapter 3 has been published in Physical Biology in 2010 and has been highlighted by Institute of Physics (IOP) as a featured article of the year (Fu et al, 2010).

1.3 Reference

Akira S, Takeda K (2004) Toll-like receptor signalling. *Nat Rev Immunol* **4:** 499-511

Alon U (2007) *An introduction to systems biology: Design principles of biological circuits*, 1 edn.: Chapman and Hall/CRC.

Alon U, Mangan S (2003) Structure and function of the feed-forward loop network motif. *P Natl Acad Sci USA* **100:** 11980-11985

Bagchi A, Herrup EA, Warren HS, Trigilio J, Shin HS, Valentine C, Hellman J (2007) MyD88-dependent and MyD88-independent pathways in synergy, priming, and tolerance between TLR agonists. *J Immunol* **178:** 1164-1171

Balaban NQ, Merrin J, Chait R, Kowalik L, Leibler S (2004) Bacterial Persistence as a Phenotypic Switch. *Science* **305:** 1622-1625

Barth TK, Imhof A (2010) Fast signals and slow marks: the dynamics of histone modifications. *Trends in Biochemical Sciences* **35:** 618-626

Behar M, Dohlman HG, Elston TC (2007) Kinetic insulation as an effective mechanism for achieving pathway specificity in intracellular signaling networks. *Proc Natl Acad Sci U S A* **104:** 16146-16151

Chen KC, Calzone L, Csikasz-Nagy A, Cross FR, Novak B, Tyson JJ (2004) Integrative Analysis of Cell Cycle Control in Budding Yeast. *Molecular Biology of the Cell* **15:** 3841-3862

Cheng CS, Feldman KE, Lee J, Verma S, Huang D-B, Huynh K, Chang M, Ponomarenko JV, Sun S-C, Benedict CA, Ghosh G, Hoffmann A (2011) The Specificity of Innate Immune Responses Is Enforced by Repression of Interferon Response Elements by NF-{kappa}B p50. *Sci Signal* **4**

Cheong R, Hoffmann A, Levchenko A (2008) Understanding NF-[kappa]B signaling via mathematical modeling. *Mol Syst Biol* **4**

Foster SL, Hargreaves DC, Medzhitov R (2007) Gene-specific control of inflammation by TLR-induced chromatin modifications. *Nature* **447:** 972-978

Fu Y, Glaros T, Zhu M, Wang P, Wu Z, Tyson JJ, Li L, Xing J (2012) Network Topologies and Dynamics Leading to Endotoxin Tolerance and Priming in Innate Immune Cells. *PLoS Comput Biol* **8:** e1002526

Fu Y, Zhu M, Xing J (2010) Resonant activation: a strategy against bacterial persistence. *Physical Biology* **7:** 016013

Gardy JL, Lynn DJ, Brinkman FSL, Hancock REW (2009) Enabling a systems biology approach to immunology: focus on innate immunity. *Trends Immunol* **30:** 249-262

Gilchrist M, Thorsson V, Li B, Rust AG, Korb M, Kennedy K, Hai T, Bolouri H, Aderem A (2006) Systems biology approaches identify ATF3 as a negative regulator of Toll-like receptor 4. *Nature* **441:** 173-178

Heintzman ND, Hon GC, Hawkins RD, Kheradpour P, Stark A, Harp LF, Ye Z, Lee LK, Stuart RK, Ching CW, Ching KA, Antosiewicz-Bourget JE, Liu H, Zhang X, Green RD, Lobanenkov VV, Stewart R, Thomson JA, Crawford GE, Kellis M et al (2009) Histone modifications at human enhancers reflect global cell-type-specific gene expression. *Nature* **459:** 108-112

Hoffmann A, Levchenko A, Scott ML, Baltimore D (2002) The IκB-NF-κB Signaling Module: Temporal Control and Selective Gene Activation. *Science* **298:** 1241-1245

Hoffmann A, Natoli G, Ghosh G (2006) Transcriptional regulation via the NF-[kappa]B signaling module. *Oncogene* **25:** 6706-6716

Hu X, Ivashkiv LB (2009) Cross-regulation of Signaling Pathways by Interferon-[gamma]: Implications for Immune Responses and Autoimmune Diseases. *Immunity* **31:** 539-550

Huang W, Ghisletti S, Perissi V, Rosenfeld MG, Glass CK (2009) Transcriptional Integration of TLR2 and TLR4 Signaling at the NCoR Derepression Checkpoint. *Molecular Cell* **35:** 48-57

Johnson DS, Mortazavi A, Myers RM, Wold B (2007) Genome-Wide Mapping of in Vivo Protein-DNA Interactions. *Science* **316:** 1497-1502

Litvak V, Ramsey SA, Rust AG, Zak DE, Kennedy KA, Lampano AE, Nykter M, Shmulevich I, Aderem A (2009) Function of C/EBP delta in a regulatory circuit that discriminates between transient and persistent TLR4-induced signals. *Nat Immunol* **10:** 437-443

Ma W, Trusina A, El-Samad H, Lim WA, Tang C (2009) Defining Network Topologies that Can Achieve Biochemical Adaptation. *Cell* **138:** 760-773

Natarajan M, Lin KM, Hsueh RC, Sternweis PC, Ranganathan R (2006) A global analysis of cross-talk in a mammalian cellular signalling network. *Nat Cell Biol* **8:** 571-580

Oda K, Kitano H (2006) A comprehensive map of the toll-like receptor signaling network. *Mol Syst Biol* **2**

Schmid CD, Bucher P (2007) ChIP-Seq Data Reveal Nucleosome Architecture of Human Promoters. *Cell* **131:** 831-832

Shnyra A, Brewington R, Alipio A, Amura C, Morrison DC (1998) Reprogramming of lipopolysaccharide-primed macrophages is controlled by a counterbalanced production of IL-10 and IL-12. *J Immunol* **160:** 3729-3736

Tyson JJ, Chen KC, Novak B (2003) Sniffers, buzzers, toggles and blinkers: dynamics of regulatory and signaling pathways in the cell. *Curr Opin Cell Biol* **15:** 221-231

Tyson JJ, Novak B (2010) Functional motifs in biochemical reaction networks. *Annu Rev Phys Chem* **61:** 219-240

West MA, Koons A (2008) Endotoxin tolerance in sepsis: concentration-dependent augmentation or inhibition of LPS-stimulated macrophage TNF secretion by LPS pretreatment. *J Trauma* **65:** 893-898; discussion 898-900

Yao G, Tan CM, West M, Nevins JR, You LC (2011) Origin of bistability underlying mammalian cell cycle entry. *Mol Sys Biol* **7:** 485

Zhang XK, Morrison DC (1993) Lipopolysaccharide-Induced Selective Priming Effects on Tumor-Necrosis-Factor-Alpha and Nitric-Oxide Production in Mouse Peritoneal-Macrophages. *J Exp Med* **177:** 511-516

Chapter 2. Network Topologies and Dynamics Leading to Endotoxin Tolerance and Priming in Innate Immune Cells

Yan Fu[1,2], Trevor Glaros[1], Meng Zhu[3], Ping Wang[1], Zhanghan Wu[1,2], John J Tyson[1], Liwu Li[1,*], Jianhua Xing[1,*]

[1]Department of Biological Sciences and [2]Interdisciplinary PhD Program of Genetics, Bioinformatics and Computational Biology, Virginia Polytechnic Institute and State University, Blacksburg, VA 24060, USA. [3]School of Computing, Clemson University, Clemson, SC 29634, USA.

* Send correspondence to jxing@vt.edu and lwli@vt.edu

2.1 Abstract

The innate immune system, acting as the first line of host defense, senses and adapts to foreign challenges through complex intracellular and intercellular signaling networks. Endotoxin tolerance and priming elicited by macrophages are classic examples of the complex adaptation of innate immune cells. Upon repetitive exposures to different doses of bacterial endotoxin (lipopolysaccharide) or other stimulants, macrophages show either suppressed or augmented inflammatory responses compared to a single exposure to the stimulant. Endotoxin tolerance and priming are critically involved in both immune homeostasis and the pathogenesis of diverse inflammatory diseases. However, the underlying molecular mechanisms are not well understood. By means of a computational search through the parameter space of a coarse-grained three-node network with a two-stage Metropolis sampling approach, we enumerated all the network topologies that can generate priming or tolerance. We discovered three major mechanisms for

priming (pathway synergy, suppressor deactivation, activator induction) and one for tolerance (inhibitor persistence). These results not only explain existing experimental observations, but also reveal intriguing test scenarios for future experimental studies to clarify mechanisms of endotoxin priming and tolerance.

2.2 Introduction

Innate immune cells such as macrophages and dendritic cells constitute the first layer of host defense. Like policemen constantly patrolling the streets for criminal activity, these cells are responsible for initiating the first attack against invading pathogens (Akira & Takeda, 2004; Gordon & Martinez, 2010). For example, using Toll-like receptor 4 (TLR4), macrophages recognize lipopolysaccharide (LPS, also called endotoxin), a pathogen-associated molecular pattern (PAMP) that is expressed on the outer membrane of gram-negative bacteria. Within hours of stimulation, hundreds of regulatory genes, kinases, cytokines, and chemokines are activated in sequential waves, leading to a profound inflammatory and anti-microbial response in macrophages (Medzhitov & Horng, 2009). Although effective levels of inflammation require potent cytokine production, excessive or prolonged expression can be detrimental, resulting in various immune diseases, such as autoimmunity, atherosclerosis, sepsis shock and cancers (Lin & Karin, 2007; Medzhitov & Horng, 2009). Owing to this double-edged nature of innate immunity, living organisms have evolved a highly complex signaling network to fine-tune the expression of cytokines (Ezekowitz & Hoffmann, 1996). A fundamental question in this field is what kinds of network topologies and dynamics in the signaling network ensure the appropriate expression of cytokines. This question is part of a larger current theme in systems biology of the design principles of biological networks. Are there small network motifs that serve as building

blocks to perform complex "information processing" functions in biological signaling networks (Alon, 2007; Kholodenko, 2006; Ma et al, 2006; Ma et al, 2009; Milo et al, 2002; Shen-Orr et al, 2002; Tyson et al, 2003)? In this context, a systems and computational biology approach may greatly deepen our understanding in innate immunity (Gardy et al, 2009; Gilchrist et al, 2006; Hume et al, 2007; Litvak et al, 2009; Tegner et al, 2006).

Here we focus on the signaling motifs responsible for endotoxin priming and tolerance of macrophages. The interaction between host macrophages and bacterial endotoxin is arguably one of the most ancient and highly conserved phenomena in multi-cellular eukaryotic organisms (Ezekowitz & Hoffmann, 1996). Through TLR4, LPS activates MyD88-dependent and MyD88-independent pathways, which eventually lead to the regulation of a number of downstream genes and pathways, including the mitogen-activated protein kinase (MAPK), phosphoinositide 3-kinase (PI3K), and nuclear factor κB (NFκB). The integration of these intracellular pathways leads to measured induction of pro-inflammatory mediators. Intriguingly, the induction of inflammatory mediators is also finely controlled by the quantities and prior history of LPS challenges. The latter is physiologically relevant since cells are likely repetitively exposed to stimulants in their natural environment. For example, numerous *in vitro* studies have found that significant induction of cytokine TNF-α and IL-6 requires at least 10 ng/mL LPS in mouse peritoneal macrophages (Hirohashi & Morrison, 1996; Shnyra et al, 1998) and macrophage cell lines (Hume et al, 2001), and a high dose of LPS (100 ng/mL) is sufficient to trigger a catastrophic "cytokine storm". Strikingly, however, the dose-response relationship can be reprogrammed by two successive treatments with LPS, to give either a reduced or an augmented expression of cytokines (Figure 2.1A). *In vitro*, preconditioning macrophages with a high dose

(HD) of LPS (10−100 ng/mL) renders the cells much less responsive to a subsequent HD stimulation in terms of pro-inflammatory cytokine expression. This phenomenon, known as "endotoxin tolerance" or "LPS tolerance" (Biswas & Lopez-Collazo, 2009), is reported to last up to 3 weeks *in vivo* (West & Heagy, 2002). On the other hand, macrophages primed by a low dose (LD) of LPS (0.05−1 ng/mL) show an augmented production of cytokine in response to a subsequent HD challenge, a phenomenon known as "LPS priming" (Henricson et al, 1993; Hirohashi & Morrison, 1996; Shnyra et al, 1998; West & Koons, 2008; Zhang & Morrison, 1993). Both priming and tolerance are present in other cells of the innate immune system including monocytes and fibroblasts, and are highly conserved from mice to humans. Our own studies on murine macrophages show both effects (Figure 2.1B).

Endotoxin priming and tolerance may confer significant survival advantages to higher eukaryotes. Priming of innate immune cells may enable robust and expedient defense against invading pathogens, a mechanism crudely analogous to vaccination of the adaptive immune system. On the other hand, tolerance may promote proper homeostasis following robust innate immune responses. However, despite these survival advantages, endotoxin priming and tolerance are also closely associated with the pathogenesis of both chronic and acute human diseases. For example, despite the potential ability to limit pro-inflammatory cytokine production, endotoxin tolerance is responsible for the induction of immunosuppression in patients with sepsis shock, and this suppression leads to increased incidence to secondary infections and mortality (West & Heagy, 2002). Endotoxin priming, on the other hand, reprograms macrophages to super-induction of proinflammatory cytokines. Increasing evidence relates this phenomenon to low-grade metabolic endotoxemia, where an elevated but physiological level of LPS in the host's

bloodstream results in a higher incidence of insulin resistance, diabetes and atherosclerosis (Kiechl et al, 2001; Moreno-Navarrete et al, 2010; Slofstra et al, 2006; Wiesner et al, 2010). Augmented IL-6 expression has also been observed in human blood cells that were primed by LD and challenged by HD LPS (Nakamura et al, 2004).

Despite the significance and intense research efforts, molecular mechanisms responsible for endotoxin priming and tolerance are not well understood, apparently due to the complex nature of intracellular signaling networks. Tolerance has been attributed to the negative regulators at multiple levels of the TLR4 signaling pathway. These include signaling molecules (*e.g.* SHIP, ST2, induction of IRAK-M and suppression of IRAK-1), transcriptional modulators (*e.g.* ATF3, p50/p50 homodimers), soluble factors (*e.g.* IL-10 and TGFβ), and gene-specific chromatin modifications (Biswas & Lopez-Collazo, 2009; Brint et al, 2004; Chang et al, 2009; El Gazzar et al, 2007; Foster et al, 2007; Jacinto et al, 2002; Kobayashi et al, 2002; Li et al, 2000; Sly et al, 2004). These negative regulators are likely to work together to drive macrophages into a transient refractory state for cytokine expression after LPS pretreatment (Sly et al, 2004). Molecular mechanisms for priming are rarely studied and even less well understood than tolerance. Early studies suggest that like endotoxin tolerance, both intra- and inter-cellular events may be involved in LPS priming (Zhang & Morrison, 1993). Morrison and coworkers first revealed that LPS priming of cytokine TNF-α production is induced, at least in part, by a reprogrammed counterbalance between endogenous IL-10 and IL-12 in an autocrine fashion (Shnyra et al, 1998). However, it is still elusive exactly how the change in two counteracting soluble secretory products can contribute to the priming effect, and whether LPS priming is exclusively an intercellular event or it takes place at both intra- and inter-cellular levels.

These published observations and our own new experimental results have inspired us to look for all possible mechanisms for LPS priming and tolerance. To do this, we computationally searched the high-dimensional parameter space associated with a generic mathematical model of a three-node regulatory network. The search reveals only three mechanisms accounting for priming (pathway synergy, suppressor deactivation, activator induction) and one for tolerance (inhibitor persistence). Existing experimental results support these mechanisms.

In summary, our approach provides a systematic, quantitative framework for understanding numerous experimental observations, and it suggests new experimental procedures to identify the players and investigate the dynamics of priming and tolerance. Our analysis suggests that endotoxin tolerance and priming are rooted in the basic structure of the immune regulatory network: a signal often triggers synergizing pathways to ensure that sufficient responses can be elicited efficiently, as well as opposing pathways to ensure that the responses can be resolved eventually (Akira & Takeda, 2004). Therefore, in addition to shedding light on LPS-induced tolerance and priming, our approach is applicable in the more general context of cross-priming and cross-talk in the signal transduction mechanisms of the innate immune system (Bagchi et al, 2007; Hu et al, 2008; Hu & Ivashkiv, 2009).

2.3 Materials and Methods

Mathematical description

The following mathematical formalism is used to describe the dynamics of the three-node system,

$$\frac{dx_j}{dt} = \gamma_j (G(\sigma_j W_j) - x_j)$$

where $G(a) = \frac{1}{1+e^{-a}}$, and $W_j = \omega_{j0} + \sum_{i=1}^{3} \omega_{ji} x_i + S_j$. Notice that $x_j(t)$ lies between 0 and 1 for all *t*. All variables and parameters are dimensionless. $G(\sigma_j W_j)$ is a generic "sigmoidal" function with steepness (slope at $W_j = 0$) that increases with σ_j. Each ω_{ji} is a real number in [-1, 1] with its absolute value denoting the strength of the regulation; $\omega_{ji} > 0$ for the "activators" and $\omega_{ji} < 0$ for "inhibitors" of node *j*. The sum, W_j, is the net activation or inhibition on node *j*, and ω_{j0} determines whether node *j* is "on" or "off" when all input signals are 0. The parameters γ_j determine how quickly each variable approaches its goal value, $G(\sigma_j W_j)$ for the present value of W_j. Because the magnitudes of the weights are bounded, $|\omega_{ji}| < 1$, it is possible to do a thorough and systematic search of all possible weight matrices, even for networks of moderate complexity, *e.g.*, *K* (= number of non-zero ω_{ji}'s) < 20. The formalism is close to that used by Vohradsky (Vohradsky, 2001; Weaver et al, 1999) and others (Jaeger et al, 2004; Perkins et al, 2006) previously. More detailed discussions and applications of the formalism can be found in (Hong et al, 2011; Tyson et al, 2011; Tyson & Novak, 2010).

The model contains 18 parameters: 9 ω_{ji}'s, 3 γ_j's, 3 σ_j's and 3 ω_{j0}'s. By setting $\gamma_3 = 1$, we fix the time scale of the model to be the response time of the output variable, $x_3(t)$. We set $\omega_{30} = -0.50$, so that the response variable is close to $x_3 = 0$ in the absence of input. We also chose $\sigma_3 = 6$ as a moderate value for the sigmoidicity of the output response. Apart from that, ω_{20} is set to be -0.25 so that the x_2 pathway is responsive to LD stimulation.

Monte Carlo sampling algorithm

Our goal is to sample points in a 14-dimensional parameter space that is bounded and continuous. The sampling algorithm needs to search the parameter space thoroughly and generate sample parameter sets that are statistically unbiased and significant. Our strategy is a random walk based on the Metropolis Algorithm (Metropolis et al, 1953) through parameter space according to the following rules:

0. Choose an initial parameter set $\boldsymbol{\theta}_0$ and determine its score: $\Omega_0 = 0$ if it is a "good" set, or $\Omega_0 = 1$ if it is not. (See Text S1 for the definition of a good set of parameters for priming or for tolerance.)

1. Generate parameter set $\boldsymbol{\theta}_{k+1}$ from $\boldsymbol{\theta}_k$ by $\boldsymbol{\theta}_{k+1} = \boldsymbol{\theta}_k + \lambda\boldsymbol{\zeta}$, where $\lambda = 0.025$ specifies the maximum displacement per step, and $\boldsymbol{\zeta}$ is a vector of random numbers with uniform distribution between -0.5 and 0.5.

2. Compute Ω_{k+1}. If $\Omega_{k+1} \le \Omega_k$, then accept the step from *k* to *k*+1. If $\Omega_{k+1} > \Omega_k$, then accept the step from *k* to *k* + 1 with probability ρ. Otherwise, reject the step *k* to *k*+1.

3. Update *k*. If *k* is larger than a maximum step number, stop. Otherwise return to step 1.

We pursue this strategy in two stages. In stage 1, we set $\rho = 0.0025$ (see Text S1), so that the random walk has larger tendency to stay in "good" regions of parameter space, but can also jump out of a good region and searches randomly until it falls into another good region (which may be the same region it left). Stage 1 generates a random walk of 10^9 steps, which is sampled every 100 steps. From this sample of 10^7 parameter sets only the good ones are saved, giving a sample of $\sim 8\times10^4$ good parameter sets. These data are then analyzed as described below:

1. The K-means algorithm is applied to identify possible clusters of good parameter sets in the 14-dimensional parameter space. The clustering result is then visualized through the first two principal components (which account for ~60% of the data variance) under Principal Component Analysis.

2. One parameter set is chosen from each possible cluster to serve as starting points for stage 2.

Stage 2 is a repeat of stage 1 with $\rho = 0$. In this case the random walk never leaves a good region. The purpose of stage 3 is to generate a large sample of good parameter sets that may occupy different regions of parameter space. The random walks are sampled every 100 steps, generating 10^6 good parameter sets from each starting point. Each parameter set must pass an additional test for "biological relevance" (see Text S1 for details) before further analysis.

While the results reported in the main text are from one run of the search procedure, the whole procedure was repeated several times with random initial starting point in stage 1. The final results of these repeated runs agree with each other, confirming the convergence of our search procedure.

Discretization of continuous parameter matrix into topology matrix

In order to analyze the topological feature of each priming/tolerance mechanism, one needs to map the continuous parameters ω_{ji} into a discretized topological matrix τ_{ji}. In the topological space, variables are only described by (−, 0, +) representing inhibition, no regulation and activation, respectively. A cut off value (= 0.1) is used to perform the discretization, following the rules below:

$$\tau_{ji} = \begin{cases} -1, & if \ \omega_{ji} \le -0.1 \\ 0, & if \ -0.1 < \omega_{ji} < 0.1 \\ 1, & if \ \omega_{ji} \ge 0.1 \end{cases}$$

Experimental studies of LPS priming and tolerance

Murine bone marrow derived macrophages from C57BL/6 wild type mice were harvested as described previously (Maitra et al, 2011). Cells were cultured in DMEM medium (Invitrogen) supplemented with 100 units/mL penicillin, 100 μg/mL streptomycin, 2 mM l-glutamine, and 10% fetal bovine serum (Hyclone) in a humidified incubator with 5% CO_2 at 37 ℃. Cells were treated with LPS (*E. coli* 0111:B4, Sigma) as indicated in the figure legend. RNAs were harvested using Trizol reagent (Invitrogen) as previously described (Maitra et al, 2011). Quantitative real-time reverse-transcription (RT)-PCR were performed as described (Maitra et al, 2009). The relative levels of *IL-6* message were calculated using the ΔΔCt method, using *GAPDH* as the internal control. The relative levels of mRNA from the untreated samples were adjusted to 1 and served as the basal control value.

2.4 Results

Inducing priming and tolerance in a well-controlled experimental setting

Although separate experimental studies of priming and tolerance have been carried out in many laboratories, no systematic study of both effects has been performed in the same setting. Thus, we first set out to measure priming and tolerance in the same experimental system. We used murine bone marrow derived macrophages (BMDMs), which are widely used for measuring LPS responses. BMDM were treated with various combinations of LD (50 pg/mL) and HD (100 ng/mL) LPS for times indicated in Figure 2.1B. Cells were washed with PBS and fresh medium

between consecutive treatments. Figure 2.1B shows that 50 pg/mL LPS induced negligible *IL-6*, while 100 ng/mL LPS induced robust expression of *IL-6* in BMDM (~3300 fold). Consistent with previous findings, cells pre-treated for 4 h with 50 pg/mL LPS exhibited ~4500 fold induction of *IL-6* when challenged with 100 ng/mL LPS, a ~36% augmentation as compared to cells treated with 100 ng/mL LPS alone ($p < 0.05$). In contrast, cells pretreated for 4 h with 100 ng/mL LPS exhibited only ~700 fold induction of *IL-6* when re-challenged with 100 ng/mL LPS, a ~80% reduction as compared to cells treated with 100 ng/mL LPS alone ($p < 0.05$).

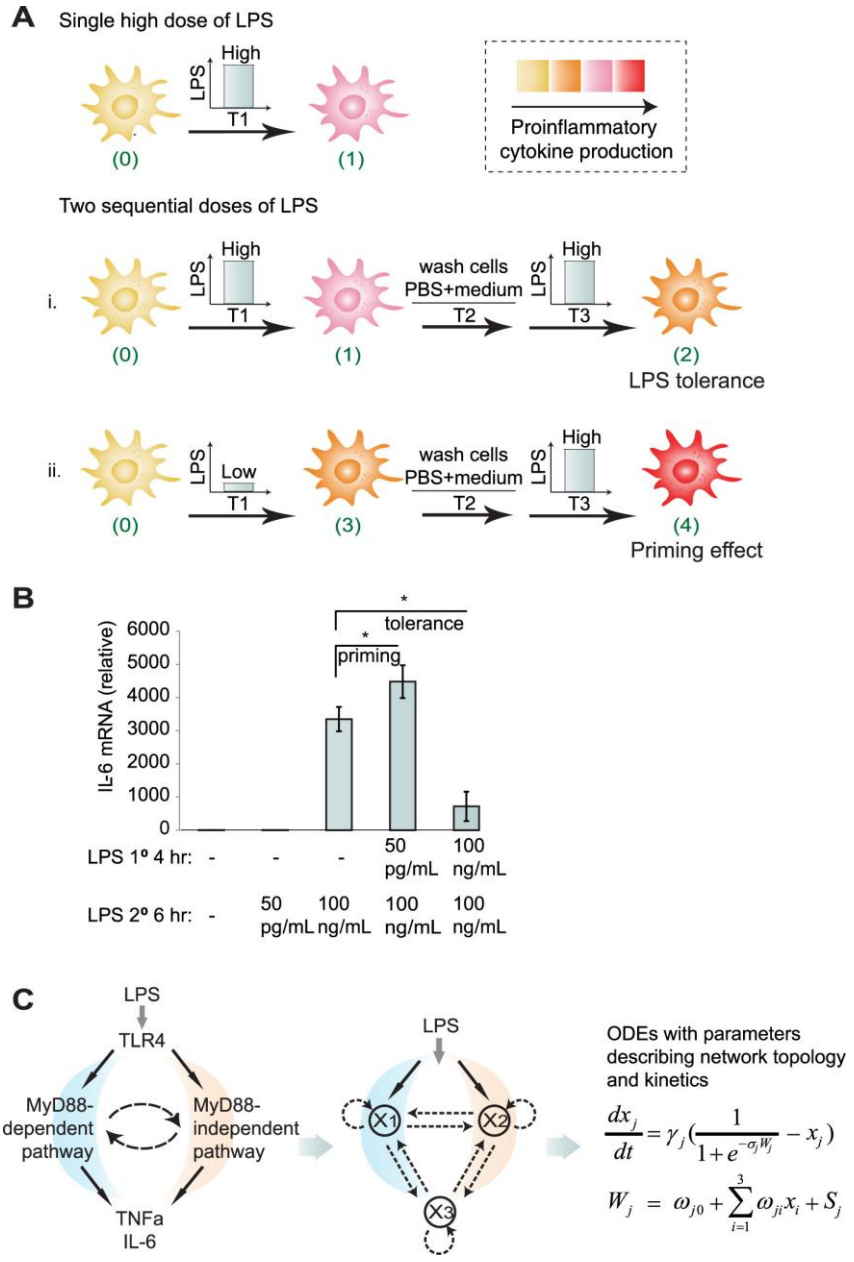

Figure 2.1. Formulation of the problem. (A) Schematic illustration of *in vitro* experimental studies of LPS-induced tolerance and priming effect in macrophages. (B) *IL-6* mRNA levels of murine bone marrow derived macrophages treated with various combinations of LPS. * $p<0.05$. (C) Abstraction of the parallel LPS associated pathways into a three-node network motif and the corresponding mathematical model based on ordinary differential equations. Refer to Materials and Methods for details.

Identifying motifs that generate priming effect

Figure 2.1C shows that LPS binding to TLR4 triggers two groups of parallel pathways: MyD88-dependent and (several) MyD88-independent pathways. Together, these pathways control the expression of different but overlapping inflammatory mediators in a delicate time-dependent and dose-dependent manner. Based on these parallel pathways, we proposed a three-node model in Figure 2.1C as a minimal abstraction of the system. Each node can positively or negatively regulate the activity of itself and the other two nodes. The interactions are governed, we assume, by a standardized set of nonlinear ordinary differential equations (Figure 2.1C) for x_j = activity of the j^{th} node ($0 \leq x_j \leq 1$, j = 1,2,3). For a complete description of the mathematical model, see the section on Materials and Methods. The "network topology" of the model is determined by the sign pattern of the nine interaction coefficients ($-1 \leq \omega_{ji} \leq 1$, j,i = 1,2,3) which express the magnitude and direction of the effect of node i on node j. This is a coarse-grained model, with no distinction between intra- and inter-cellular events. For example, in a real cell the self-regulation of a node may correspond to a feedback loop involving many intermediates, including extracellular cytokines. The simplicity of the model allows full search of the 14-dimensional parameter space (although there are 18 parameters in Table 2.1, four of them are held constant, as explained in Materials and Methods). Similar three-node models have been studied in other contexts (Ma et al, 2009; Yang et al, 2008; Yao et al, 2011).

We searched the 14-dimensional parameter space of the model for priming and then for tolerance. The behavior of the model is defined as "priming" if the maximum level of the output variable x_3 under the priming dose (step 3 in Figure 2.1A) is small ($x_3 < 0.3$), but with the subsequent high dose (step 4 in Figure 2.1A) x_3 is at least 50% higher than the level reached

without priming (step 1 in Figure 2.1A). Similarly, for "tolerance" the maximum level of x_3 must be high enough under the first HD exposure ($x_3 > 0.3$) but less intense by at least 50% under the second HD challenge (step 2 in Figure 2.1A). Precise criteria for priming and tolerance are provided in Table 2.S1. Brute force search of the parameter space is impractical. Unbiased searching results in <1000 parameter sets exhibiting priming after 10^8 Monte Carlo steps. Noticing that parameter sets giving priming or tolerance (called "good sets" for convenience) are clustered into a small number of isolated regions in parameter space, we designed a two-stage sampling procedure. First we perform a Metropolis search slightly biased for good sets. Next, to identify any isolated regions of parameter space where good sets are clustered, we analyzed the good sets using K-means clustering and Principal Component Analysis (see Text S1). The good sets then serve as seeds in the second stage of sampling, which restricts Metropolis searching to each local region of good sets. This two-stage procedure allows us to search the parameter space thoroughly and to obtain good-set samples that are large enough for statistical analysis. The overall procedure is illustrated schematically in Figure 2.S1 and discussed in Supporting Text.

Three basic mechanisms for the priming effect of LPS

By trial-and-error, we found that the two experimentally measurable quantities, Δx_1 and Δx_2 (see Figure 2.2A), are effective in dividing the "good" parameter sets into three regions (see Figure 2.2B). Here Δx_1 = maximum difference between x_1 during the LD priming stage and the steady state value of x_1 in the absence of any stimulus, and Δx_2 = difference between the maximum values of x_2 during the HD period with and without the priming pretreatment (Figure 2.2A). Further analysis (discussed below) revealed that the three groups correspond to three distinct priming mechanisms: "Pathway Synergy" (PS), "Activator Induction" (AI), and "Suppressor

Deactivation" (SD). All AI and PS parameter sets show considerable increase in x_2 (> 0.1) after the priming stage, while SD does not (Figure 2.S2).

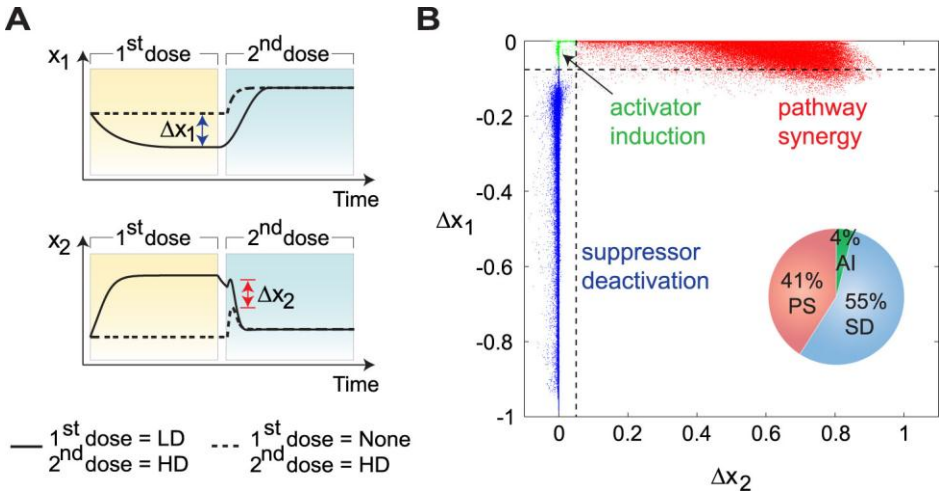

Figure 2.2. Three priming mechanisms revealed by time-course patterns. (A) Definition of clustering axis x_1 and x_2. x_1 refers to the maximum difference between x_1 during the LD priming stage and the steady state value of x_1 in the absence of any stimulus. x_2 refers to the difference between the maximum values of x_2 during the HD period with and without priming pretreatment. (B) The time courses of the priming data sets naturally divide into three clusters, corresponding to three priming mechanisms. The pie chart shows the relative frequencies of the priming mechanisms among all the priming parameter sets.

To characterize these priming mechanisms, we next examined the parameter sets within each group for shared topological features. The topology of a regulatory motif is defined as the sign pattern (+, − or 0) of the nine interaction coefficients, ω_{ji}, with the proviso that ω_{ji}'s in the interval [−0.1, 0.1] are set = 0. We define a backbone motif as the simplest network topology that is shared by most of the good priming sets in each group and that is able to generate a priming

effect on its own. Therefore, a backbone motif represents a core network structure in each group. Figure 2.3A shows that each group has its unique backbone motif(s), directly revealing different priming mechanisms in each group. Figure 2.S3 and Supporting Text provide detailed statistical methods used to identify the backbone motifs. The two-dimensional parameter histograms in Figure 2.S4 provide further support for the backbone motifs we have identified.

Figure 2.3B-D shows typical time-courses and state-space trajectories for the three priming mechanisms (see Table 2.S2 for the parameter values used to generate this figure).

***Pathway Synergy* (*PS*):** As shown in the upper left panel of Figure 2.3A, the backbone motif of PS mechanism contains both pathways through x_1 and x_2 activating x_3. Under a single HD, the faster pathway through x_1 prevents activation of x_2, either directly or through x_3. Consequently there is no synergy between the two pathways after a single HD. With LD pretreatment, however, x_2 is partially activated. During the following HD treatment, this partial activation allows x_2 to increase significantly, either transiently (Figure 2.3B left panel, called "monostable") or persistently (Figure 2.3B right panel, called "bistable"), despite inhibition from x_1 and/or x_3. Simultaneous activation of both pathways leads to synergy between them and a priming effect for x_3.

***Activator Induction* (*AI*):** In the backbone motif (see upper right panel of Figure 2.3A), the pathway through x_1 (with high activation threshold) inhibits x_3, whereas the pathway through x_2 (with a low activation threshold) activates x_3. Consequently, under a single HD, the two pathways work against each other to prevent full activation of x_3. A LD pretreatment partially

activates x_2 without significantly affecting x_1. Then, during the following HD treatment, x_2 gets a head start on x_1 to induce greater activation of x_3 than observed under a single HD. The activation of x_3 can be either transient (monostable) or persistent (bistable), as illustrated in Figure 2.3C and Figure 2.S5A.

***Suppressor Deactivation* (*SD*):** In this case there are two backbone motifs slightly different from each other (the lower panel of Figure 2.3A). Both motifs contain an inhibition pathway ($x_1 \dashv x_3$) with slow dynamics and low sensitivity to LPS, and an activation pathway ($x_2 \rightarrow x_3$) with fast dynamics and high sensitivity to LPS. The basal level of the suppressor x_1 is relatively high, which is typical of some suppressors (*e.g.* TOLLIP, TRAILR, PI3K and nuclear receptors) that are constitutively expressed in macrophages to prevent unwanted expression of downstream pro-inflammatory genes under non-stimulated conditions (Liew et al, 2005; Necela et al, 2008). Compared to AI, in this case the LD pretreatment decreases the level of suppressor x_1, through direct inhibition of x_1 by x_2. The basic SD effect is amplified either by x_2 self-activation (backbone motif I) or by negative feedback from x_3 to x_1 (backbone motif II). As before, the activation of x_3 can be either transient (monostable) or persistent (bistable), as illustrated in Figure 2.3B and Figure 2.S5B.

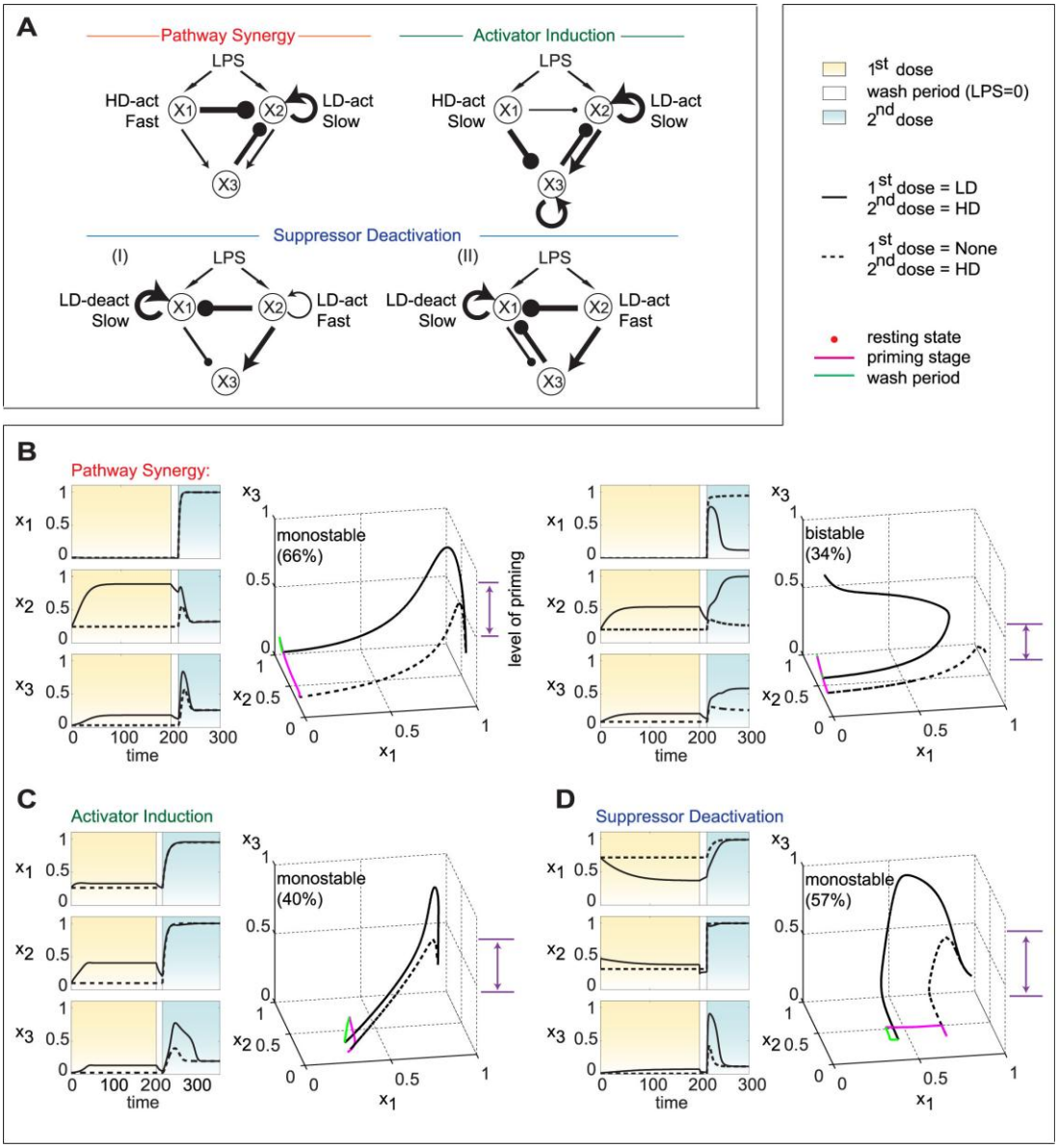

Figure 2.3. Details of the three priming mechanisms. (A) Backbone motifs (topological features shared by most of the good parameter sets) of each priming mechanism (see Figure 2.S3 and Text S1 for details). The width of a line is proportional to the mean value of the corresponding γ_{ji} among data sets under each priming mechanism. The "slow" and "fast" time scales reflect the values of γ_j in comparison to $\gamma_3 = 1$. (B-D) Typical time courses and corresponding phase space trajectories with or without LD pretreatment. Bistable results for AI and SD are shown in Figure 2.S5.

Combined backbone motifs may enhance the robustness of the priming effect

Each of these groups contains many different network topologies (187 in PS, 139 in SD, and 82 in AI). Taking SD as an example, Figure 2.4A shows the sorted density distribution of the 139 unique topologies represented by the SD parameter sets. The top 7 of these topologies (Figure 2.4B) comprise 31% of all the SD parameter sets. Consistent with other studies (Ma et al, 2009; Yao et al, 2011), the most highly represented topologies contain more links than the corresponding backbone motif, indicating that additional links may increase the robustness of a network. While the two backbone motifs rank Top 27 and Top 10 respectively (Figure 2.4B), their combination ranks Top 4. The Venn diagram in Figure 2.4C shows that of the 93% of SD parameter sets that contain at least one of the two backbone motifs, 64% contain both. Notice that the two backbone motifs use different helpers to deactivate the suppressor (x_1) under LD, the combination of motifs (Top 4) integrates both helpers so that deactivation of the suppressor can be enhanced (Figure 2.4C). The results of a similar analysis applied to PS and AI mechanisms are given in Figure 2.S7.

Additionally, in the Figure 2.S8 and Supporting Text, we discuss a parameter compensation effect that further expands the priming region in the parameter space.

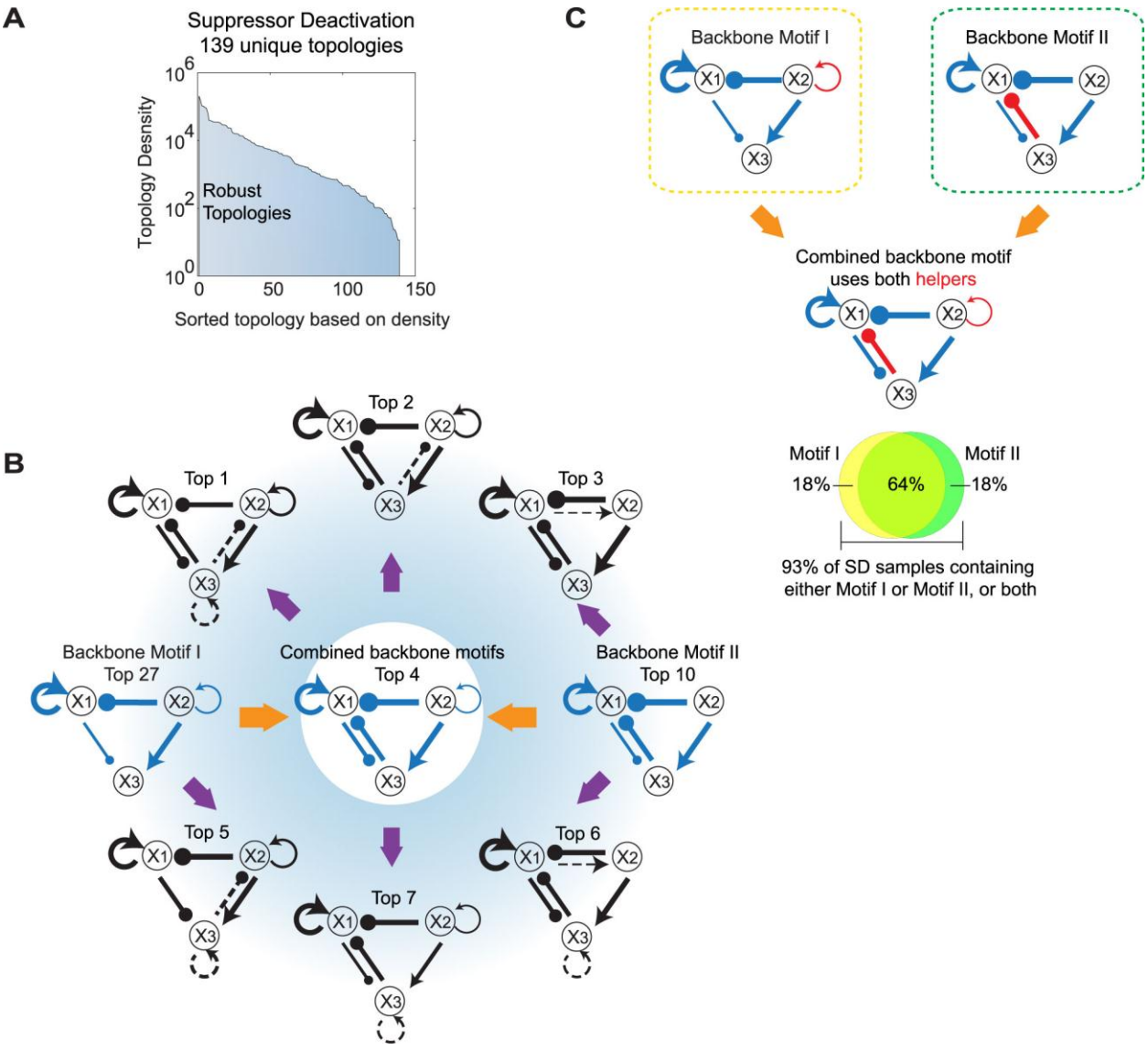

Figure 2.4. Analysis of the robust priming topologies in the SD mechanism. (A) 139 unique topologies under SD mechanism sorted by topology density (see Figure 2.S6 and Supporting Text for detailed discussion). (B) The highest seven density topologies and the backbone motifs. Line widths are proportional to the mean value of samples of the corresponding topology. Dashed lines denote the additional link present in the top topologies but absent in the backbone motif. (C) Combination of the two backbone motifs is common in the SD data sets. 93% of SD data sets are found to contain either Motif I or Motif II as the backbone motif. Among them, 64% contain both Motif I and Motif II.

Slow inhibitor relaxation dynamics is essential for the induction of tolerance

We used the 3-node model to search for endotoxin-tolerance motifs. The tolerance effect requires that pro-inflammatory cytokine expression (x_3) is markedly reduced (by at least 1.5 fold) under two sequential HD treatments with LPS, compared to the level induced by a single HD (see Table 2.S1 for details). Over 1660 unique topologies are found to give a tolerance effect (Figure 2.5A), indicating that the requirements for tolerance are much lower than for priming. A typical time course (Figure 2.5B, left panel) highlights the essential dynamical requirement for tolerance — to sustain a sufficiently high level of inhibitor (x_1 in this case) after the first HD of LPS so that x_3 is less responsive to the second HD stimulus. The effect is transient: if the second HD stimulus is delayed long enough for the suppressor to return to its basal level, then the tolerance effect is lost (Figure 2.5B, right panel). This "memory" effect has been noticed in other modeling studies (An & Faeder, 2009; Day et al, 2006; Riviere et al, 2009; Vodovotz et al, 2009) and is consistent with experimental observations. For example, the tolerance status of IL-6 is reported to persist for 48 h after the initial HD of LPS, but beyond this time a re-challenge started to recover the expression of IL-6 (Foster et al, 2007). Figure 2.5C shows two backbone motifs that support temporary persistence of the inhibitor: by slow removal or by positive auto-regulation of the inhibitor.

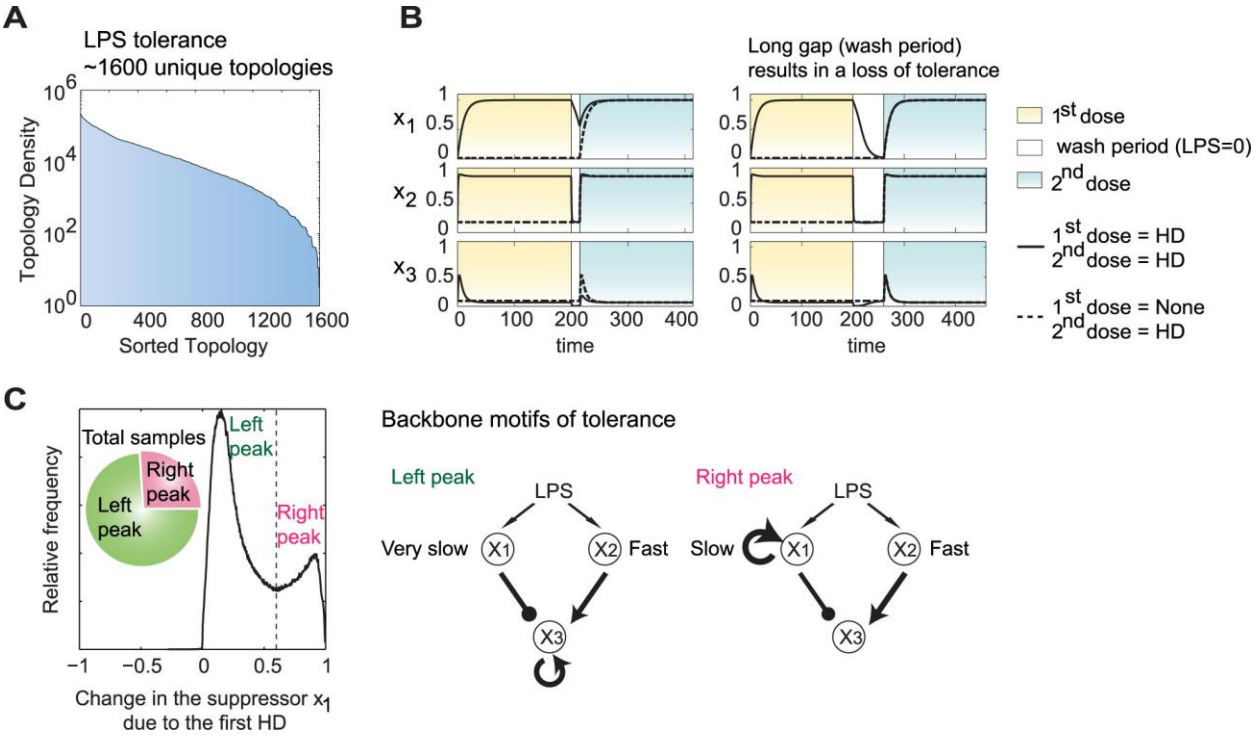

Figure 2.5. Analysis of the tolerance data sets. (A) The unique topologies generating a tolerance effect sorted by topology density. (B) Typical time courses shown with normal (left panel) or elongated (right panel) gap period between the two doses. Solid line: time course tracking the dynamics of the system under the first HD stimulation, in gap period and under a second HD stimulation. Dashed line: time course tracking the dynamics under a single HD treatment; in this case the system is treated with no LPS during the otherwise first HD period. (C) Distribution of the change of x_1 level due to the initial HD stimulation reveals two mechanisms to achieve slow relaxation dynamics in the inhibitor (left panel) and the corresponding two backbone motif (right panel).

The dosing scenarios for priming and tolerance are well separated

It is of interest to ask whether priming and tolerance can be observed in a single 3-node network given the corresponding dosing conditions. It turns out that about 11% of the priming motifs

exhibit tolerance as well, and most of them belong to the SD or the AI mechanism. Figure 2.6A shows qualitatively the dose-response relationship for priming and tolerance in a typical network motif. First, both priming and tolerance require a relatively large second dose (>0.5). Second, the dosing regions for priming and tolerance are well separated. A low first dose (0.1−0.4) leads to priming while a higher one (0.5−1) leads to tolerance. There exists a range separating the priming and the tolerance region where neither are observed.

Signaling durations affect the induction of priming and tolerance

Most experimental studies of priming and tolerance are performed with fixed durations of the three time periods (T_1, T_2, and T_3 in Figure 2.1A). Time-course measurements are rarely reported. The phase diagrams in Figure 2.6B & C show how varying each time period can affect the induction of priming and tolerance in a typical network motif. Altogether, these results reveal important dynamical requirement in priming and tolerance and suggest systematic studies in real biological experiments.

The left panel of Figure 2.6B shows the effects of varying stimulus durations (T_1 and T_3) at fixed gap duration (T_2). To generate priming, T_1 must be sufficiently long, while T_3 can be relatively short (left panel of Figure 2.6B). A sufficient priming duration is crucial because the system utilizes this time to activate/deactivate the regulatory pathway with slower dynamics, *i.e.*, the synergizing pathway in PS and the suppressor pathway in SD. Therefore, if T_1 is too short, one may erroneously conclude that priming does not exist in the system. On the other hand, tolerance is less dependent on T_1 (right panel of Figure 2.6B).

Figure 2.6C shows results when all durations are varied under the constraint $T_1 = T_3$. In this case, both priming and tolerance require that T_2 is sufficiently short compared to the time required for the system to relax to its basal state after the first stimulus. This result reveals priming and tolerance as essentially the result of cellular memory of the first stimulation.

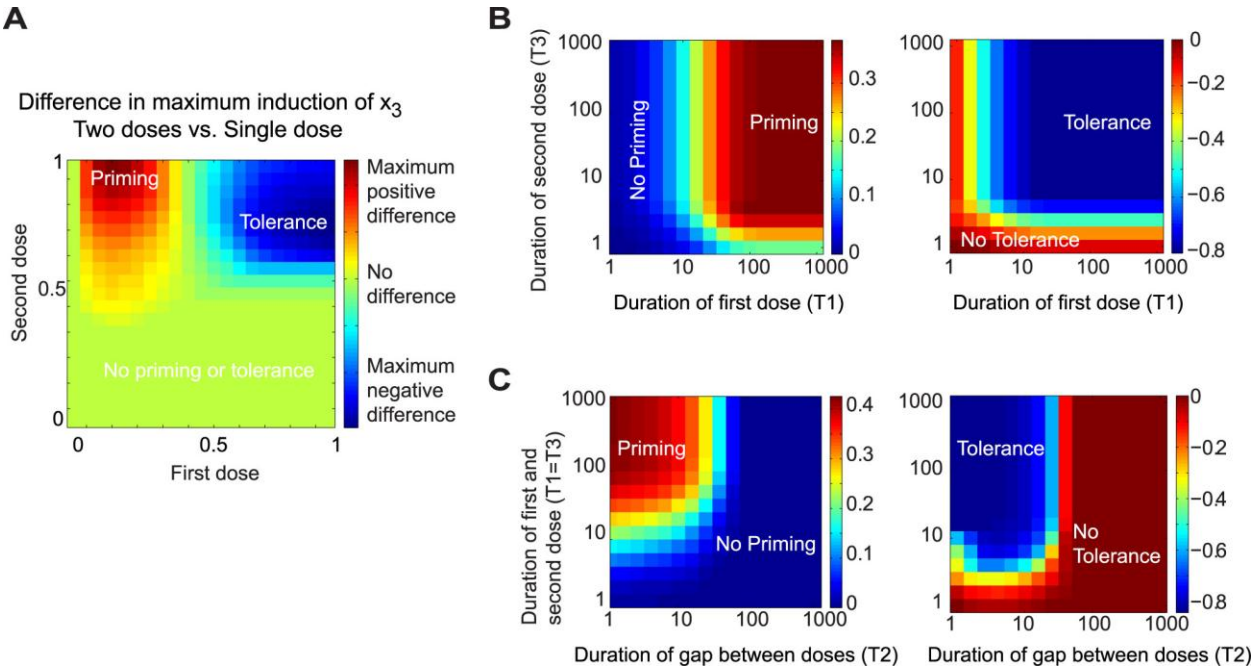

Figure 2.6. Phase diagrams for priming and tolerance in a typical network motif. (A) Regions of dosing conditions for tolerance and priming are well separated. (B) Both priming and tolerance effects are affected by the duration of two sequential treatments (with the gap period between two doses being fixed). (C) Priming and tolerance are also affected by the duration of the gap between two doses. Very long gaps fail to exhibit either priming or tolerance.

2.5 Discussion

Using a simple yet flexible model of cellular signaling pathways, we have carried out a systematic study of the topological and dynamic requirements for endotoxin priming and

tolerance in cells of the innate immune system. Our study reveals that the phenomena of priming and tolerance can be attributed to a few characteristic network motifs (called "backbone" motifs) that are simple yet effective combinations of feed-forward loops, negative feedback signals, and auto-activation. In addition to reconciling the limited available experimental data on endotoxin priming and tolerance, our models suggest novel, testable hypotheses regarding the molecular mechanisms responsible for these effects.

Essential modalities for priming and tolerance

Our *in silico* analysis identifies three basic mechanisms for priming (Figure 2.7). In these mechanisms two pathways interact either constructively (pathway synergy−PS) or destructively (activator induction−AI, suppressor deactivation−SD). Compared to the response of these systems to a single high dose (HD) of LPS, a priming dose of LPS modifies the relative phases of the two pathways so as to strengthen pathway synergy (for PS mechanism) or weaken pathway interference (for SD and AI mechanisms).

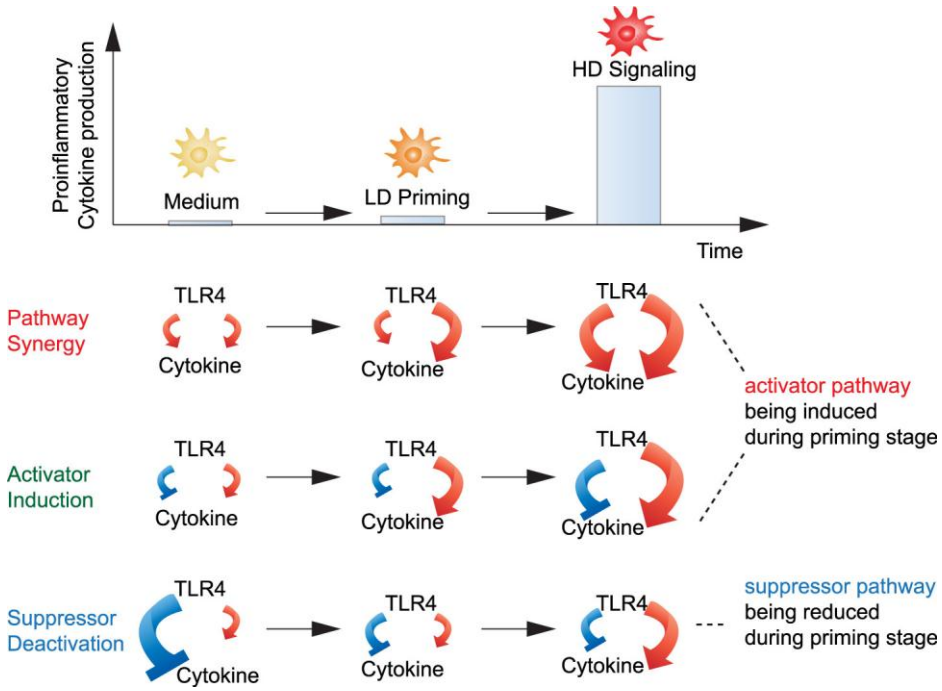

Figure 2.7. Schematic illustration of constructive (PS) and destructive (AI, SD) pathway interference leading to priming effect. PS results from the activation of the LD-responsive pathway (x_2) which cooperates with the other HD-responsive pathway (x_1) to boost cytokine expression in response to the following HD stimulus. AI results from activating a LD-responsive pathway (x_2), which cancels the inhibition coming from the other HD-responsive inhibitor (x_1) during the HD stage. SD results from deactivating a constitutively expressed suppressor (x_1) during the priming stage. Red line with arrow head: activation pathway. Blue line with bar head: inhibition pathway. Line width denotes strength of the pathway controlling the downstream cytokine expression.

In this work we define the priming effect as a response of x_3 that is at least 50% higher with priming than without. The threshold of 50% is consistent with experimental observations (Henricson et al, 1993; West & Koons, 2008), but to be sure that our conclusions are robust, we also performed the computational analysis at two other thresholds: 30% augmentation or 70%

augmentation (i.e., λ=1.3 or λ=1.7 in Table 2.S1). In both cases we obtained results similar to those shown in Figure 2.2B, corresponding to the three priming mechanisms, although the exact percentage of each priming mechanism among the data sets varies with the priming threshold.

The priming effect may be viewed as a primitive counterpart of the more sophisticated memory mechanisms of the adaptive immune system. For a limited period of time after exposure to a weak stimulus, the system is prepared to launch a stronger response to a second exposure to the (same or another) stimulus (Hu et al, 2008; Taniguchi & Takaoka, 2001). On the other hand, tolerance reflects a transient refractory status to produce inflammatory cytokines due to the memory of an earlier exposure.

Supporting experimental evidences at intra- and inter-cellular levels

The actual molecular and cellular networks responsible for endotoxin priming and tolerance are highly complex, involving both intra- and inter-cellular signaling modalities. A combination of priming/tolerance motifs most likely coexist in real signaling networks, and their interactions will determine the specific properties of the priming/tolerance effect *in vivo*. LPS is known to activate multiple intracellular pathways through TLR4, including MyD88-dependent, TRIF-dependent pathways (Takeda & Akira, 2004). Cross-talk among these pathways may be differentially modulated by low *vs.* high dosages of LPS, and thus contribute to differential priming and tolerance (Laird et al, 2009; Li et al, 2000; Maitra et al, 2011).

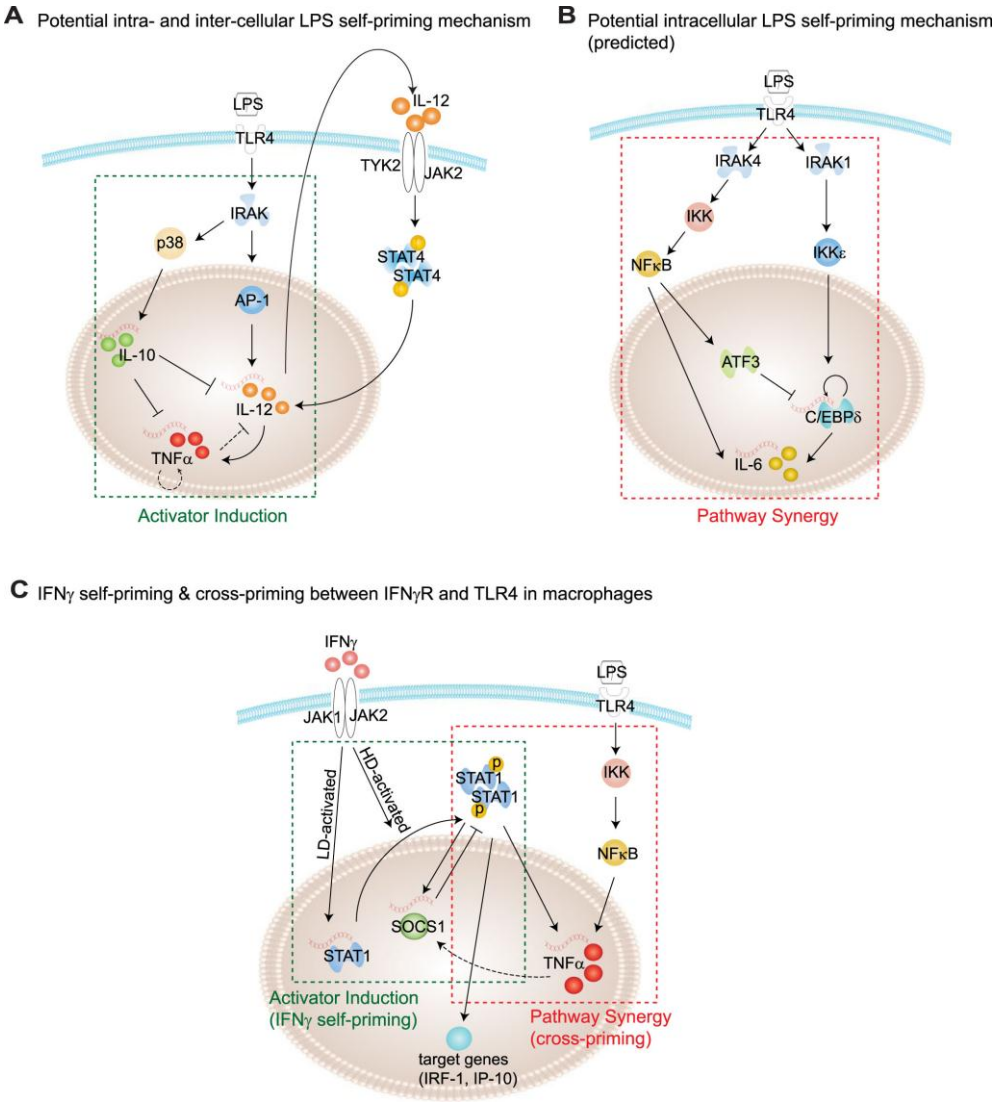

Figure 2.8. Example regulatory networks supporting the priming mechanisms. (A) The AI mechanism is consistent with observed intra- and inter-cellular molecular mechanisms for LPS priming, based on counterbalanced IL-10 and IL-12 signaling (Shnyra et al, 1998). (B) The PS mechanism inspires this predicted intracellular molecular mechanism based on the selective activation of C/EBPδ by LD LPS. (C) IFN-γ self-priming and cross-priming to LPS follows the AI and PS mechanisms. Network details are retrieved from the database IPA (@Ingenuity) as well as the experimental literature listed in Table 2.S3. Dashed lines refer to indirect regulations involving autocrine signaling loops.

Endotoxin tolerance has drawn significant attention in the past due to its relevance to septic shock. Existing literature reveals the involvement of multiple negative regulators (SHIP, ST2, IL-10, IRAK-M, SOCS1) at either intracellular or intercellular levels. Many of them are shown to be persistently elevated during endotoxin tolerance, a key feature (confirmed by our systems analysis) creating a refractory state that suppresses the expression of pro-inflammatory mediators (see Table 2.2). For example, SHIP and ST2 are documented to have very slow degradation rates. On the other hand, negative regulators with faster turn-over rates, such as A20 and MKP1 (induced between 2−4 h by LPS), are known not to be required for LPS tolerance (Biswas & Lopez-Collazo, 2009; van 't Veer et al, 2007).

In terms of priming, our *in silico* results are consistent with limited experimental data regarding potential molecular mechanisms. For example (Figure 2.8A), IL-12 and IL-10 are differentially induced by low *vs.* high dose LPS, and subsequently serve as autocrine mediators to modulate LPS priming (Shnyra et al, 1998). Figure 2.8B provides a second example. Low dose LPS (50 pg/mL) can selectively activate transcription factor C/EBPδ, yet fails to activate the classic NFκB pathway (Maitra et al, 2011). Hence, by a pathway synergy motif, the selective activation of C/EBPδ by low dose LPS may synergize with NFκB under the subsequent high dose to induce the priming effect. While the removal of nuclear repressor by low dose LPS is reported (Maitra et al, 2011), further evidence for the predicted suppressor deactivation mechanism awaits additional, targeted experimentation. In this context, one needs to be aware that our predicted network motifs are simple topologies that have the potential to generate priming or tolerance, within proper parameter ranges. Our predictions warrant further experimental studies to

determine the physiologically relevant ranges of signaling parameters required for priming and tolerance.

Our analysis of priming and tolerance is not limited to LPS. Bagchi *et al.* showed that cross-priming may happen between specific TLRs (Bagchi et al, 2007). Ivashkiv and coworkers reported that IFN-γ can prime macrophage for an augmented response to a variety of stimulants, including bacterial LPS, virus, IFN-α/β and IFN-γ itself (Hu et al, 2008; Hu & Ivashkiv, 2009). IFN-γ self-priming is similar to LPS self-priming: a low dose can prime for boosted expression of interferon-responsive genes. The priming mechanism as reported by Hu *et al.* resembles the AI strategy (Hu et al, 2002). Interferon-responsive genes such as IRF1 and IP-10 are transcriptionally induced by transcription factor STAT1, and are inhibited by SOCS1 through a negative feedback mechanism. Low dose IFN-γ (1 U/ml) is able to elevate the expression level of STAT1, preparing macrophage for a boosted activation of STAT1 (through phosphorylation and dimerization of STAT1) under the high dose IFN-γ stimulation. With STAT1 being active, however, the inhibitor SOCS1 cannot be expressed during the priming stage, resulting in an augmented expression of IRF-1 and IP-10 (Figure 2.8C). Furthermore, Figure 2.8C suggests a possible cross-priming between IFN-γ and TLR4 via a PS mechanism. Priming of macrophage by a low dose IFN-γ promotes STAT1 expression, which may synergistically cooperate with NFκB to give boosted cytokine expression to secondary stimulation by LPS (Hu et al, 2002; Schroder et al, 2004). Further experimental studies are needed to confirm the prediction.

Limitations of three-node models and further theoretical studies

Three-node models have been used to analyze functional network motifs in several contexts (Alon, 2007; Ma et al, 2009; Yao et al, 2011). The simplicity of three-node models allows a thorough search of the parameter space. However, the model should be viewed as a minimal system. A typical biochemical network surely has more than three nodes. Therefore each node or link in the three-node model is normally coarse-grained from more complex networks. The model parameters are also composite quantities. Three-node models are limited in their ability to generate certain dynamic features such as time delays. Figure 2.3A shows the backbone motifs of the three mechanisms we have identified. Further studies of models with additional nodes will be necessary to determine whether all of the links are necessary. For example, in Figure 2.8B, we cannot find evidence for IL-6 inhibiting C/EBPδ (either by direct or indirect links). This lack of evidence may indicate a missing link waiting for experimental confirmation, or it may indicate a limitation of the three-node model. The parameter search algorithm developed in this work can be applied to models with 4 or more nodes, although the search space grows rapidly with the number of nodes.

Despite the above-mentioned limitations, we expect that the three priming mechanisms and the one tolerance mechanism discovered here are quite general, holding beyond the three-node model. We expect that the present work can serve as a basis for analyzing larger networks with more mechanistic details. As illustrated in Figure 2.8, motifs can be combined together in series or in parallel, and these combined structures may lead to new dynamic properties of functional importance.

Suggested experimental design

Our analysis in Figure 2.6 suggests that systematic studies of signal durations (T_1, T_2 and T_3) may reveal important details of the dynamics of priming and tolerance. For example, both relatively short (4 h, as the experiment in this paper) and longer priming duration ($\geq$ 20 h) are exhibit priming effects in macrophages (Henricson et al, 1993). Relatively fast transcriptional regulators like NFκB and AP-1, as well as numerous signaling repressors such as PI3K and nuclear receptors, may be involved in intracellular priming motifs, inducing priming in response to short pretreatments. On the other hand, a longer pretreatment orchestrates more complex intercellular pathways whereby autocrine or paracrine signaling of cytokines (e.g. IL-10, IL-12 and type I IFNs) might dominate the induction of priming effects (Shnyra et al, 1998). Therefore, measurements of the full time spectrum are necessary to reveal different parts of the network contributing to priming/tolerance.

Furthermore, our analysis predicts that priming networks may respond in two distinct fashions: monostable (transient super-induction of cytokine) or bistable (sustained super-induction of cytokines). Time-course measurements can distinguish between these two responses, keeping in mind that the bistable behavior predicted here is relative to the effective time-scale of the model. Each motif considered here is embedded in a larger network. Eventually, in a healthy organism pro-inflammatory cytokines have to be cleared out by some other slow processes that resolve the inflammation. On this longer time scale, the sustained induction of cytokines predicted by some of our models would be resolved.

The analysis presented in Figure 2.2B suggests a plausible hypothesis to characterize underlying mechanisms of endotoxin priming. High-throughput techniques can be used to identify genes and proteins that are significantly changed by low dose pretreatment. Likely candidates can be assayed during the course of a priming experiment, and the time-course data analyzed as in Figure 2.2B to identify the critical regulatory factors.

Our analyses and simulations reveal that the priming effect is quite sensitive to system dynamics, *i.e.*, to parameter values and initial conditions. It is well documented that many biological control systems, especially those involving gene expression, are stochastic in nature. Consequently a population of seemingly identical cells may respond heterogeneously to a fixed experimental protocol. In this case, single-cell measurements may reveal cell-to-cell variations in priming and tolerance responses (Diercks et al, 2009; Lee & Covert, 2010; Ravasi et al, 2002).

Taken together, our integrated and systems analyses reconcile the intriguing paradigm of priming and tolerance in monocytes and macrophages. Given the significance and prevalence of this paradigm in immune cells to diverse stimulants other than LPS, our identified functional motifs will serve as potential guidance for future experimental works related to macrophage polarization as well as dynamic balance of immune homeostasis and pathogenesis of inflammatory diseases.

2.6 Acknowledgements

We thank Dr Xiaoyu Hu for helpful discussions.

2.7 References

Akira S, Takeda K (2004) Toll-like receptor signalling. *Nat Rev Immunol* 4: 499-511

Alon U (2007) *An introduction to systems biology: Design principles of biological circuits*, 1 edn.: Chapman and Hall/CRC.

An GC, Faeder JR (2009) Detailed qualitative dynamic knowledge representation using a BioNetGen model of TLR-4 signaling and preconditioning. *Math Biosci* 217: 53-63

Bagchi A, Herrup EA, Warren HS, Trigilio J, Shin HS, Valentine C, Hellman J (2007) MyD88-dependent and MyD88-independent pathways in synergy, priming, and tolerance between TLR agonists. *J Immunol* 178: 1164-1171

Benkhart EM, Siedlar M, Wedel A, Werner T, Ziegler-Heitbrock HW (2000) Role of Stat3 in lipopolysaccharide-induced IL-10 gene expression. *J Immunol* 165: 1612-1617

Biswas SK, Lopez-Collazo E (2009) Endotoxin tolerance: new mechanisms, molecules and clinical significance. *Trends Immunol* 30: 475-487

Brint EK, Xu D, Liu H, Dunne A, McKenzie AN, O'Neill LA, Liew FY (2004) ST2 is an inhibitor of interleukin 1 receptor and Toll-like receptor 4 signaling and maintains endotoxin tolerance. *Nat Immunol* 5: 373-379

Chang J, Kunkel SL, Chang CH (2009) Negative regulation of MyD88-dependent signaling by IL-10 in dendritic cells. *Proc Natl Acad Sci U S A* 106: 18327-18332

Chen X, El Gazzar M, Yoza BK, McCall CE (2009) The NF-kappaB factor RelB and histone H3 lysine methyltransferase G9a directly interact to generate epigenetic silencing in endotoxin tolerance. *J Biol Chem* 284: 27857-27865

Day J, Rubin J, Vodovotz Y, Chow CC, Reynolds A, Clermont G (2006) A reduced mathematical model of the acute inflammatory response II. Capturing scenarios of repeated endotoxin administration. *J Theor Biol* 242: 237-256

de Waal Malefyt R, Abrams J, Bennett B, Figdor CG, de Vries JE (1991) Interleukin 10(IL-10) inhibits cytokine synthesis by human monocytes: an autoregulatory role of IL-10 produced by monocytes. *J Exp Med* 174: 1209-1220

Diercks A, Kostner H, Ozinsky A (2009) Resolving cell population heterogeneity: real-time PCR for simultaneous multiplexed gene detection in multiple single-cell samples. *PLoS ONE* 4: e6326

El Gazzar M, Yoza BK, Hu JY, Cousart SL, McCall CE (2007) Epigenetic silencing of tumor necrosis factor alpha during endotoxin tolerance. *J Biol Chem* 282: 26857-26864

Ezekowitz RAB, Hoffmann JA (1996) Innate immunity. *Curr Opin Immunol* 8: 1-2

Foster SL, Hargreaves DC, Medzhitov R (2007) Gene-specific control of inflammation by TLR-induced chromatin modifications. *Nature* 447: 972-978

Gardy JL, Lynn DJ, Brinkman FSL, Hancock REW (2009) Enabling a systems biology approach to immunology: focus on innate immunity. *Trends Immunol* 30: 249-262

Gilchrist M, Thorsson V, Li B, Rust AG, Korb M, Kennedy K, Hai T, Bolouri H, Aderem A (2006) Systems biology approaches identify ATF3 as a negative regulator of Toll-like receptor 4. *Nature* 441: 173-178

Gordon S, Martinez FO (2010) Alternative Activation of Macrophages: Mechanism and Functions. *Immunity* 32: 593-604

Henricson BE, Manthey CL, Perera PY, Hamilton TA, Vogel SN (1993) Dissociation of lipopolysaccharide (LPS)-inducible gene expression in murine macrophages pretreated with smooth LPS versus monophosphoryl lipid A. *Infect Immun* 61: 2325-2333

Hirohashi N, Morrison DC (1996) Low-dose lipopolysaccharide (LPS) pretreatment of mouse macrophages modulates LPS-dependent interleukin-6 production in vitro. *Infect Immun* 64: 1011-1015

Hong T, Xing J, Li L, Tyson JJ (2011) A Mathematical Model for the Reciprocal Differentiation of T Helper 17 Cells and Induced Regulatory T Cells. *PLoS Comput Biol* 7: e1002122

Hu X, Chakravarty SD, Ivashkiv LB (2008) Regulation of interferon and Toll-like receptor signaling during macrophage activation by opposing feedforward and feedback inhibition mechanisms. *Immunol Rev* 226: 41-56

Hu X, Herrero C, Li W-P, Antoniv TT, Falck-Pedersen E, Koch AE, Woods JM, Haines GK, Ivashkiv LB (2002) Sensitization of IFN-[gamma] Jak-STAT signaling during macrophage activation. *Nat Immunol* 3: 859-866

Hu X, Ivashkiv LB (2009) Cross-regulation of Signaling Pathways by Interferon-[gamma]: Implications for Immune Responses and Autoimmune Diseases. *Immunity* 31: 539-550

Hume DA, Ravasi T, Wells CA (2007) Systems biology of transcription control in macrophages. *BioEssays* 29: 1215-1226

Hume DA, Underhill DM, Sweet MJ, Ozinsky AO, Liew FY, Aderem A (2001) Macrophages exposed continuously to lipopolysaccharide and other agonists that act via toll-like receptors exhibit a sustained and additive activation state. *BMC Immunol* 2: 11

Jacinto R, Hartung T, McCall C, Li L (2002) Lipopolysaccharide- and lipoteichoic acid-induced tolerance and cross-tolerance: distinct alterations in IL-1 receptor-associated kinase. *J Immunol* 168: 6136-6141

Jaeger J, Surkova S, Blagov M, Janssens H, Kosman D, Kozlov KN, Manu, Myasnikova E, Vanario-Alonso CE, Samsonova M, Sharp DH, Reinitz J (2004) Dynamic control of positional information in the early Drosophila embryo. *Nature* 430: 368-371

Kholodenko BN (2006) Cell-signalling dynamics in time and space. *Nat Rev Mol Cell Biol* 7: 165-176

Kiechl S, Egger G, Mayr M, Wiedermann CJ, Bonora E, Oberhollenzer F, Muggeo M, Xu Q, Wick G, Poewe W, Willeit J (2001) Chronic Infections and the Risk of Carotid Atherosclerosis : Prospective Results From a Large Population Study. *Circulation* 103: 1064-1070

Kobayashi K, Hernandez LD, Galan JE, Janeway CA, Medzhitov R, Flavell RA (2002) IRAK-M is a negative regulator of toll-like receptor signaling. *Cell* 110: 191-202

Laird MH, Rhee SH, Perkins DJ, Medvedev AE, Piao W, Fenton MJ, Vogel SN (2009) TLR4/MyD88/PI3K interactions regulate TLR4 signaling. *J Leukoc Biol* 85: 966-977

Lee TK, Covert MW (2010) High-throughput, single-cell NF-[kappa]B dynamics. *Curr Op Genet Dev* 20: 677-683

Li L, Cousart S, Hu J, McCall CE (2000) Characterization of interleukin-1 receptor-associated kinase in normal and endotoxin-tolerant cells. *J Biol Chem* 275: 23340-23345

Liew FY, Xu D, Brint EK, O'Neill LA (2005) Negative regulation of toll-like receptor-mediated immune responses. *Nat Rev Immunol* 5: 446-458

Lin WW, Karin M (2007) A cytokine-mediated link between innate immunity, inflammation, and cancer. *J Clin Invest* 117: 1175-1183

Litvak V, Ramsey SA, Rust AG, Zak DE, Kennedy KA, Lampano AE, Nykter M, Shmulevich I, Aderem A (2009) Function of C/EBP delta in a regulatory circuit that discriminates between transient and persistent TLR4-induced signals. *Nat Immunol* 10: 437-443

Ma W, Lai L, Ouyang Q, Tang C (2006) Robustness and modular design of the Drosophila segment polarity network. *Mol Syst Biol* 2: 70

Ma W, Trusina A, El-Samad H, Lim WA, Tang C (2009) Defining Network Topologies that Can Achieve Biochemical Adaptation. *Cell* 138: 760-773

Maitra U, Gan L, Chang S, Li L (2011) Low-Dose Endotoxin Induces Inflammation by Selectively Removing Nuclear Receptors and Activating CCAAT/Enhancer-Binding Protein {delta}. *J Immunol* 186: 4467-4473

Maitra U, Singh N, Gan L, Ringwood L, Li L (2009) IRAK-1 contributes to lipopolysaccharide-induced reactive oxygen species generation in macrophages by inducing NOX-1 transcription

and Rac1 activation and suppressing the expression of antioxidative enzymes. *J Biol Chem* 284: 35403-35411

Medzhitov R, Horng T (2009) Transcriptional control of the inflammatory response. *Nat Rev Immunol* 9: 692-703

Metropolis N, Rosenbluth AW, Rosenbluth MN, Teller AH (1953) Equation of State Calculations by Fast Computing Machines. *The Journal of chemical physics* 21: 1087

Milo R, Shen-Orr S, Itzkovitz S, Kashtan N, Chklovskii D, Alon U (2002) Network motifs: simple building blocks of complex networks. *Science* 298: 824-827

Moreno-Navarrete JM, Manco M, Ibanez J, Garcia-Fuentes E, Ortega F, Gorostiaga E, Vendrell J, Izquierdo M, Martinez C, Nolfe G, Ricart W, Mingrone G, Tinahones F, Fernandez-Real JM (2010) Metabolic endotoxemia and saturated fat contribute to circulating NGAL concentrations in subjects with insulin resistance. *Int J Obes (Lond)* 34: 240-249

Nakagawa R, Naka T, Tsutsui H, Fujimoto M, Kimura A, Abe T, Seki E, Sato S, Takeuchi O, Takeda K, Akira S, Yamanishi K, Kawase I, Nakanishi K, Kishimoto T (2002) SOCS-1 participates in negative regulation of LPS responses. *Immunity* 17: 677-687

Nakamura T, Nitta H, Ishikawa I (2004) Effect of low dose Actinobacillus actinomycetemcomitans lipopolysaccharide pretreatment on cytokine production by human whole blood. *J Periodontal Res* 39: 129-135

Necela BM, Su W, Thompson EA (2008) Toll-like receptor 4 mediates cross-talk between peroxisome proliferator-activated receptor gamma and nuclear factor-kappaB in macrophages. *Immunology* 125: 344-358

Perkins TJ, Jaeger J, Reinitz J, Glass L (2006) Reverse engineering the gap gene network of Drosophila melanogaster. *PLoS Comput Biol* 2: e51

Ravasi T, Wells C, Forest A, Underhill DM, Wainwright BJ, Aderem A, Grimmond S, Hume DA (2002) Generation of diversity in the innate immune system: macrophage heterogeneity arises from gene-autonomous transcriptional probability of individual inducible genes. *J Immunol* 168: 44-50

Riviere B, Epshteyn Y, Swigon D, Vodovotz Y (2009) A simple mathematical model of signaling resulting from the binding of lipopolysaccharide with Toll-like receptor 4 demonstrates inherent preconditioning behavior. *Math Biosci* 217: 19-26

Schroder K, Hertzog PJ, Ravasi T, Hume DA (2004) Interferon-gamma: an overview of signals, mechanisms and functions. *J Leukoc Biol* 75: 163-189

Shen-Orr SS, Milo R, Mangan S, Alon U (2002) Network motifs in the transcriptional regulation network of Escherichia coli. *Nat Genet* 31: 64-68

Shnyra A, Brewington R, Alipio A, Amura C, Morrison DC (1998) Reprogramming of lipopolysaccharide-primed macrophages is controlled by a counterbalanced production of IL-10 and IL-12. *J Immunol* 160: 3729-3736

Slofstra S, Cate H, Spek CA (2006) Low dose endotoxin priming is accountable for coagulation abnormalities and organ damage observed in the Shwartzman reaction. A comparison between a single-dose endotoxemia model and a double-hit endotoxin-induced Shwartzman reaction. *Thromb J* 4: 13

Sly LM, Rauh MJ, Kalesnikoff J, Song CH, Krystal G (2004) LPS-Induced Upregulation of SHIP Is Essential for Endotoxin Tolerance. *Immunity* 21: 227-239

Staples KJ, Smallie T, Williams LM, Foey A, Burke B, Foxwell BM, Ziegler-Heitbrock L (2007) IL-10 induces IL-10 in primary human monocyte-derived macrophages via the transcription factor Stat3. *J Immunol* 178: 4779-4785

Takeda K, Akira S (2004) TLR signaling pathways. *Semin Immunol* 16: 3-9

Taniguchi T, Takaoka A (2001) A weak signal for strong responses: interferon-alpha/beta revisited. *Nat Rev Mol Cell Biol* 2: 378-386

Tegner J, Nilsson R, Bajic VB, Bjorkegren J, Ravasi T (2006) Systems biology of innate immunity. *Cell Immunol* 244: 105-109

Tyson JJ, Baumann WT, Chen C, Verdugo A, Tavassoly I, Wang Y, Weiner LM, Clarke R (2011) Dynamic modelling of oestrogen signalling and cell fate in breast cancer cells. *Nat Rev Cancer* 11: 523-532

Tyson JJ, Chen KC, Novak B (2003) Sniffers, buzzers, toggles and blinkers: dynamics of regulatory and signaling pathways in the cell. *Curr Opin Cell Biol* 15: 221-231

Tyson JJ, Novak B (2010) Functional motifs in biochemical reaction networks. *Annu Rev Phys Chem* 61: 219-240

van 't Veer C, van den Pangaart PS, van Zoelen MA, de Kruif M, Birjmohun RS, Stroes ES, de Vos AF, van der Poll T (2007) Induction of IRAK-M is associated with lipopolysaccharide tolerance in a human endotoxemia model. *J Immunol* 179: 7110-7120

Vodovotz Y, Constantine G, Rubin J, Csete M, Voit EO, An G (2009) Mechanistic simulations of inflammation: current state and future prospects. *Math Biosci* 217: 1-10

Vohradsky J (2001) Neural network model of gene expression. *Faseb J* 15: 846-854

Weaver DC, Workman CT, Stormo GD (1999) Modeling regulatory networks with weight matrices. *Pac Symp Biocomput*: 112-123

West MA, Heagy W (2002) Endotoxin tolerance: A review. *Crit Care Med* 30: S64-S73

West MA, Koons A (2008) Endotoxin tolerance in sepsis: concentration-dependent augmentation or inhibition of LPS-stimulated macrophage TNF secretion by LPS pretreatment. *J Trauma* 65: 893-898; discussion 898-900

Wiesner P, Choi SH, Almazan F, Benner C, Huang W, Diehl CJ, Gonen A, Butler S, Witztum JL, Glass CK, Miller YI (2010) Low doses of lipopolysaccharide and minimally oxidized low-density lipoprotein cooperatively activate macrophages via nuclear factor kappa B and activator protein-1: possible mechanism for acceleration of atherosclerosis by subclinical endotoxemia. *Circ Res* 107: 56-65

Yang K, Bai H, Ouyang Q, Lai L, Tang C (2008) Finding multiple target optimal intervention in disease-related molecular network. *Mol Syst Biol* 4: 228

Yao G, Tan CM, West M, Nevins JR, You LC (2011) Origin of bistability underlying mammalian cell cycle entry. *Mol Sys Biol* 7: 485

Zhang XK, Morrison DC (1993) Lipopolysaccharide-Induced Selective Priming Effects on Tumor-Necrosis-Factor-Alpha and Nitric-Oxide Production in Mouse Peritoneal-Macrophages. *J Exp Med* 177: 511-516

Table 2.1. Description of modeling parameters.

Parameter	**Description**
x_j	Concentration (or activity) of species j
γ_j	Time scale of x_j dynamics
ω_{ji}	Regulation strength of x_i on x_j
ω_{j0}	Activation threshold of x_j
σ_j	Nonlinearity of the regulation relation associated to species x_j
S_j	External signal strength acting on x_j. (S_3=0, S_1=S_2)

Table 2.2. Experimental evidence supporting the proposed tolerance mechanism.

Molecular Candidate	**Inhibition Target**	**Persistent Strategy**	**Reported Evidence**	**Reference**
IRAK-M	IRAK-1 and IRAK-4 signaling	Slow time scale	Both mRNA and protein level of IRAK-M kept increased until 24 h with LPS stimulation.	(Kobayashi et al, 2002)
SHIP	NFκB pathway	Slow time scale; Positive auto-regulation of upstream regulator	Slow but sustained production of SHIP (peaked at 24 h and remained high until 48 h with LPS stimulation), regulated via autocrine-acting TGF-β; long half-life of SHIP protein.	(Sly et al, 2004)
SOCS1 (under debate)	IRAK and NFκB pathway	Slow time scale	SOCS1 mRNA levels remains detectable 24 h post LPS stimulation.	(Nakagawa et al, 2002)
ST2	MyD88 and Mal	Slow time scale	ST2 is induced at 4 h and lasts until 48 h with LPS stimulation.	(Brint et al, 2004)
IL-10 (required but not necessary for tolerance)	MyD88-dependent pathway (IRAK, TRAF6)	Slow time scale; Positive autoregulation	Significant level of IL-10 was detected with prolonged (24 h) LPS stimulation, and the level is sustained until 48 h. The IL-10-activated STAT3 is required for efficient induction of IL-10.	(Benkhart et al, 2000; Chang et al, 2009; de Waal Malefyt et al, 1991; Staples et al, 2007)

DNA methylation and chromatin remodeling	Proinflammatory cytokine (TNF-α) gene expression	Slow time scale	Sustained methylation of H3 (lys9), increased and sustained binding of RelB (as transcriptional repressor) on TNF-α promoter in tolerant THP-1 cells.	(Chen et al, 2009; El Gazzar et al, 2007)

2.8 Supporting Information

Detailed criteria for priming and tolerance in the Metropolis searching algorithm

We used the Metropolis algorithm (Metropolis et al, 1953) to search for parameter values for which the system exhibits priming or tolerance effects. Table 2.S1 gives the criteria for identifying priming or tolerance parameter sets. In general, both priming and tolerance require the system to generate a dose-response curve having the following qualitative features: small signal (LD) gives small response and large signal (HD) gives large response; priming requires that LD+HD LPS gives a larger response than does a single HD LPS (positive control); tolerance requires that HD+HD LPS gives lower response than does a single HD LPS (positive control). Parameter sets that satisfy these conditions (either for priming or for tolerance) are called "good" sets.

Two-stage Metropolis search for parameter sets that exhibit priming or tolerance

It is impractical to perform a brute force search for priming/tolerance samples in a high dimensional parameter space. Figure 2.S1A illustrates an alternative two-stage strategy. In the first stage, we searched widely over the parameter space with some bias to stay in a good

parameter region and some chance to wander off in search of another good region. Then K-means Clustering and Principal Component Analysis was applied to the samples of good parameter sets generated in stage 1 to see if the data form several separate clusters. Each potential cluster provides a random seed for a second round of Metropolis searching. This time the search is restricted to stay within a good region, in order to search each region thoroughly and to obtain a representative sample of good parameter sets.

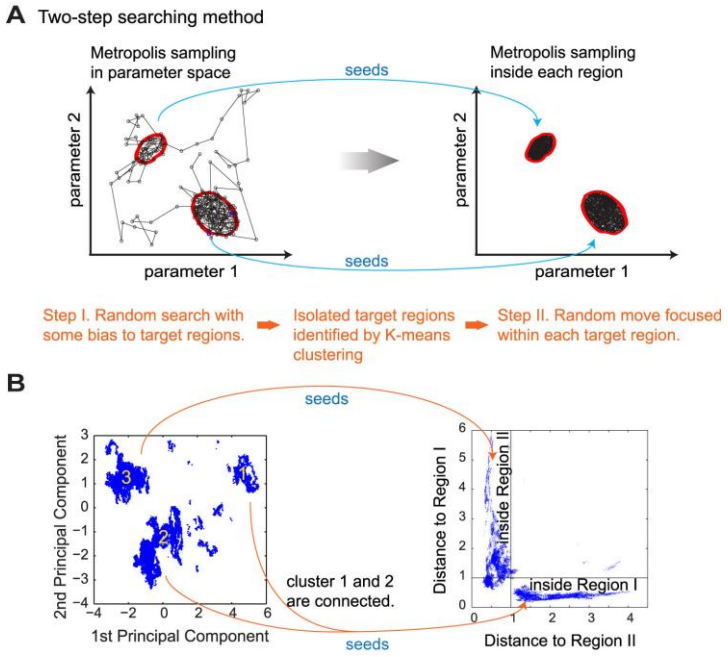

Figure 2.S1. Illustration of the two-stage Metropolis search procedure. (A) Schematic illustration of the two-stage Metropolis search method for priming/tolerance parameter sets. In the first stage one randomly searches the whole parameter space. K-means clustering algorithm identifies one or more clusters of the data. Then one performs a second Metropolis step to search thoroughly inside each cluster. (B) As a result, we got three priming set clusters with K-means clustering. By calculating the minimum volume bounding ellipsoid, we found that cluster 1 and 2 belong to a single region (Region I) whereas cluster 3 belong to a separate region (Region II).

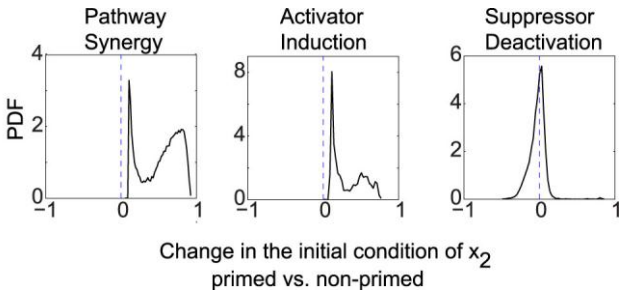

Figure 2.S2. Distribution of change in x_2's initial condition prior to HD without or without priming treatment. Both PS and AI show considerable increase in x_2 in the primed system. PDF: probability distribution function.

To apply the Metropolis Algorithm, we relate the current problem of searching in the parameter space to sampling the partition function of a pseudo-statistical physics system. The bias controlling the probability of wandering out of a good region ($\Omega_k = 0,\ \Omega_{k+1} = 1$) is defined by a Boltzmann-type expression $\rho = e^{-\beta(\Omega_{k+1}-\Omega_k)}$ where β represents an "inverse temperature" variable. There exists a trade-off value of β for the Metropolis search in stage I. If β is too large, the search will stay in a local minimum and fail to explore the parameter space thoroughly. If β is too small, the search cannot yield enough samples for the clustering analysis. Through trial and error, we found that β = 6 is a good value for the stage I Metropolis search, which gives ρ = 0.0025. Note that the priming region is very small compared to the whole parameter space. Therefore, although ρ = 0.0025 is very small, it still guarantees that the system has sufficient probability to leave the good regions and thoroughly search the parameter space.

In the above procedure, the score function Ω_k plays the role of "energy" in a physical system. In general it can be a continuous function, and its gradient can guide the Metropolis search to the

favorable region. For the current problem, the score function we use essentially behaves as a two-state system. Therefore we assign the value of Ω_k to be 0 or 1.

We chose to use the Metropolis method for the first stage, but other methods will probably work equally well, e.g. genetic algorithm (Singhania, 2011) and the methods used by Ma et al. (Ma et al, 2009) and Yao et al. (Yao et al, 2011).

Figure 2.S1B provides the result of the two-stage Metropolis search. In the left panel the priming sets obtained from the first stage form three main clusters under the K-means Clustering. For visualization purpose the clusters in the high-dimensional parameter space are plotted using the first two components of Principal Component Analysis. Using the Khachiyan Algorithm (Khachiyan, 1996), we calculated the minimal volume ellipsoid to embrace 99% of the parameter sets of each region. As shown in the right panel of Figure 2.1B which calculates the distance of a parameter set to the center of each bounding ellipsoid, it turns out that a single ellipsoid embraces clusters 1 and 2, thus forming one single region (we call it "Region I"). This result is independently confirmed with the following Metropolis simulation with ρ = 0: a trajectory starting from one cluster can generate parameter sets belonging to the other cluster. On the other hand, cluster 3 forms a separate region (Region II). Notice that a small portion of samples locate within both ellipsoids, indicating these two ellipsoids (regions) are barely connected. We found that Region II is actually (part of) the mirror image of Region I with the roles of x_1 and x_2 exchanged, reflecting the symmetry of the 3-node system. Therefore, the results discussed below and in the main text focus on the motifs found in Region I.

About 10^6 output samples are generated out of 10^8 Metropolis steps in stage 2. Of these 10^6 samples, some appear to be biologically irrelevant and are removed from the sample set. For example, in some cases $x_3(t)$ increases to a much higher level after the HD stimulation is removed, this would be a pathological response of the system. Other samples show unrealistically large sensitivity to initial conditions, i.e., although LD induced only small changes in x_1, x_2 and x_3 (less than 10%), the system still exhibited priming effect. If priming were due to such small differences, then (in our opinion) the response would not be robust to the stochastic fluctuation expected in real systems (Chang et al, 2008; Cohen et al, 2008; Sigal et al, 2006; Spencer et al, 2009).

While the results reported in the main text are from one trajectory result, the procedure was repeated several times with random initial start of the searching in stage 1. Results analyzed from different trajectories agree with each other, confirming the convergence of our two-stage Metropolis searching procedure.

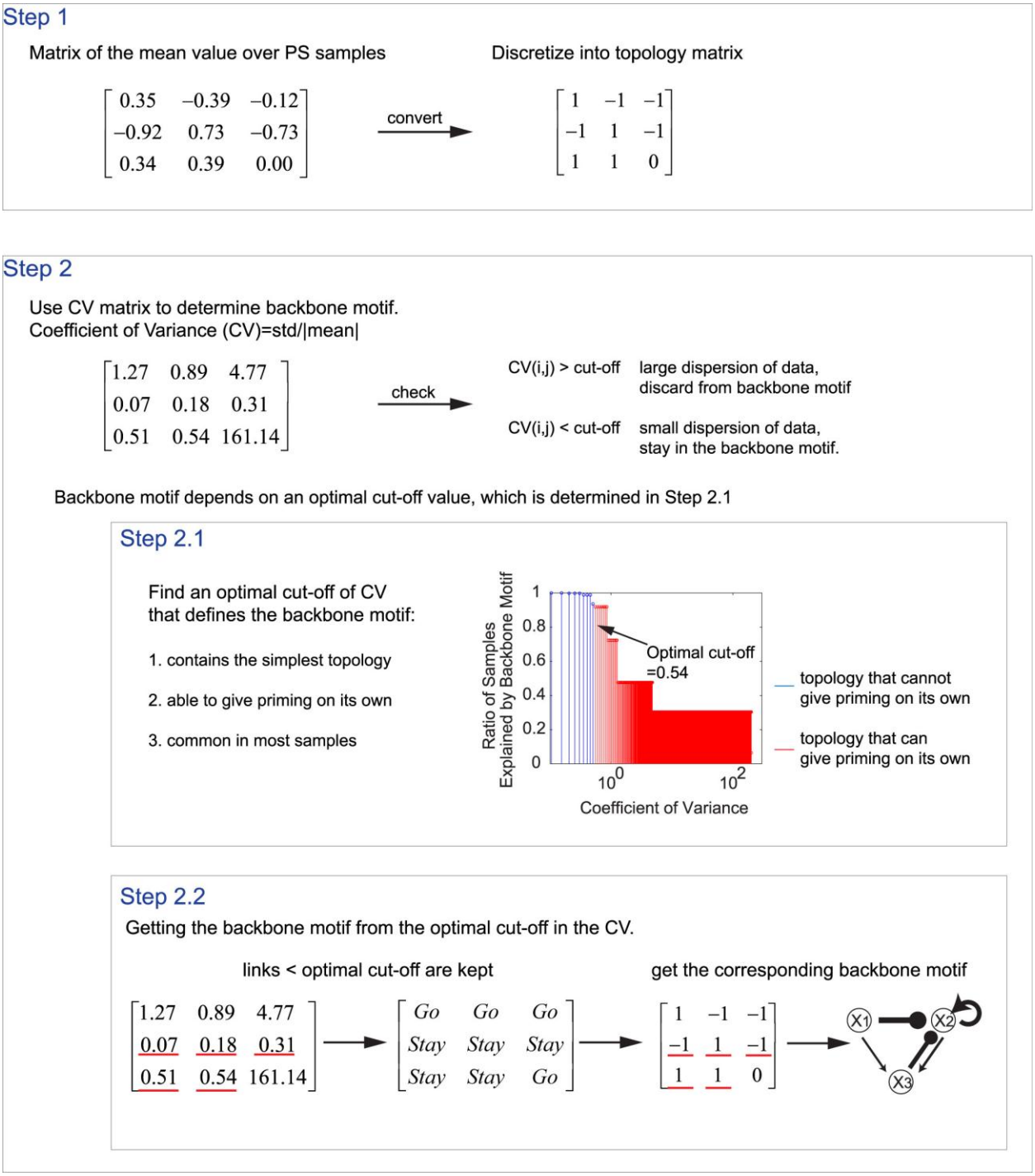

Figure 2.S3. Statistical method used to identify backbone motifs from priming/tolerance data.

Statistical method used to identify backbone motifs

A backbone motif is defined to be the simplest motif (the fewest number of non-zero ω_{ji}'s) that is shared by most of the priming/tolerance network structures in a particular region. A backbone motif must be able to generate a priming/tolerance effect by itself. Identification of backbone motifs helps to define the core mechanism of priming or tolerance. Figure 2.S3 shows the statistical method used to obtain the backbone motifs for the pathway synergy group.

Step 1: calculate the mean of each interaction coefficient ω_{ji} among all samples of the group, and map the mean values into a topological matrix τ_{ji} (see Material and methods in the main text for the method of parameter discretization).

Step 2: for each ω_{ji} calculate its coefficient of variation (CV = standard deviation divided by |mean|). The value of CV measures the dispersion of the data along each parameter dimension. A large value of CV suggests that a link is not essential and should not be part of the backbone motif. Only links with CV < *CutOff* should be part of a backbone motif. For CV > *CutOff*, $\tau_{ji} = 0$ in the backbone motif.

Step 2.1: determine the optimal value of *CutOff*. As *CutOff* decreases, the corresponding motif becomes simpler and therefore more samples contain this motif. However, the motif is a backbone motif only if it gives priming by itself. Therefore, there exists an optimal *CutOff* value so that the corresponding motif has the simplest topology that is still able to generate priming for some specific parameter sets. In this case the optimal *CutOff* = 0.54 (see the right figure in Step 2.1 of Supplement Figure 2.3).

Step 2.2: compare each dimension in the CV matrix to this optimal *CutOff* value, and obtain the corresponding backbone motif.

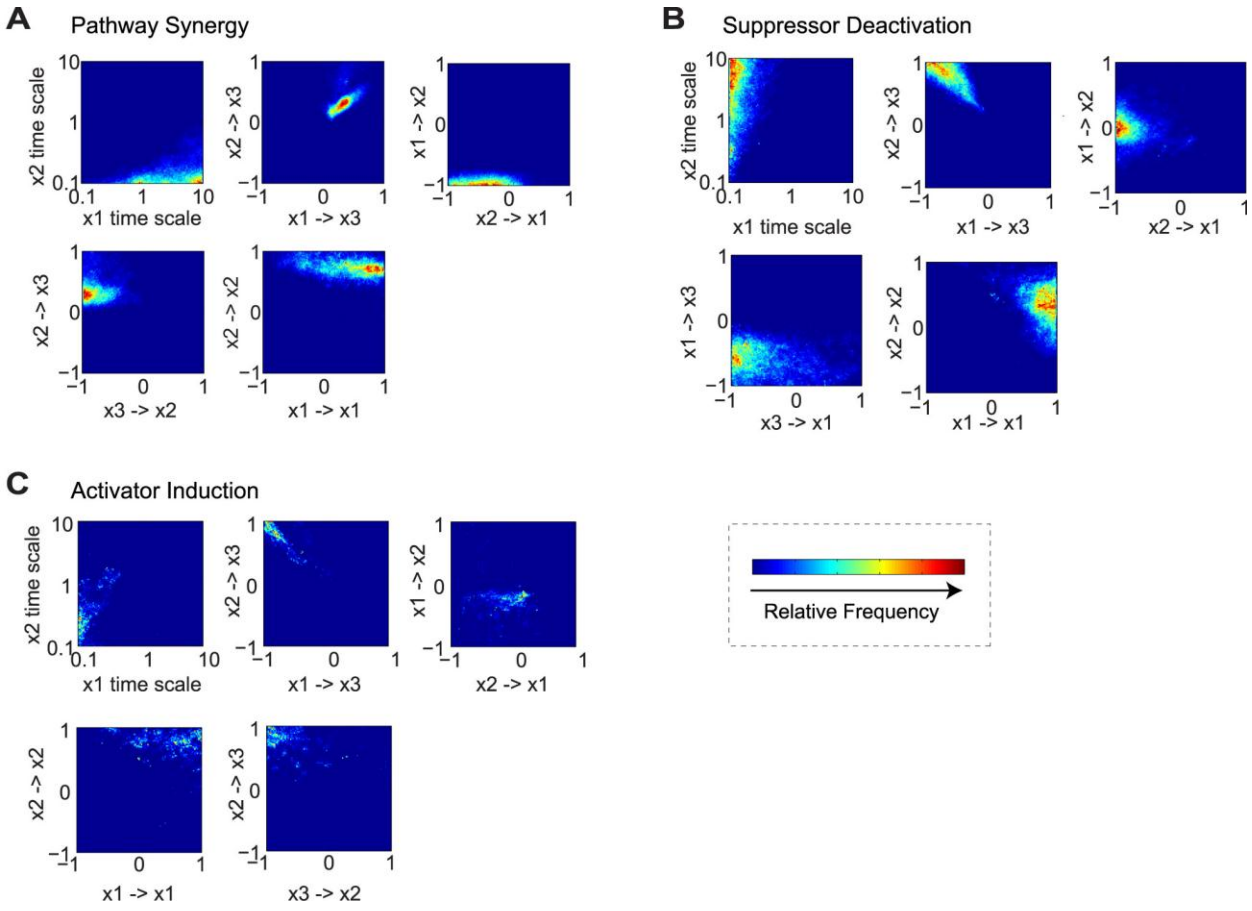

Figure 2.S4. Parameter correlations highlight the backbone motifs of each priming mechanism: (A) Pathway Synergy, (B) Suppressor Deactivation, and (C) Activator Induction.

Figure 2.S4 shows 2D histograms of parameter distributions under each priming mechanism (PS, SD and AI). These histograms clearly highlight the corresponding backbone motifs. For example, for the 2D histogram shown in Supplemental Figure 2.4A, the PS data form clusters where both x_1 and x_2 activate x_3 (2nd figure), and x_3 feeds back negatively on x_2 (4th figure). Also

x_2 shows significant auto-activation but x_1 does not (data spread out horizontally in the 5th figure); this is in line with the backbone motif where x_1 auto-regulation is not essential for priming. Similarly, x_1 exerts strong inhibition on x_2, whereas the regulation from x_2 to x_1 can be either negative, zero or positive (the 3rd figure), in line with the backbone motif where this regulation is missing. In addition, the 1st figure indicates that x_1 should change on a much faster time-scale than x_2. This is a dynamical requirement of pathway synergy in addition to the topological features as illustrated by the backbone motif.

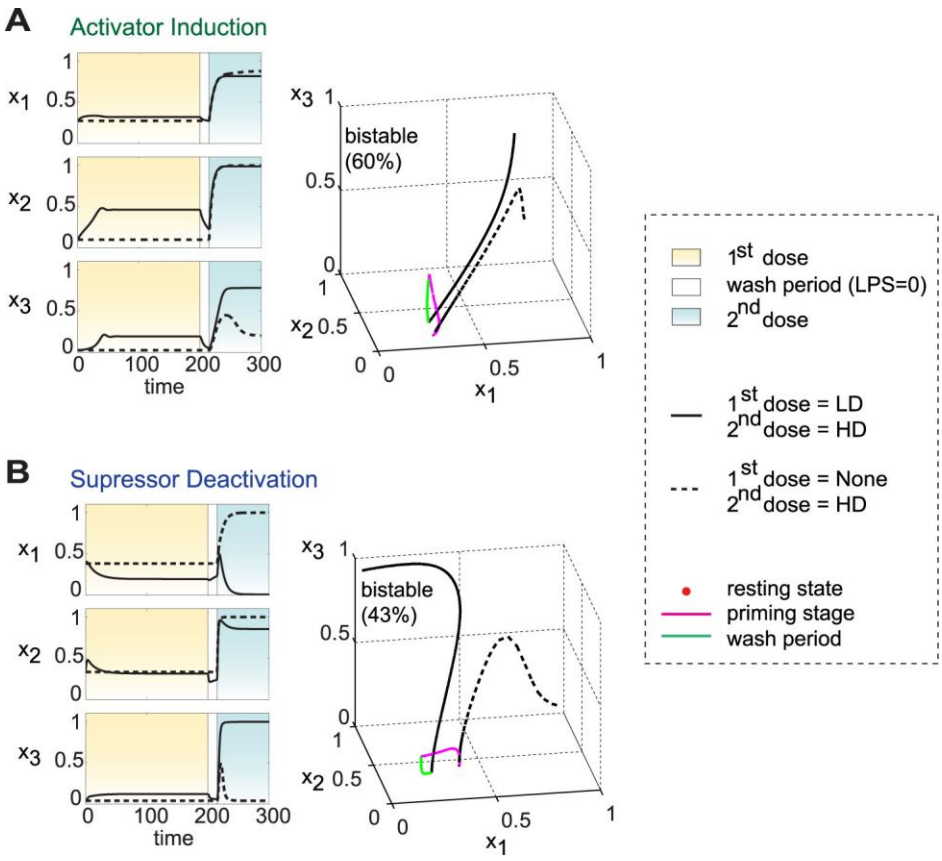

Figure 2.S5. Typical time course and corresponding trajectory in the phase space. (A) bistable case of AI mechanism. (B) bistable case of SD mechanism. Refer to Figure 2.3 of the main text for the time course trajectories in other cases.

Motif density is more robust than frequency to variation in the topological cut-off

To map from the continuous space of interaction coefficients ω_{ji} to the discrete space of network topologies τ_{ji}, one must choose a cut-off value τ_0 for mapping ω_{ji}'s to −1, 0 or +1. We have chosen this cut-off τ_0 (somewhat arbitrarily) to be 0.1. The simplest way to order these topologies from "more robust" to "less robust" is in terms of the number of parameter sets that map into each topology, i.e., the frequency of each topology in the total data set. However, we find that topology-frequency is sensitive to the choice of the cut-off value for ω_{ji}. A better measure is topology density (Figure 2.S6), defined as follows. The total volume of the 9-dimensional space of interaction coefficients is 2^9, because each ω_{ji} can continuously vary over [−1, 1]. For a motif with m non-zero τ_{ji}'s, the volume of its subspace is $(1-\tau_0)^m = (0.9)^m$. The density of the motif is defined as the number of samples corresponding to this motif divided by the volume of its subspace.

In Figure 2.S6 we compared the two ways of ordering the topologies using the SD data set as an example. The figure shows how the rank of robustness of each topology changes due to 10%, 30% and 50% positive or negative variations from the original cut-off $\tau_0 = 0.1$. A point on the figure with coordinate (x, y) means that the rank of a given topology is x with $\tau_0 = 0.1$, but y with the varied τ_0. Scattering from the diagonal indicates changing of the ranking due to τ_0 variation. The density-sorted rank (top panel) is less sensitive than the frequency-sorted one (lower panel) to the change of τ_0.

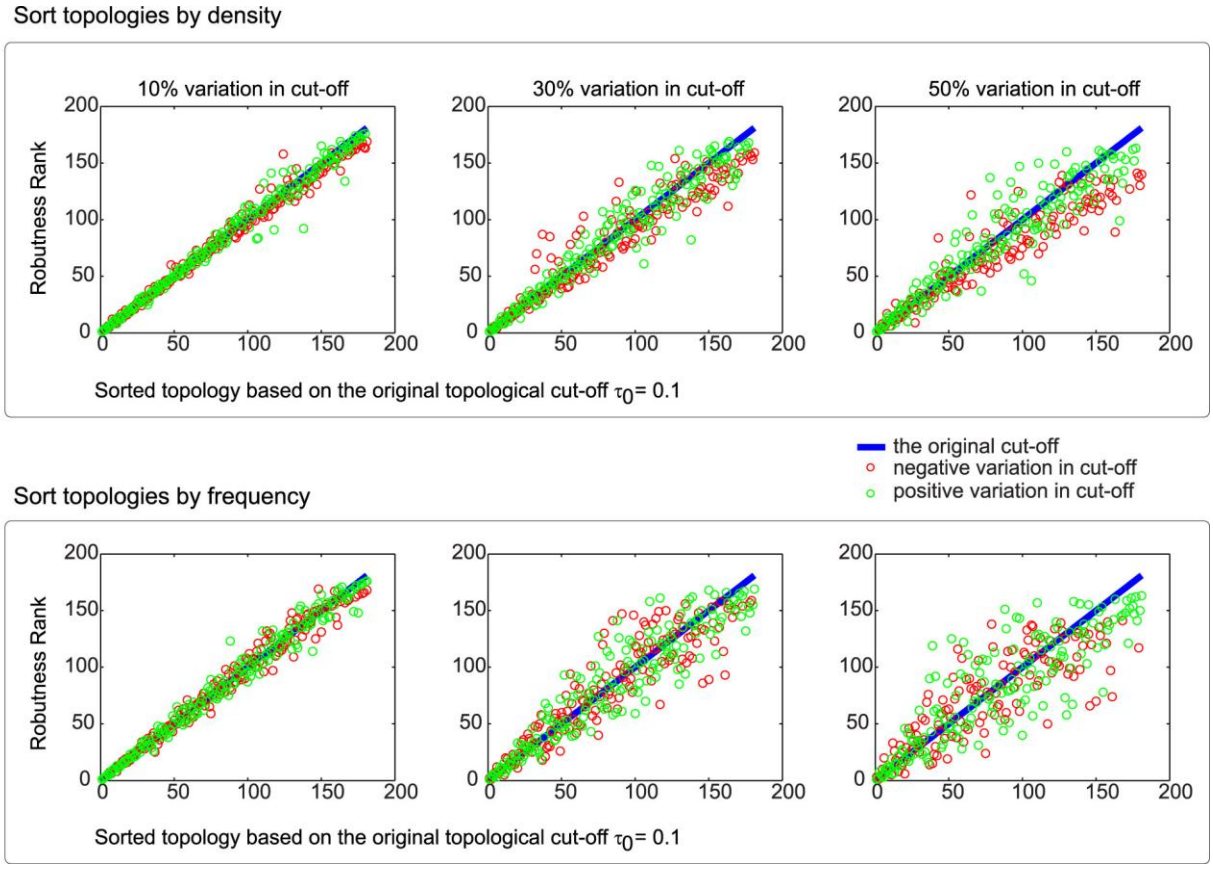

Figure 2.S6. Change in the robustness rank as a result of variations in the topology cut-off. SD datasets are used as an example. The robustness rank is calculated based on density (top panel) or sample frequency (lower panel) of the unique topologies. Changes in the robustness rank is compared with 10% (left column), 30% (center column), and 50% (right column) variation in the topology cut-off τ_0=0.1.

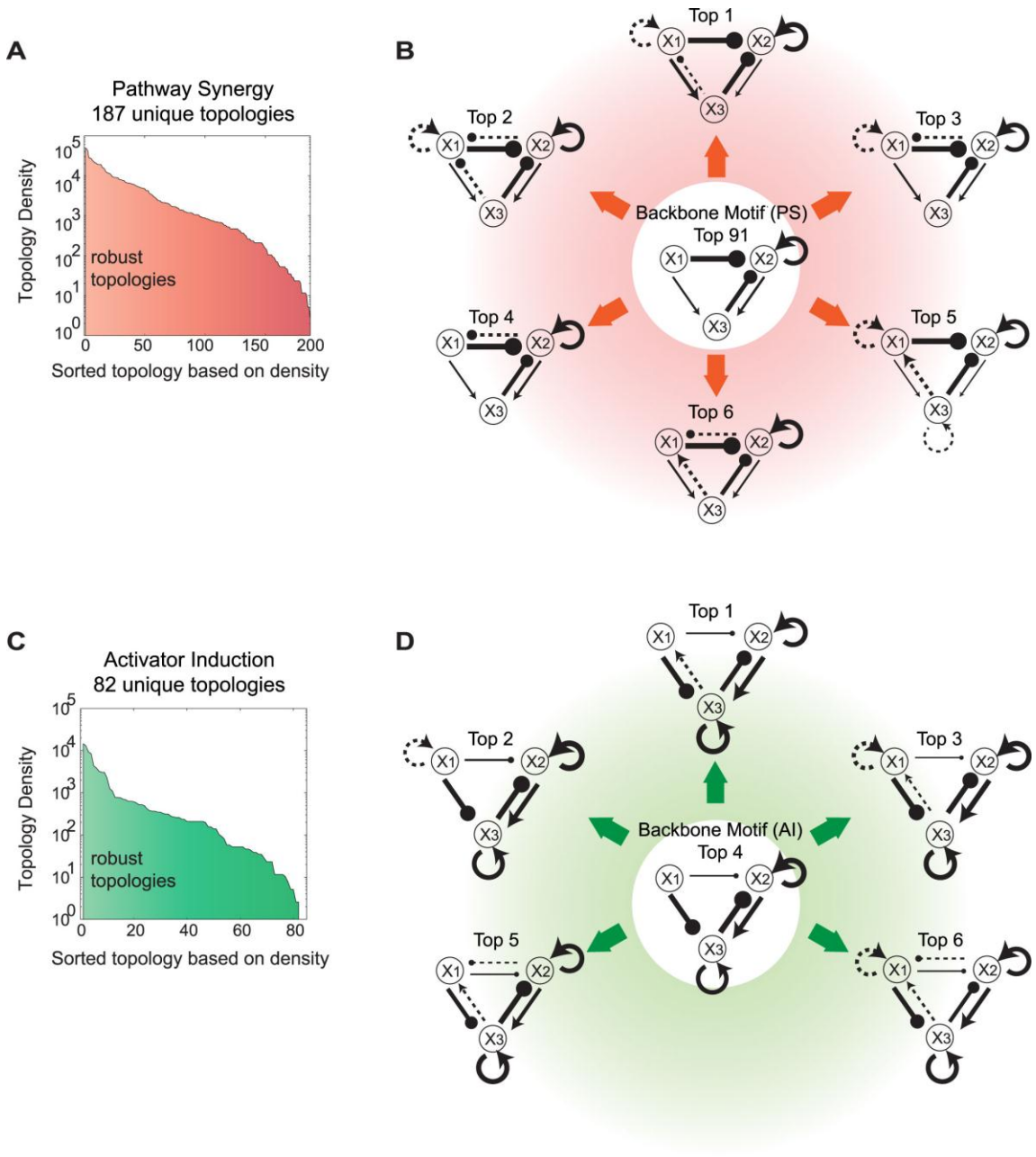

Figure 2.S7. Topologies of PS and AI mechanisms. (A) The topology density distribution for the PS mechanism. (B) Top six PS topologies and the backbone motif. (C) The topology density distribution for the AI mechanism. (D) Top six AI topologies and the backbone motif. Line widths are proportional to the mean value of samples of the corresponding topology. Dashed lines denote the additional links present in the top topologies but absent in the backbone motif.

2D parameter correlations demonstrate how parameter compensation affects topological robustness

We calculated the correlation matrix of each priming mechanism from the corresponding samples. As can be seen from Figure 2.S8A, some parameters show strong anti-correlations. For a pair of anti-correlated parameters, increasing one can be compensated by decreasing the other (or negatively increasing the other if the regulation is inhibition), so the overall dynamics remains (approximately) the same. This is because in the modeling equations,

$$\frac{dx_j(t)}{dt} = \gamma_j\left(\frac{1}{1+e^{-\sigma_j W_j}} - x_j(t)\right)$$

$$W_j = \sum_{i=1}^{3} \omega_{ji} x_i(t) + \omega_{j0} + S_j$$

the activation of species x_j is dependent on the overall net input W_j. As W_j sums inputs from all regulating nodes, a change in one parameter (e.g. ω_{j1}) can be compensated by a change in a second parameter (e.g. ω_{j2}) if the sum stays the same. Such parameter compensation expands the region of parameter space where priming or tolerance is observed and therefore affects the robustness of the model.

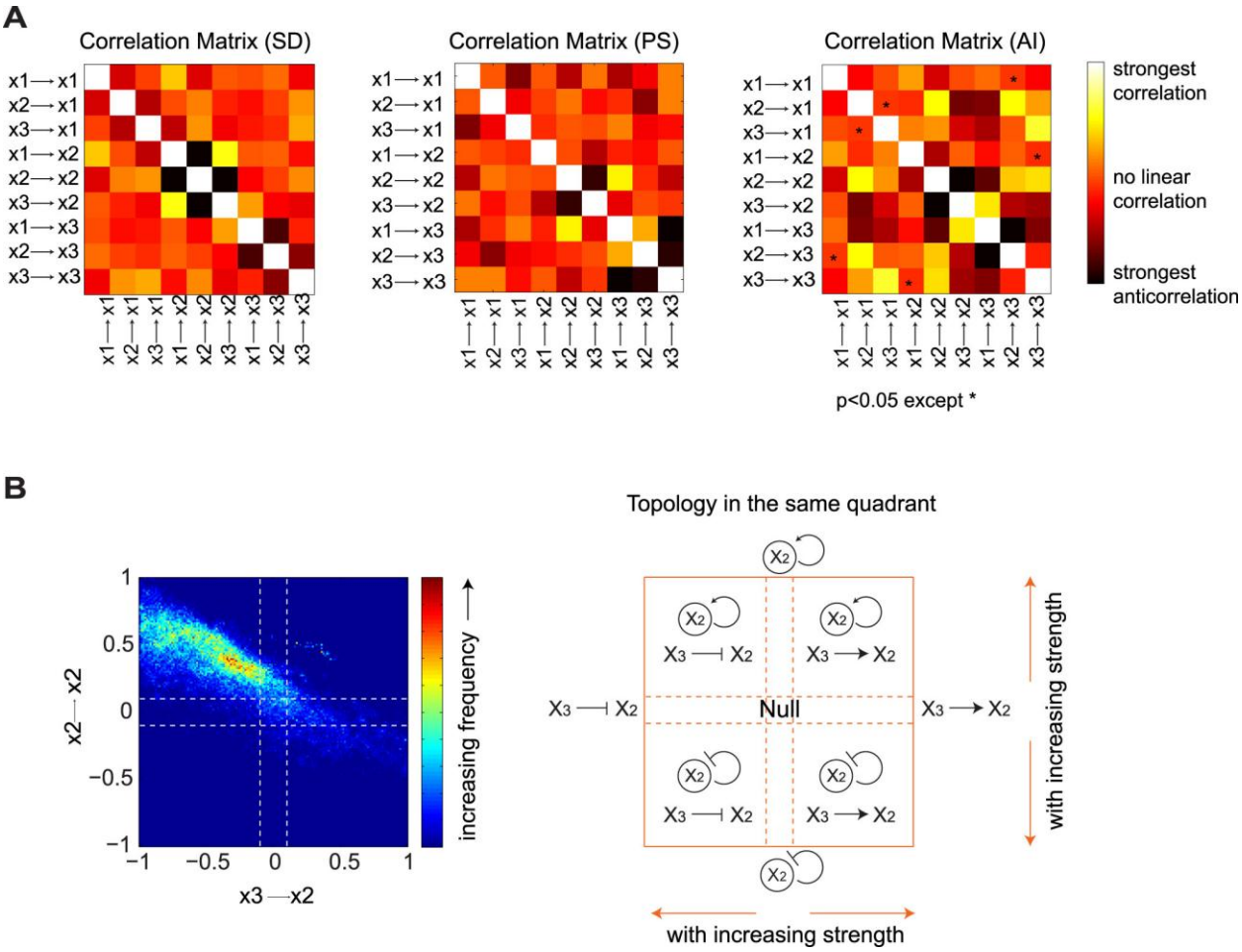

Figure 2.S8. Parameter correlation and compensation affects the robustness of the model. A) Correlation matrix calculated based on the samples of each priming mechanism. The *p*-value is smaller than 0.05 except where marked. B) The parameter compensation mechanism is illustrated by the 2D correlation histogram of the SD samples (left) and the corresponding connection diagrams (right).

For example, the left panel of Figure 2.S8B shows that the feedback from x_3 to x_2 strongly anti-correlated with x_2's auto-regulation among SD datasets. With $\omega_{23} = 0$, the absolute value of ω_{22} needs to be also small (the Null region in the right panel of Figure 2.S8B), otherwise priming is abolished. However, since ω_{23} and ω_{22} are anti-correlated, the effect of an increasing ω_{22} can be

canceled off by increasing ω_{23}, thus expand the priming region in the parameter space (the upper left and bottom right regions of the right panel of Figure 2.S8B).

Supporting References

Chang HH, Hemberg M, Barahona M, Ingber DE, Huang S (2008) Transcriptome-wide noise controls lineage choice in mammalian progenitor cells. *Nature* **453:** 544-547

Cohen AA, Geva-Zatorsky N, Eden E, Frenkel-Morgenstern M, Issaeva I, Sigal A, Milo R, Cohen-Saidon C, Liron Y, Kam Z, Cohen L, Danon T, Perzov N, Alon U (2008) Dynamic proteomics of individual cancer cells in response to a drug. *Science* **322:** 1511-1516

Khachiyan LG (1996) Rounding of Polytopes in the Real Number Model of Computation. *Math Oper Res* **21:** 307-320

Ma W, Trusina A, El-Samad H, Lim WA, Tang C (2009) Defining Network Topologies that Can Achieve Biochemical Adaptation. *Cell* **138:** 760-773

Metropolis N, Rosenbluth AW, Rosenbluth MN, Teller AH (1953) Equation of State Calculations by Fast Computing Machines. *The Journal of chemical physics* **21:** 1087

Sigal A, Milo R, Cohen A, Geva-Zatorsky N, Klein Y, Liron Y, Rosenfeld N, Danon T, Perzov N, Alon U (2006) Variability and memory of protein levels in human cells. *Nature* **444:** 643-646

Singhania R (2011) Modeling Protein Regulatory Networks that Control Mammalian Cell Cycle Progression and that Exhibit Near-Perfect Adaptive Responses. Virginia Polytechnic Institute and State University, Blacksburg, Va: University Libraries

Spencer SL, Gaudet S, Albeck JG, Burke JM, Sorger PK (2009) Non-genetic origins of cell-to-cell variability in TRAIL-induced apoptosis. *Nature* **459:** 428-432

Yao G, Tan CM, West M, Nevins JR, You LC (2011) Origin of bistability underlying mammalian cell cycle entry. *Mol Sys Biol* **7:** 485

Table 2.S1. Criteria identifying priming and tolerance for a given parameter set *x*.

A Good set of	**Single LD**	**Single HD**	**LD+HD**	**HD+HD**
Priming	$R_{LD}(x) < \delta_{LD}$	$R_{HD}(x) \geq \delta_{HD}$	$R_{LD+HD}(x)/R_{HD}(x) \geq \lambda$	-
Tolerance	$R_{LD}(x) < \delta_{LD}$	$R_{HD}(x) \geq \delta_{HD}$	-	$R_{HD}(x)/R_{HD+HD}(x) \geq \lambda$
Description	LD signal stimulates small response.	HD signal stimulates large response.	Two sequential signals (LD followed by HD) gives a larger response than a single HD.	Two sequential signals (HD followed by HD) gives a smaller response than a single HD.

R denotes the maximum response of "cytokine" x_3 under a specific stimulation protocol. LD: low dose; HD: high dose; LD+HD: LD followed by HD with maximum response measured in the HD period; HD+HD: HD followed by HD with maximum response measured in the second HD period. δ_{LD} and δ_{HD} denote the threshold of response under LD and HD, respectively. $\lambda > 1$ is the threshold of fold-change in the maximum response. The values we have chosen for these parameters (LD=0.1, HD=1, $\delta_{LD}=\delta_{HD}=0.3$, $\lambda=1.5$) are in qualitative agreement with experimental observations.

Table 2.S2. Parameter sets used to generate time course and phase-space trajectory in Figure 2.3 and Figure 2.S5.

	PS	**PS**	**AI**	**AI**	**PS**	**PS**
	bistable	monostable	bistable	monostable	bistable	monostable
ω_{11}	0.26	0.19	-0.54	0	0.86	0.84
ω_{12}	-0.92	-0.27	0.05	-0.11	-0.78	-0.90
ω_{13}	0.61	0.23	-0.24	0.04	-0.86	-0.36
ω_{21}	-0.95	-0.93	-0.61	-0.52	0.36	0.08
ω_{22}	0.53	0.54	0.99	0.95	0.06	0.16
ω_{23}	-0.54	-0.35	-0.69	-0.89	-0.53	-0.45
ω_{31}	0.18	0.18	-0.80	-0.75	-0.96	-0.85
ω_{32}	0.47	0.27	0.83	0.82	0.89	0.93
ω_{33}	0.12	0.40	0.69	0.77	0.61	0.54
γ_1	1.56	0.43	0.10	0.11	0.14	0.15
γ_2	0.11	0.11	0.19	0.16	0.76	9.96
γ_3	1.00	1.00	1.00	1.00	1.00	1.00
σ_1	6.84	8.00	4.36	4.37	7.96	5.36
σ_2	7.19	8.00	6.55	6.89	6.33	5.50
σ_3	6.00	8.00	6.00	6.00	6.00	6.00
ω_{10}	-0.75	-0.50	-0.07	-0.22	-0.10	-0.15
ω_{20}	-0.25	-0.25	-0.25	-0.25	-0.25	-0.25
ω_{30}	-0.50	-0.50	-0.50	-0.50	-0.50	-0.50

Table 2.S3. Experimental literature supporting the network details in Figure 2.8.

Figure 2.8 Panel	**Source**	**Target**	**Regulatory Type**	**Reference**	**Comment**
A	TLR4	IRAK	Activation	(Hacker & Karin, 2006; O'Neill et al, 2003)	
A	IRAK	P38	Activation	(Akira & Takeda, 2004; Koziczak-Holbro et al, 2007)	
A	P38	IL-10	Transcription	(De et al, 2000)	
A	IL-10	IL-12	inhibition	(Sica et al, 2000; Uyemura et al, 1996)	
A	IL-10	TNFα	inhibition	(Fiorentino et al, 1991;	

				Shnyra et al, 1998)	
A	IRAK	AP-1	Activation	(Thompson & Locarnini, 2007)	
A	AP-1	IL-12	Transcription	(Ma et al, 2004; Matsumoto et al, 2004)	
A	IL-12	TNFα	Transcription	(Jana et al, 2003; Shnyra et al, 1998)	
A	TNFα	TNFα	Positive auto-regulation involving an autocrine loop	(Spriggs et al, 1987)	
A	IL-12	IL-12	Positive auto-regulation involving an autocrine loop	(Grohmann et al, 2001)	IL-12 auto-regulates itself through Jak/Stat pathway with STAT4 being the major transcription factor.
A	TNFα	IL-12	inhibition	(Hodge-	TNFα inhibits IL-12p40

				Dufour et al, 1998; Zakharova & Ziegler, 2005)	through TNFα signaling pathway.
B	IRAK4	IKK	Activation	(Hacker & Karin, 2006)	
B	IKK	NFκB	Activation	(Hacker & Karin, 2006)	
B	NFκB	ATF3	Transcription	(Kawai & Akira, 2010)	
B	ATF3	C/EBPδ	Inhibition	(Gilchrist et al, 2006; Litvak et al, 2009)	
B	NFκB	IL-6	Transcription	(Litvak et al, 2009)	
B	IRAK1	IKKε	Activation	(Maitra et al, 2011)	
B	IKKε	C/EBPδ	Activation	(Maitra et	Low dose LPS induces the

				al, 2011)	expression of C/EBPδ through IRAK1 and IKKε.
B	C/EBPδ	C/EBPδ	Transcription	(Litvak et al, 2009)	C/EBPδ can bind onto its own promoter to enhance the transcription.
B	C/EBPδ	IL-6	Transcription	(Litvak et al, 2009)	
C	IFNγ	STAT1	Transcription	(Hu et al, 2002)	Low dose IFNγ elevates STAT1 transcription, but not STAT1 phosphorylation.
C	IFNγ	P-STAT1	Activation	(Hu et al, 2002)	Phosphorylation of STAT1 is activated only under high dose IFNγ.
C	P-STAT1	SOCS1	Transcription	(Hu et al, 2002)	
C	SOCS1	P-STAT1	Inhibit	(Hu et al, 2002)	SOCS1 inhibits the phosphorylation and activation of STAT1.
C	P-STAT1	IRF-1, IP-10	Transcription	(Hu et al, 2002)	
C	P-STAT1	TNFα	Transcription	(Kalliolias & Ivashkiv,	P-STAT1 may synergistically cooperate

				2008)	with NFκB to activate the transcription of TNFα.
C	TNFα	SOCS1	Transcription	(Federici et al, 2002)	TNFα might be able to negatively feedback on P-STAT1 through enhancing the production of SOCS1.

Table 2.S3 References

Akira S, Takeda K (2004) Toll-like receptor signalling. *Nat Rev Immunol* **4:** 499-511

De AK, Kodys KM, Yeh BS, Miller-Graziano C (2000) Exaggerated Human Monocyte IL-10 Concomitant to Minimal TNF-α Induction by Heat-Shock Protein 27 (Hsp27) Suggests Hsp27 Is Primarily an Antiinflammatory Stimulus. *J Immunol* **165:** 3951-3958

Federici M, Giustizieri ML, Scarponi C, Girolomoni G, Albanesi C (2002) Impaired IFN-γ-Dependent Inflammatory Responses in Human Keratinocytes Overexpressing the Suppressor of Cytokine Signaling 1. *J Immunol* **169:** 434-442

Fiorentino D, Zlotnik A, Mosmann T, Howard M, O'Garra A (1991) IL-10 inhibits cytokine production by activated macrophages. *J Immunol* **147:** 3815-3822

Gilchrist M, Thorsson V, Li B, Rust AG, Korb M, Kennedy K, Hai T, Bolouri H, Aderem A (2006) Systems biology approaches identify ATF3 as a negative regulator of Toll-like receptor 4. *Nature* **441:** 173-178

Grohmann U, Belladonna ML, Vacca C, Bianchi R, Fallarino F, Orabona C, Fioretti MC, Puccetti P (2001) Positive Regulatory Role of IL-12 in Macrophages and Modulation by IFN-γ. *J Immunol* **167:** 221-227

Hacker H, Karin M (2006) Regulation and function of IKK and IKK-related kinases. *Sci STKE* **2006:** re13

Hodge-Dufour J, Marino MW, Horton MR, Jungbluth A, Burdick MD, Strieter RM, Noble PW, Hunter CA, Puré E (1998) Inhibition of interferon γ induced interleukin 12 production: A potential mechanism for the anti-inflammatory activities of tumor necrosis factor. *P Natl Acad Sci USA* **95:** 13806-13811

Hu X, Herrero C, Li W-P, Antoniv TT, Falck-Pedersen E, Koch AE, Woods JM, Haines GK, Ivashkiv LB (2002) Sensitization of IFN-[gamma] Jak-STAT signaling during macrophage activation. *Nat Immunol* **3:** 859-866

Jana M, Dasgupta S, Saha RN, Liu X, Pahan K (2003) Induction of tumor necrosis factor-α (TNF-α) by interleukin-12 p40 monomer and homodimer in microglia and macrophages. *J Neurochem* **86:** 519-528

Kalliolias GD, Ivashkiv LB (2008) IL-27 Activates Human Monocytes via STAT1 and Suppresses IL-10 Production but the Inflammatory Functions of IL-27 Are Abrogated by TLRs and p38. *J Immunol* **180:** 6325-6333

Kawai T, Akira S (2010) The role of pattern-recognition receptors in innate immunity: update on Toll-like receptors. *Nat Immunol* **11:** 373-384

Koziczak-Holbro M, Joyce C, Glück A, Kinzel B, Müller M, Tschopp C, Mathison JC, Davis CN, Gram H (2007) IRAK-4 Kinase Activity Is Required for Interleukin-1 (IL-1) Receptor- and Toll-like Receptor 7-mediated Signaling and Gene Expression. *J Biol Chem* **282:** 13552-13560

Litvak V, Ramsey SA, Rust AG, Zak DE, Kennedy KA, Lampano AE, Nykter M, Shmulevich I, Aderem A (2009) Function of C/EBP delta in a regulatory circuit that discriminates between transient and persistent TLR4-induced signals. *Nat Immunol* **10:** 437-443

Ma W, Gee K, Lim W, Chambers K, Angel JB, Kozlowski M, Kumar A (2004) Dexamethasone Inhibits IL-12p40 Production in Lipopolysaccharide-Stimulated Human Monocytic Cells by Down-Regulating the Activity of c-Jun N-Terminal Kinase, the Activation Protein-1, and NF-κB Transcription Factors. *J Immunol* **172:** 318-330

Maitra U, Gan L, Chang S, Li L (2011) Low-Dose Endotoxin Induces Inflammation by Selectively Removing Nuclear Receptors and Activating CCAAT/Enhancer-Binding Protein δ. *The Journal of Immunology* **186:** 4467-4473

Matsumoto M, Einhaus D, Gold ES, Aderem A (2004) Simvastatin Augments Lipopolysaccharide-Induced Proinflammatory Responses in Macrophages by Differential Regulation of the c-Fos and c-Jun Transcription Factors. *J Immunol* **172:** 7377-7384

O'Neill LAJ, Dunne A, Edjeback M, Gray P, Jefferies C, Wietek C (2003) Mal and MyD88: adapter proteins involved in signal transduction by Toll-like receptors. *J of Endotoxin Res* **9:** 55-59

Shnyra A, Brewington R, Alipio A, Amura C, Morrison DC (1998) Reprogramming of lipopolysaccharide-primed macrophages is controlled by a counterbalanced production of IL-10 and IL-12. *J Immunol* **160:** 3729-3736

Sica A, Saccani A, Bottazzi B, Polentarutti N, Vecchi A, Damme JV, Mantovani A (2000) Autocrine Production of IL-10 Mediates Defective IL-12 Production and NF-κB Activation in Tumor-Associated Macrophages. *J Immunol* **164:** 762-767

Spriggs D, Imamura K, Rodriguez C, Horiguchi J, Kufe DW (1987) Induction of tumor necrosis factor expression and resistance in a human breast tumor cell line. *P Natl Acad Sci USA* **84:** 6563-6566

Thompson AJV, Locarnini SA (2007) Toll-like receptors, RIG-I-like RNA helicases and the antiviral innate immune response. *Immunol Cell Biol* **85:** 435-445

Uyemura K, Demer LL, Castle SC, Jullien D, Berliner JA, Gately MK, Warrier RR, Pham N, Fogelman AM, Modlin RL (1996) Cross-regulatory roles of interleukin (IL)-12 and IL-10 in atherosclerosis. *J Clin Invest* **97:** 2130-2138

Zakharova M, Ziegler HK (2005) Paradoxical Anti-Inflammatory Actions of TNF-α: Inhibition of IL-12 and IL-23 via TNF Receptor 1 in Macrophages and Dendritic Cells. *J Immunol* **175:** 5024-5033

Chapter 3. Resonant activation: a strategy against bacterial persistence

Yan Fu[1,2], Meng Zhu[3], Jianhua Xing[2,*]

[1]Interdisciplinary Program of Genetics, Bioinformatics, and Computational Biology,

[2]Department of Biological Sciences, Virginia Polytechnic Institute and State University, Blacksburg, VA 24060

[3]School of Computing, Clemson University, Clemson, SC 29631

* Corresponding author: jxing@vt.edu

3.1 Abstract

A bacterial colony may develop a small number of cells genetically identical to, but phenotypically different from other normally growing bacteria. These so-called persister cells keep themselves in a dormant state and thus are insensitive to antibiotic treatment, resulting in serious problems of drug resistance. In this paper, we proposed a novel strategy to "kill" persister cells by triggering them to switch, in a fast and synchronized way, into normally growing cells that are susceptible to antibiotics. The strategy is based on resonant activation (RA), a well-studied phenomenon in physics where the internal noise of a system can constructively facilitate fast and synchronized barrier crossings. Through stochastic Gilliespie simulation with a generic toggle switch model, we demonstrated that RA exists in the phenotypic switching of a single bacterium. Further, by coupling single cell level and population level simulations, we showed that with RA, one can greatly reduce the time and total amount of antibiotics needed to sterilize a

bacterial population. We suggest that resonant activation is a general phenomenon in phenotypic transition, and can find other applications such as cancer therapy.

3.2 Introduction

Noise has often been viewed as a nuisance for many years in biology. Robustness of large biological systems requires noise from both intracelluar and intercelluar sources being canceled or filtered in one way or another. Yet growing evidence indicates that noise actually plays fundamental roles in many biological processes, as in cell fate decision and in mutation and evolution (Rao et al, 2002). In this paper, we suggest that the functional role of noise can go even beyond: the internal noise in bacterial gene expression can be utilized to counteract antibiotic resistance, by inducing resonant activation that can facilitate a fast and synchronized phenotypic switching in bacteria population.

Antibiotic resistance is a severe and growing problem in clinical practice. It refers to a phenomenon that certain phenotypes of microorganisms, e.g. bacteria, are able to withstand (and requires prolonged) antibiotic treatment. It may be acquired from horizontal gene transfer and mutations in the pathogenic chromosome(Cirz et al, 2005; Miller et al, 2004; Ochman et al, 2000), or from the existence of phenotypic heterogeneity within bacteria population(Balaban et al, 2004; Gefen & Balaban, 2009; Levin & Rozen, 2006). The latter links antibiotic resistance to a special bacterial phenotype called persister cell, a non-growing (or slowly growing) and non-inherited cell phenotype whose number only accounts for a small fraction of total population.

Persister cells are genetically homogeneous to normally growing cells. They are first discovered by Bigger(Bigger, 1944) and then found in higher-percentage in biofilms that are known to be responsible for a majority of recalcitrant infections such as tuberculosis(Ojha et al, 2008; Stewart et al, 2003). Several experimental and theoretical works suggested their formation during mid-exponential phase, as well as their function as an "insurance" to maximize the overall survival probability of bacterial population in changing environments(Balaban et al, 2004; Keren et al, 2004a; Kussell et al, 2005; Lou et al, 2008). The magic is that persister cells have negligible growth rate and non-negligible phenotypic switching rate. The negligible growth rate helps persister cells dodging antibiotic attack that depends mostly on active cell wall growth. The non-negligible phenotypic switching rate, on the other hand, ensures finite probability of stochastic switching from persister cells to normally growing cells taking place at a period that the stress (e.g., antibiotics) is removed. Then those newly formed normal cells serve as the "seeds" for reestablishing the population. Therefore, Kussell et al. proposed the phenotypic switching rate can be seen as a result of evolutionary adaptation of bacteria to their real fluctuating environment(Kussell et al, 2005).

The ubiquity of persister cells makes bacteria population hard to sterilize. The time-series of the survival fraction under antibiotic treatment obeys a two-phase exponential decay, with the majority of cells being killed at a fast rate at the beginning while the rest being killed much slowly afterwards. *hipA7*, a mutant strain of *E.coli* that contains higher percentage (10^{-5}~10^{-2}) of persister cells, has been reported survival in a fraction about 10^{-5} even after continuous ampicillin treatment for 50 h (Balaban et al, 2004). Therefore, it is of concern how to efficiently sterilize bacteria populations, especially for strains with more fractions of persister cells. In 2008,

Gefen et al. observed that persister cells of *hipA7* assume normal growth during the first 1.5 h on exiting the stationary phase(Gefen et al, 2008). While applying ampicillin within that time window, the number of persister cells can be lowered by 1 order of magnitude. However, those still alive may adopt dormancy after that time window, and can convert to normally growing phenotype and re-grow to a new population under appropriate conditions. The essential problem here is that well-established persister cells are insensitive to antibiotics. They have to be converted into normally growing cells to get sterilized by drugs. However this transition is stochastic and may take a long time. For *hipA7*, the transition rate is $1/0.07\ h^{-1}$, which gives an exponential waiting time distribution with the average waiting time of conversion ~ 14 h. For some species, e.g. the *E coli* mutant *hipQ*, the rate can be much smaller. Therefore, bacteria sterilization requires continuous antibiotics application at least to cover this broad range of time, which may be impractical and/or detrimental to the host.

Several toxin-antitoxin (TA) modules in bacterial chromosome have been experimentally identified to regulate bacterial phenotypic transitions, though detailed mechanism has not been clearly understood (Christensen et al, 2003; Gefen & Balaban, 2009; Pedersen et al, 2002). Irrespective of the details, the basic mechanism is simple: a mutual inhibition exists between antitoxin's and cognate toxin's expression, which determines whether a single bacterium assumes normally growing phenotype (when antitoxin dominates) or persister phenotype (when toxin dominates). Therefore bistability is the major dynamical property of single cell's phenotypic transition(Lou et al, 2008). In this theoretical investigation we used the well-studied generic toggle switch to model this bistable system, Figure 3.1 (a).

Making analogy between biological networks and other familiar physical systems has led to several insightful studies (Walczak et al, 2005; Wang et al, 2006; Zhu et al, 2004). In this work we focused on resonant activation (RA), a well-studied phenomenon for thermally activated barrier-crossing systems (Doering & Gadoua, 1992; Marchi et al, 1996; Schmitt et al, 2006). If the barrier is under time varying periodic perturbation, "cooperative interplay between the barrier modulation process and thermal noise assisting barrier crossing events can cause an enhancement of the reaction kinetics" (Schmitt et al, 2006). The mean first passage time (MFPT), which is the average time the system waits for the first successful barrier crossing, reaches its minimum (by several folds or even orders of magnitude compared with that of the unperturbed system) at the resonance frequency of the perturbation. Under resonance frequency ω_c with period $T_{\omega_c} = 2\pi / \omega_c$, the system prefers to make a transition when the barrier height reaches its minimum. Consequently, the FPT distribution displays a series of peaks at odd multiples of $T_{\omega_c} / 2$, instead of a continuous exponential distribution. RA is related but different from another well studied phenomenon, stochastic resonance (SR) (Gammaitoni et al, 1998; Schmitt et al, 2006). SR focuses on synchronizing the transitions between two states by the external periodic signal with matching frequency, so it helps the system to pick up the signal from the stochastic background noise. RA emphasizes that the average time of the transition from one state to another reaches a minimum by the external modulation. To understand the latter intuitively, consider a barrier crossing system with the barrier height itself varies with time. If the barrier fluctuation is very fast compared to the mean time between two transitions, the system only experiences an averaged potential barrier; if the fluctuation is very slow compared to the mean transition time, the transition dynamics is simply a weighted average of the dynamics with

different barrier heights; RA suggests that the mean transition time reaches a minimum at some intermediate barrier fluctuation time scale.

Complementary to current efforts of searching for more efficient antibiotics, in this work we proposed to utilize the phenomenon of resonant activation to help fighting drug resistance. Noticing the similarity between thermally activated barrier crossing and cell phenotypic transition, we will first use a genetic toggle switch model to demonstrate that resonant activation exists for biological network dynamics. Then we will examine how one can shorten the time and the amount of antibiotics needed to extinct a bacteria population using resonant activation. Our strategy utilizes the two characters of RA: accelerated kinetics, and multi-peaked FPT distributions.

3.3 Model and Method

Single cell level

Currently the exact regulation mechanism for the persister-normal cell transition is not clear, and different hypotheses have been raised to give possible answers (Gefen & Balaban, 2009). For our purpose of illustrating the idea, we will use a generic toggle switch to represent the mutual inhibition within T-A module. As shown in Figure 3.1 (a), the network contains two genes mutually inhibiting each other through their dimerized protein products. The two types of protein dimers compete for the promoter binding site. Ten chemical reactions shown below control the dynamics of the generic toggle switch shown in Figure 3.1 (a):

$$
\begin{array}{llll}
O \to O + A & (k_1^0), & O \to O + B & (k_2^0) \\
A \to \phi & (k_3^0), & B \to \phi & (k_4^0) \\
A + A \rightleftarrows A_2 & (k_5, k_{-5}), & B + B \rightleftarrows B_2 & (k_6, k_{-6}) \\
O + A_2 \rightleftarrows OA_2 & (k_7, k_{-7}), & O + B_2 \rightleftarrows OB_2 & (k_8, k_{-8}) \\
OA_2 \to OA_2 + A\ (k_9), & & OB_2 \to OB_2 + B & (k_{10})
\end{array}
$$

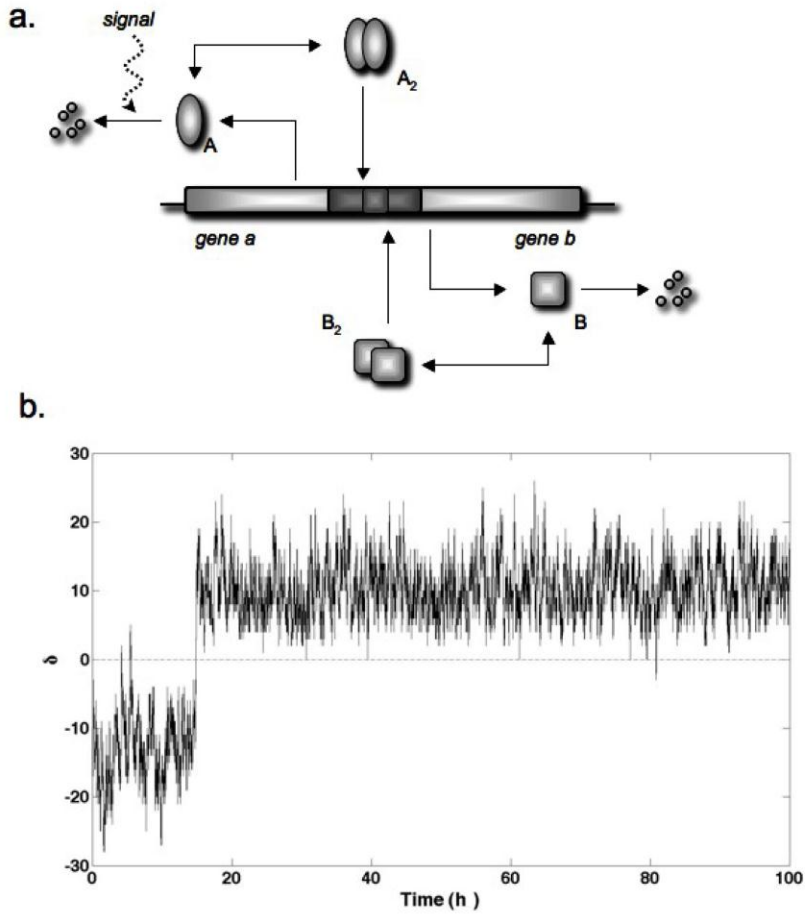

Figure 3.1. A schematic toggle switch model controlling single cell phenotype switch. (a) The toggle switch model. Periodic signal is added to the system, perturbing the degradation rate of protein A. (b) Gillespie simulations show that the model behaves like a two-state system, corresponding to two phenotypes of bacterium.

Table 3.1 gives the corresponding rate constants. Define δ to be the difference between the total number of free and bound protein B and the total number of free and bound protein A. Therefore, with these parameters and mass-action type dynamics, the system gives two stable states corresponding to the persister ($\delta < 0$), and normally growing ($\delta > 0$) phenotypes, respectively (see Figure 3.1 (b)). Stochastic fluctuations of the reactions drive the system to transit between the two states. These parameters are modified from the model of Allen et al. (Allen et al, 2005), so the model gives *hipA7* *p*2*n* (persister cell to normally growing cell) and *n*2*p* (normally growing cell to persister cell) switching rates 0.07 h^{-1} and 0.008 h^{-1}, respectively, as used by others (Balaban et al, 2004; Kussell et al, 2005). The abstract toggle switch model also places the present work in a broader context. Many microorganisms, including viruses and bacteria, coexist in a dormant and an active phenotype (Dubnau & Losick, 2006). The toggle switch is a frequently occurred generic regulation mechanism and a good model for phenotypic transitions in bacteria (Gardner et al, 2000; Smits et al, 2006).

To be specific and for practical considerations of computational feasibility, we chose model parameters in most simulations in this work to mimic the dynamics of *hipA7*. However, we want to emphasize that the proposed approach below works best for the following situation. First, we assume that one can regulate some of the rate constants through an external oscillating perturbing signal. Consequently some rates (the degradation rate of A for the results reported in the main text) are oscillating with time. The strength of the perturbing signal should be restricted due to the consideration of toxicity to the host. Second, we focus on the case that the transition from the persister to the normally growing phenotype is very slow, so that the sterilization of the total

population requires a long term antibiotic treatment, which may bring severe side-effect like liver damage.

Population level

At the population level, a cell is subject to an environment alternating between growing and antibiotics stress conditions. A normally growing cell has faster net proliferation rate than a persister cell does under growth condition, but also a larger death rate under antibiotic stress (see also(Kussell et al, 2005).

Three types of cellular events can take place for each cell: cell division (the cell including the molecular state of the toggle switch are cloned into two identical copies), cell death, and phenotypic transition. Table 3.2 gives all the related rate constants based on experimental observations (Balaban et al, 2004; Kussell et al, 2005). For a given cell with phenotype *n* (normally growing) or *p* (persister), the reactions for stochastic simulations additional to the 10 toggle switch reactions are

$$n \xrightarrow{g_n} 2n$$
$$n \xrightarrow{d_n} \phi$$
$$p \xrightarrow{g_p} 2p$$
$$p \xrightarrow{d_p} \phi$$

Unlike the work of Kussell et al, in our model we did not simulate the cell phenotypic transitions directly. Instead we propagate the 10 toggle switch reactions for each cell, which determine the phenotype of the cell (see above).

Each population level simulation initiates from a stationary-phase colony including 10^4 normal cells and 10^2 persister cells. The population is then put into fresh medium with/without antibiotics, as determined by each different strategy. The phenotype of a single cell is determined by its own toggle switch dynamics based on the value of δ. We use τ-leap Gillespie algorithm to propagate the 10 chemical reactions of each toggle switch and cell birth/death simultaneously(Gillespie, 2001). For the rates with periodic time-dependence, we approximate them as constant within one Gillespie step, which is much smaller than the rate varying period. For simplicity, we do not consider quorum sensing, thus each cell behaves independently and does not communicate with others except for competing resources as discussed below. To prevent the population from overgrowth in our simulations, we rescaled the growth rate g as a decreasing function of the number of normally growing cells n, $g_n(t+\tau) = g_n^0 / [1+\alpha \cdot n(t)]$ where τ is the time step in τ-leap Gillespie algorithm, α controls the scaling strength (here α = 0.001), and g_n^0 represents the original growth rate of normal cells without rescaling. We didn't rescale the persister cells' growth rate since the value before rescaling is already negligible. A physical justification of the rescaling is that the accessible nutrients and volume of a cell colony are usually limited against unrestricted massive replications.

3.4 Results

Resonant activation exists in cellular phenotypic switch

For the model we examined, the switching rate from *n*2*p* is much smaller than that of *p*2*n* at the exponential phase. This dynamics mimics that of *hipA7* (Balaban et al, 2004), and resembles to barrier crossing rates in an asymmetric double well potential, with one deeper well representing normally growing phenotype, and the other well representing persister phenotype. Let's define

t_{p2n} as the first passage time for *p*2*n* switching. The distribution of t_{p2n}, apart from an initial transient time period, follows an exponential form

$$P(t_{p2n}) \propto e^{-t_{p2n}/t_K}$$

(see Figure 3.2 (a)), where t_K is the inverse of the Kramers rate (Gammaitoni et al, 1998; Hänggi, 2002; Pechukas & Hanggi, 1994). The prolonged distribution contributes to bacterial persistence.

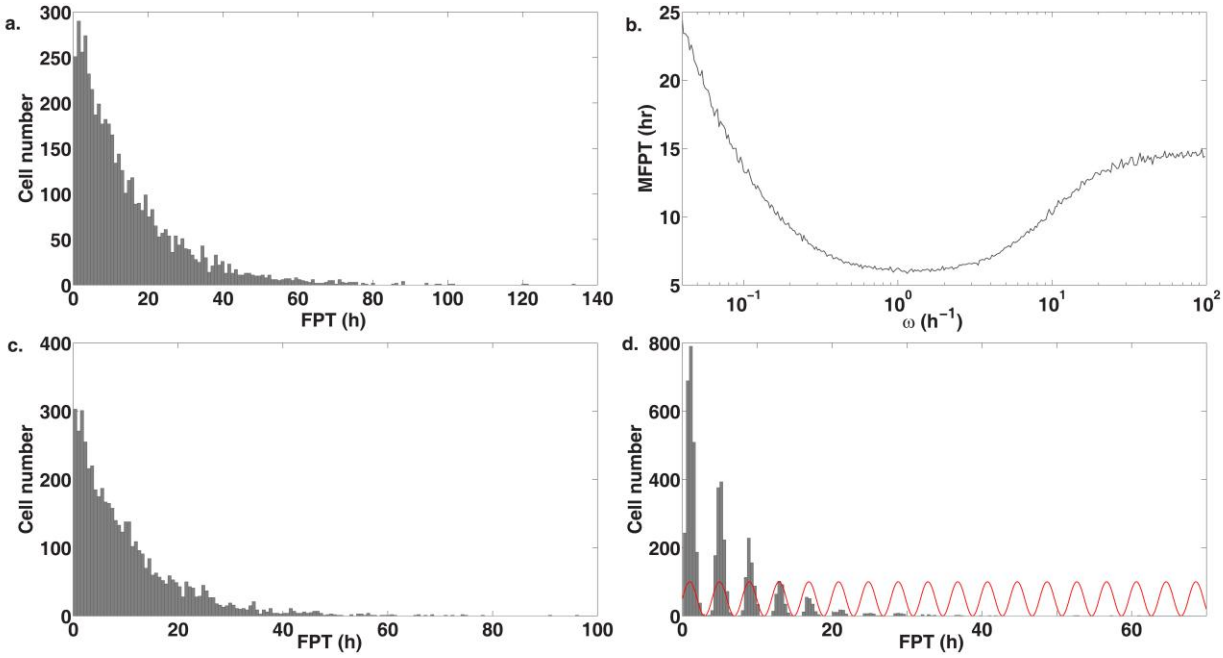

Figure 3.2. Results of single cell simulations. (a) $P(t_{p2n})$ in the absence of the perturbing signal. (b) The mean first passage time (MFPT) versus frequency ω of the sine-formed perturbation signal. (c) A weak perturbing signal with off-resonance frequency still gives an exponential distribution of $P(t_{p2n})$, here $\omega = 10\,\mathrm{h}^{-1}$. (d) A weak perturbing signal with resonance frequency (red curve) changes $P(t_{p2n})$ into several separated spikes. Each spike overlaps with a peak of the periodic signal (red curve) with $\omega_c = 1.6\ \mathrm{h}^{-1}$ and $\theta = 0$.

Next, we perturbed the protein *A*'s degradation rate with sine-formed signal (see Figure 3.1), $k_3 = k_3^0(1+\gamma\sin(\omega t+\theta))$, with $0<\gamma<1$. For each simulation the phase θ is randomly drawn from a uniform distribution between 0 and 2π. This is because in the population level simulations below, the relative phase between the birth time of a persister cell and the added signal can be seen as a random variable. Figure 3.2 (b) shows that the mean first passage time (MFPT) as a function of ω, averaged over 5000 independent simulations, shows a minimum around $\omega_c = 1.6\,\mathrm{h}^{-1}$, and the curve is rather flat over a range of ω values. Resonant activation occurs at the frequency ω_c where MFPT reaches minimum (Marchi et al, 1996; Schmitt et al, 2006) despite the current system is described by discrete dynamics.

Figure 3.2 also shows $P(t_{p2n})$ under a perturbing signal with different frequency. At a high ω, the system cannot respond fast enough, and the perturbation is equivalent to an averaged constant one. The distribution is exponential, Figure 3.2 (c). Under resonance frequency ω_c, however, t_{p2n} distribution changes into several separated spikes, Figure 3.2 (d). Note that the peaks of spikes overlap with the peaks of the periodic signal. Therefore transition takes place more frequently when the signal reaches the peak value, thus the degradation rate of protein A is the fastest, and the transition from A dominant to B dominant is the easiest(Gammaitoni et al, 1998). If the system misses one peak of the signal for a *p*2*n* transition, it prefers waiting for the next peak. We observed this type of localized distribution over a broad range of ω values corresponding to the flat bottom region of the MFPT- ω curve (see Figure 3.2 (b) and Figure 3.S1 in the Supplementary Information). Further increase of ω leads to gradual merge of the spikes, and eventually reduction to a single exponential distribution. These observations are

consistent with studies with barrier crossings in a double well potential(Schmitt et al, 2006), further supporting the existence of RA in the system.

For all the results reported here, we added the perturbing signal on protein A's degradation for illustrative purpose (see Figure 3.1 (a)). In real experiments and applications, one can also perturb other reactions (e.g. protein synthesis as well as degradation), depending on the actual practical feasibility. For example, one possible implementation of this perturbation may be through varying the activity of protease through specific regulating molecules. We further presented results with perturbations on A's synthesis rate, and B's synthesis and degradation rates in the Supplementary Information, Figure 3.S2. In all these cases we observed resonant activation with the same resonant frequency, but with varying fold of change of the MFPT. We provided a theoretical explanation there. It depends on the system to identify the reactions most sensitive to the perturbations. Figure 3.S3 in the Supplementary Information also showed that existence of RA is independent of the detailed form of the periodic perturbation signal.

Resonant activation accelerates bacteria colony sterilization

The stochastic simulations on single cell dynamics discussed above show that resonant activation can facilitate fast and synchronized *p2n* switches. Next we coupled the single cell level dynamics with population level proliferation/death under changing environment.

First we define a killing strategy K to be the combination of a perturbing signal *S* and an antibiotic environment *E*, characterized by their frequency (ω_1 and ω_2), strength, and duration, respectively.

For a given population initialized with 10^4 normally growing cells and 10^2 persister cells, our simulations allow it to evolve until no bacterium exists, or a maximum time reaches. Because the stochastic nature of the dynamics, for each population the sterilization time T_{kill} is random. To quantitatively compare different strategies, for each strategy we performed independent simulations with 1000 populations, and recorded T_{kill} of each population sample. Figure 3.S4 in Supplementary Information gives the killing time distribution of 1000 population samples under strategies K1 and K3. To compare the different strategies, we used the time needed to sterilize 90% of the 1000 population samples, *Q*, as a criterion. Practically this is a more relevant quantity than the average killing time, although we reached similar conclusion below with the latter.

The stochastic simulation results are summarized in Figure 3.3 and Table 3.3. Figure 3.4 give several typical trajectories. Without the perturbing signal, both the strategies with periodic (K1) and continuous (K2) antibiotics treatment require long time, since it takes long time to eradicate the persister cells. On the other hand, with the perturbation at the resonance frequency (K3 and K4), the sterilization time is greatly reduced. Because under K3, most of the *p2n* transitions take place within the period of applying antibiotics, it is difficult for the bacteria population to restore either the normally growing or the persister subpopulations (see Figure 3.S5 in the Supplementary Information). Consequently the sterilization time for K3 and K4 are about the same. To further prove this, we compute over 500 independent samples the ratio (R^g_{p2n}) between the number of *p2n* transitions that happen during growth environment and the total number of *p2n* transitions. Larger R^g_{p2n} corresponds to the inefficiency of the periodic antibiotic strategy, because the population may be easier to get re-established during growth period. Under K3,

$R^g_{p2n} = 4.3\%$, while under K1, $R^g_{p2n} = 46.8\%$. We observed similar efficient bacterial eradication with signal frequencies away from ω_c but still lying near the flat bottom of the MFPT-ω curve in Figure 1 (b). However, further change of the frequency (K5 and K6) shows less improvement over that of K1 or K2. Figure 3.3 (b) gives the total amount of antibiotics used for each case. Compared to K2, K3 requires less than half of the time, with ~25% of the total amount of antibiotics. In the Supplementary Information, we also examined how the killing time depends on the signal duration and strength, Figure 3.S6 and Figure 3.S7.

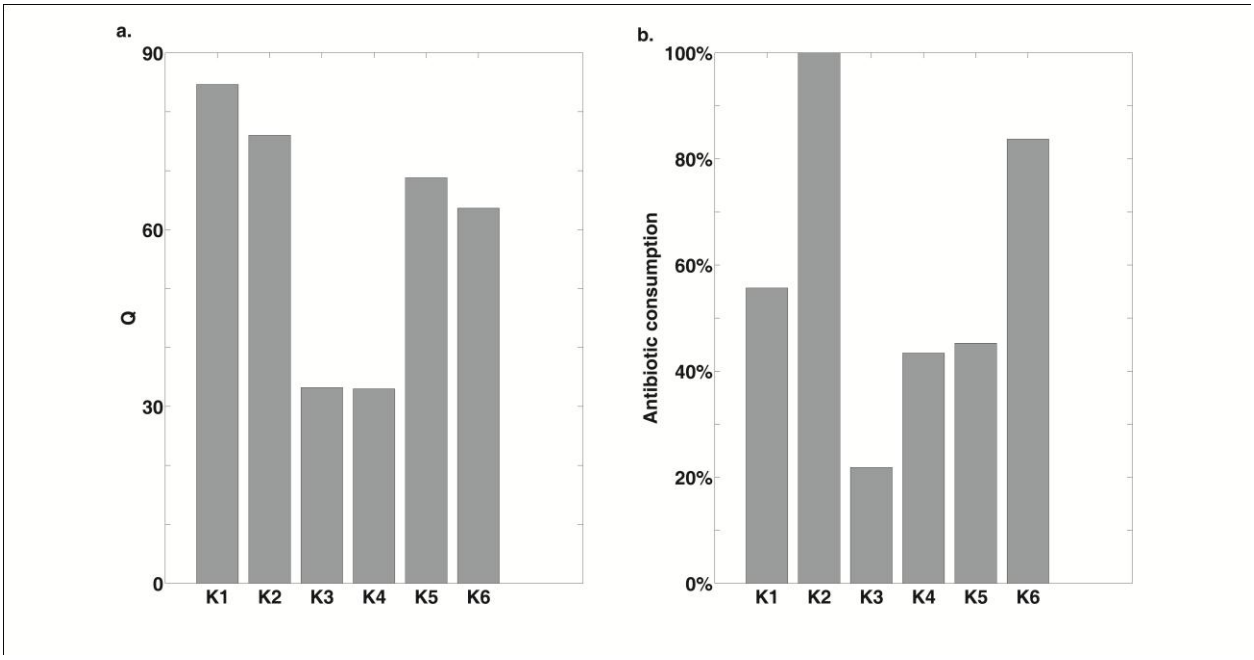

Figure 3.3. Comparison of various strategies at the population level. (a) 90% quantile (*Q*) of T_{kill} under six different killing strategies (refer to Table 3.3 for notation of each killing strategy). (b) Corresponding relative antibiotic consumption. Please refer to Table 3.1 for the illustration of killing strategies K.

To further examine the strength and limitation of our proposal, we examined a more difficult case of bacterial persistence. The model is similar to what discussed above, except that the *p2n*

transition rate is reduced by a factor of 5. Correspondingly, we extend each period of alternative antibiotics and freely growing environment. This leaves more time for the system to recover under the latter environment. Figure 3.5 gives several typical trajectories of population level simulations. For strategy K1, we had difficulty to observe population extinction even after 10^4 h. While almost all the normally growing cells are killed, and the persister subpopulation size is reduced under an antibiotics environment, both subpopulations are restored to their original levels under next freely growing period. For strategy K2, the 90% quantile of sterilization time for 1000 populations is 362 h. In comparison, the 90% quantile of sterilization time for K3 and K4 are 358 h and 168 h, respectively. Though under K3, the ratio of *p2n* transitions within growth period $R_{p2n}^{g} = 4.3\%$, in this case a single *p2n* transition under the freely growing environment is sufficient to restore both the two subpopulations. That explains why K3 requires almost the same sterilization time with K2. However, K3 uses about half of the amount of antibiotics needed under K2. In addition, since antibiotics are applied periodically, K3 might be better than K4 considering it leaves time for the host to recover from possible side effects of the antibiotics treatment. Therefore, in this case, one has to make a compromise between short sterilization time and side-effect reduction.

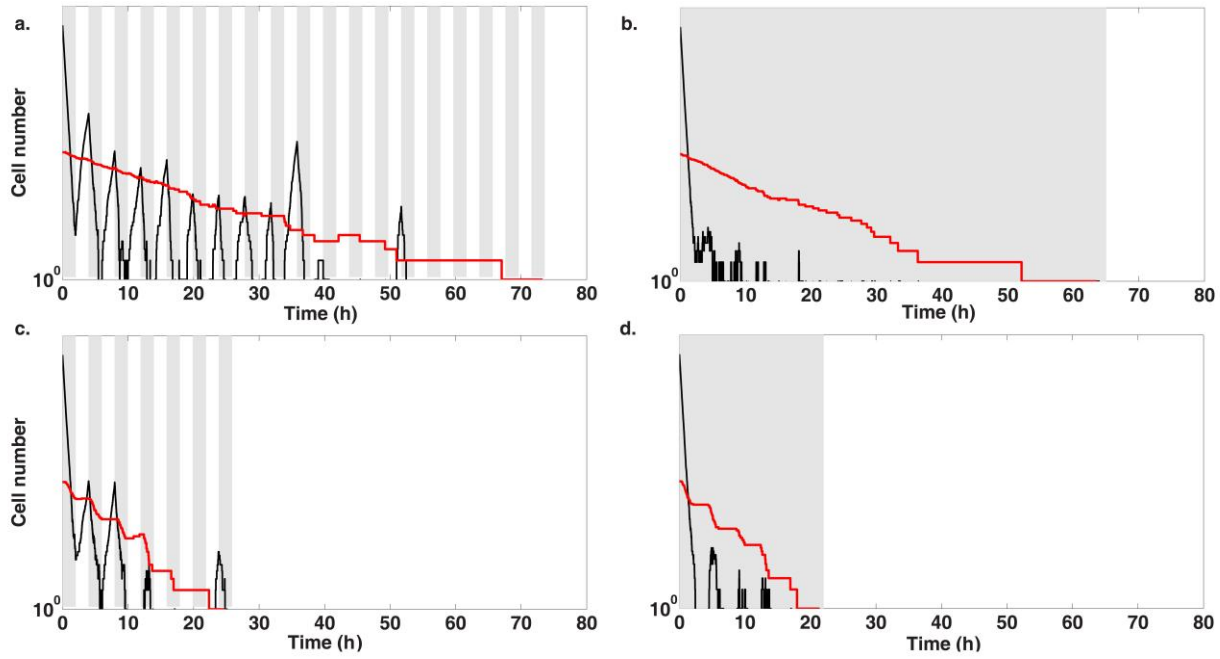

Figure 3.4. Sample population dynamics corresponding to the results in Figure 3.3. (a) K1. (b) K2. (c) K3, $\omega_c = 1.6\,\mathrm{h}^{-1}$, $T_{\omega_c} = 2\pi/\omega_c = 3.9\,\mathrm{h}$. (d) K4. Black curve shows the dynamics of normally growing population. Red curve shows the dynamics of persister population. Gray time windows in the background indicate antibiotic treatment, blank time windows represent environment good for growth.

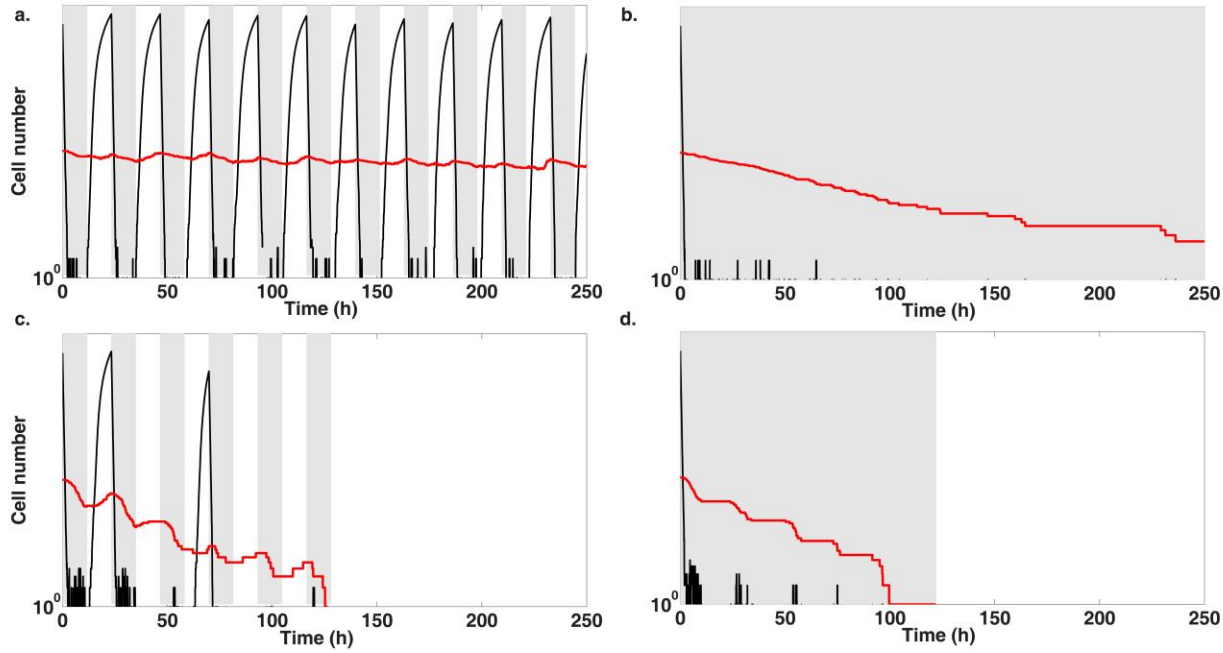

Figure 3.5. Sample population dynamics corresponding to a phenotype with slower switching rate (see the main text). Antibiotic treatment is either continuous or periodic. (a) K1. (b) K2. (c) K3, $\omega_c = 0.27\,\mathrm{h}^{-1}, T_{\omega_c} = 2\pi/\omega_c = 23.3\,\mathrm{h}$. (d) K4. Black curve shows the dynamics of normally growing population. Red curve shows the dynamics of persister population. Gray time windows in the background indicate antibiotic treatment, blank time windows represent environment good for growth.

3.5 Discussions and concluding remarks

In the past decade, bacterial persistence became a spotlight in microbiological arena. The leading actors, called persister cells, are some special dormant cells which account for only a small fraction of the total population. However, they are insensitive to antimicrobial therapy, and are able to switch back into normally growing phenotype to initiate population regrowth. The phenotypic switching property of bacteria has been experimentally identified to be regulated by

several toxin-antitoxin (TA) modules within bacterium chromosome, such as *hipBA*, *relBE* and *chpA*. For example, Keren et al. reported that *hipBA*-knocked-out *E. coli* biofilm produced 150-folder-fewer persister cells under mitomycin treatment(Keren et al, 2004b). Continuous efforts have been made to reveal the detailed molecular regulation mechanism (Christensen et al, 2003; Pedersen et al, 2002).

Now, it is believed that persister cells may evolve into maximizing the overall survival possibility of bacteria population in real fluctuation environment. Many lab experiments have proved that the existence of persister cells in biofilms is responsible for many recalcitrant diseases, such as human tuberculosis, an infectious disease caused by *Mycobacterium tuberculosis* biofilms. The typical antibiotic treatment of this disease is as long as 6-9 months. Therefore, besides the inefficiency of the therapy, the side-effect from such a long-term use of antibiotics is of serious concern. Active research is undertaken to fight against bacteria persistence through accelerating the phenotype transition rate with chemical or physical method(Gefen & Balaban, 2009; Stewart et al, 2003). In this work we assume such a mechanism exists, and focused on the optimal strategy to combine it with antibiotics treatment.

Stochastic resonance has been discovered in many biological systems(Hänggi, 2002). Similar to Schmitt et al., we also observed stochastic resonance in the present system. Resonant activation, on the other hand, is seldom discussed in the biology context. The phenomenon of RA is related to fluctuation resonance previously reported (Lipan & Wong, 2005; Mettetal et al, 2008). For a stochastic system with one steady state driven by an oscillating perturbation, there may be a resonant frequency of the perturbation so that the system shows largest fluctuation amplitude.

This is called fluctuation resonance, which resembles the peak of the energy absorption spectrum of a system. For a system with multiple steady states, larger fluctuations lead to faster transition rate to a new steady state. This is resonant activation. Here we demonstrated the existence of RA in non-thermal systems governed by discrete chemical reaction dynamics. RA has two unique properties: reduced mean first passage time, and localized transition in time. We propose to utilize the two properties of RA to help on eliminating persistent bacteria. As previously mentioned, the essential reason for bacterial persistence is the large time-scale of t_{p2n} distribution. This requires continuous antibiotic treatment to cover most of the time period to prevent bacteria population re-establishment. With RA, the distribution is narrowed through reduction of the MFPT. This is our main argument for using RA against bacteria persistence. Furthermore for some cases the localized spike shaped transition time distribution may allow dividing the antibiotics treatment into sessions without serious problem of bacteria population restoration. This is of special advantage by minimizing side effects of antibiotics treatment to patients if the treatment has to be long. On the other hand, our simulations show that even if one can accelerate the bacteria phenotype switching rate, improper procedure (strategy K5) leads to no improvement in fighting bacteria persistence.

In this work, we presented the general idea of modulating cellular phenotype switching through resonant activation. It should be viewed as illustrative. More detailed modeling and experimental studies are necessary to examine the feasibility and the optimal strategy for each specific system. Detailed molecular mechanism of the toxin-antitoxin module, its interaction with related signal transduction and metabolic pathways should be carefully considered. The detailed model will provide information on the strategies of adding the perturbing signal. In a bacterial colony,

several persistent phenotypes may coexist. In this case a more efficient strategy may be to apply antibiotics continuously for a period, then switch to the strategy we propose here for the most persistent phenotype. The broad range of resonance frequency of one phenotype (see Figure 3.2 (b)) may also allow one to choose an overlapping frequency for all the phenotypes. The perturbing signal is not limited to chemicals, but any external environmental change that can affect the phenotype switching dynamics.

We want to point out that the actual performance of each strategy depends on the property of the system, especially the unperturbed *p*2*n* transition time and the system noise level. Here we only focused on illustrating the basic idea, and the choice of the system is partly restricted by computational considerations. Orders of magnitude reduction of the MFPT with RA have been reported for some physical systems(Boguñá et al, 1998). One may expect similar result for some phenotypic transitions.

While here we focused on bacterial persistence, we want to emphasize that resonant activation is a general phenomenon for phenotypic transitions, which are analogous to thermally activated barrier crossing processes. One may find application of the idea discussed here to other problems. For example, Spencer et al. have shown that cancer cells have persistence behavior similar to bacteria(Spencer et al, 2009). Radiotherapy is a standard cancer treatment option. It normally consists of multi-session low dose of radiation in a few weeks. The radiation induces cell DNA damage, which eventually leads to apoptosis. In this case it is even easier to apply RA. Here radiation is the oscillating signal, apoptosis plays the role of antibiotics, and population restoration during the treatment intervals is not a serious problem. An optimal strategy may exist

on performing the treatment utilizing resonant activation. Similar argument applies to chemotherapy. In this case stochastic resonance does not exist since the system is not bistable.

3.6 Acknowledgements

We would like to thank Dr.Nathalie Q. Balaban for discussion in the experimental works in bacterial persistence, Drs. John J. Tyson, Katherine C. Chen, Tongli Zhang, Vlad Elgart, Zhanghan Wu and Chun Chen for discussions and comments on this paper. We would also like to thank Dr.Yang Cao for useful discussion on stochastic simulation method.

Table 3.1. Parameters for single cell level simulation.

Parameter	Value (unit[a])	Notation
k_1^0	0.05	Basal synthesis rate of A
k_2^0	1	Basal synthesis rate of B
k_3^0	0.45	Basal degradation rate of A
k_4^0	0.56	Basal degradation rate of B
k_5	5	Dimer A_2 association rate
k_{-5}	5	Dimer A_2 disassociation rate
k_6	5	Dimer B_2 association rate
k_{-6}	5	Dimer B_2 disassociation rate
k_7	5	Binding rate between operon and A_2
k_{-7}	1	Unbinding rate of A_2 from operon
k_8	5	Binding rate of B_2 from operon
k_{-8}	1	Unbinding rate of B_2 from operon
k_9	1	Synthesis rate of A
k_{10}	1	Synthesis rate of B

[a] first order reaction unit = 130 h^{-1}, second order reaction unit = 130 h^{-1} $molecule^{-1}$

Table 3.2. Parameters for population level simulation.

Parameter	Value (h^{-1})	Notation
g_n	0.2	Net growth rate of normally growing cells under the growth condition
d_n	4	Net death rate of normally growing cells under the antibiotic condition
g_p	0.02	Net growth rate of persister cells under the growth condition
d_p	1×10^{-6}	Net death rate of persister cells under the antibiotic condition

Table 3.3. 90% quantile of T_{kill} (Q) under different killing strategies.

	S_{ω_1}	E_{ω_2}	Q (h)	Notation
K_1	ϕ	$H(S_{\omega_c})$ [a]	84.6	No signal + periodic antibiotics
K_2	ϕ	E_0 [b]	76.0	No signal + continuous antibiotics
K_3	S_{ω_c}	$H(S_{\omega_c})$	33.2	Resonance signal + periodic antibiotics
K_4	S_{ω_c}	E_0	33.0	Resonance signal + continuous antibiotics
K_5	S_{10}	$H(S_{10})$	68.8	Off-resonance signal + off-resonance periodic antibiotics
K_6	S_{10}	E_0	63.7	Off-resonance signal + continuous antibiotics

[a] $H(x)$ is a Heaviside function which returns 1 if $x \geq 0$, otherwise returns 0. We assume that $H = 1$ denotes that the antibiotic treatment is switched on, and $H = 0$ denotes that the antibiotic treatment is switched off. $S_{\omega_c} = A\sin(\omega_c t)$ is the sine-formed perturbing signal under resonance frequency ω_c. [b] E_0 represents continuous antibiotic treatment.

3.7 Reference

Allen RJ, Warren PB, ten Wolde PR (2005) Sampling Rare Switching Events in Biochemical Networks. *Physical Review Letters* **94:** 018104

Balaban NQ, Merrin J, Chait R, Kowalik L, Leibler S (2004) Bacterial Persistence as a Phenotypic Switch. *Science* **305:** 1622-1625

Bigger J (1944) The bactericidal action of penicillin on Staphylococcus pyogenes. *Irish Journal of Medical Science (1926-1967)* **19:** 553-568

Boguñá Mn, Porr‡ JM, Masoliver J, Lindenberg K (1998) Properties of resonant activation phenomena. *Physical Review E* **57:** 3990

Christensen SK, Pedersen K, Hansen FG, Gerdes K (2003) Toxin-antitoxin Loci as Stress-response-elements: ChpAK/MazF and ChpBK Cleave Translated RNAs and are Counteracted by tmRNA. *Journal of Molecular Biology* **332:** 809-819

Cirz RT, Chin JK, Andes DR, de Cr√©cy-Lagard Vr, Craig WA, Romesberg FE (2005) Inhibition of Mutation and Combating the Evolution of Antibiotic Resistance. *PLoS Biol* **3:** e176

Doering CR, Gadoua JC (1992) Resonant activation over a fluctuating barrier. *Physical Review Letters* **69:** 2318

Dubnau D, Losick R (2006) Bistability in bacteria. *Molecular Microbiology* **61:** 564-572

Gammaitoni L, Hanggi P, Jung P, Marchesoni F (1998) Stochastic resonance. *Reviews of Modern Physics* **70:** 223

Gardner TS, Cantor CR, Collins JJ (2000) Construction of a genetic toggle switch in Escherichia coli. *Nature* **403:** 339-342

Gefen O, Balaban NQ (2009) The importance of being persistent: heterogeneity of bacterial populations under antibiotic stress. *FEMS Microbiology Reviews* **33:** 704-717

Gefen O, Gabay C, Mumcuoglu M, Engel G, Balaban NQ (2008) Single-cell protein induction dynamics reveals a period of vulnerability to antibiotics in persister bacteria. *Proceedings of the National Academy of Sciences* **105:** 6145-6149

Gillespie DT (2001) Approximate accelerated stochastic simulation of chemically reacting systems. *The Journal of Chemical Physics* **115:** 1716-1733

Hänggi P (2002) Stochastic resonance in biology. How noise can enhance detection of weak signals and help improve biological information processing. *Chemphyschem* **3:** 6

Keren I, Kaldalu N, Spoering A, Wang Y, Lewis K (2004a) Persister cells and tolerance to antimicrobials. *FEMS Microbiology Letters* **230:** 13-18

Keren I, Shah D, Spoering A, Kaldalu N, Lewis K (2004b) Specialized Persister Cells and the Mechanism of Multidrug Tolerance in Escherichia coli. *The Journal of Bacteriology* **186:** 8172-8180

Kussell E, Kishony R, Balaban NQ, Leibler S (2005) Bacterial Persistence: A Model of Survival in Changing Environments. *Genetics* **169:** 1807-1814

Levin BR, Rozen DE (2006) Non-inherited antibiotic resistance. *Nat Rev Micro* **4:** 556-562

Lipan O, Wong WH (2005) The use of oscillatory signals in the study of genetic networks. *Proceedings of the National Academy of Sciences of the United States of America* **102:** 7063-7068

Lou C, Li Z, Ouyang Q (2008) A molecular model for persister in E. coli. *Journal of Theoretical Biology* **255:** 205-209

Marchi M, Marchesoni F, Gammaitoni L, Menichella-Saetta E, Santucci S (1996) Resonant activation in a bistable system. *Physical Review E* **54:** 3479

Mettetal JT, Muzzey D, Gomez-Uribe C, van Oudenaarden A (2008) The frequency dependence of osmo-adaptation in Saccharomyces cerevisiae. *Science* **319:** 482-484

Miller C, Thomsen LE, Gaggero C, Mosseri R, Ingmer H, Cohen SN (2004) SOS Response Induction by {beta}-Lactams and Bacterial Defense Against Antibiotic Lethality. *Science* **305:** 1629-1631

Ochman H, Lawrence JG, Groisman EA (2000) Lateral gene transfer and the nature of bacterial innovation. *Nature* **405:** 299-304

Ojha AK, Baughn AD, Sambandan D, Hsu T, Trivelli X, Guerardel Y, Alahari A, Kremer L, Jr WRJ, Hatfull GF (2008) Growth of Mycobacterium tuberculosis biofilms containing free mycolic acids and harbouring drug-tolerant bacteria. *Molecular Microbiology* **69:** 164-174

Pechukas P, Hanggi P (1994) Rates of Activated Processes with Fluctuating Barriers. *Physical Review Letters* **73:** 2772-2775

Pedersen K, Christensen SK, Gerdes K (2002) Rapid induction and reversal of a bacteriostatic condition by controlled expression of toxins and antitoxins. *Molecular Microbiology* **45:** 501-510

Rao CV, Wolf DM, Arkin AP (2002) Control, exploitation and tolerance of intracellular noise. *Nature* **420:** 231-237

Schmitt C, Dybiec B, H‰nggi P, Bechinger C (2006) Stochastic resonance vs. resonant activation. *Europhys Lett* **74:** 937-943

Smits WK, Kuipers OP, Veening J-W (2006) Phenotypic variation in bacteria: the role of feedback regulation. *Nat Rev Micro* **4:** 259-271

Spencer SL, Gaudet S, Albeck JG, Burke JM, Sorger PK (2009) Non-genetic origins of cell-to-cell variability in TRAIL-induced apoptosis. *Nature* **459:** 428-432

Stewart GR, Robertson BD, Young DB (2003) Tuberculosis: a problem with persistence. *Nat Rev Micro* **1:** 97-105

Walczak AM, Onuchic JN, Wolynes PG (2005) Absolute rate theories of epigenetic stability. *Proceedings of the National Academy of Sciences of the United States of America* **102:** 18926-18931

Wang J, Huang B, Xia X, Sun Z (2006) Funneled Landscape Leads to Robustness of Cell Networks: Yeast Cell Cycle. *PLoS Comput Biol* **2:** e147

Zhu XM, Yin L, Hood L, Ao P (2004) Calculating biological behaviors of epigenetic states in the phage ? life cycle. *Functional & Integrative Genomics* **4:** 188-195

3.8 Supplementary Information

3.8.1 Large region of ω guarantees RA in single cell phenotypic transition

Under resonance frequency $\omega_c \sim 1.6\,\mathrm{h}^{-1}$, the mean first passage time (MFPT) reaches a minimum. Actually, the MFPT-ω curve displays a rather flat bottom, indicating a large region of the signal frequency may generate RA in our system. Figure 3.S1 shows some FPT distribution for the *p*2*n* transitions (also denoted by $P(t_{p2n})$) within this region of signal frequency. The $P(t_{p2n})$ under ω=0.3, 1.0, 2.0 h^{-1} all produce separated-spikes-like distribution. This allows some freedom in real therapeutic applications. We have repeated the double well system studied by Schmitt et al.(Schmitt et al, 2006), and found similar behaviors.

3.8.2 Choices of the perturbation target for RA

In the main text, we reported results with the degradation rate of protein A being periodically perturbed. Figure 3.S2 (a-c) shows the MFPT of *p*2*n* transitions when A's synthesis rate, B's synthesis or degradation rates are perturbed at different signal frequency, respectively. Clearly, resonant activation exists in all cases. However, the fold of change between the MFPT at the resonant frequency and that with no perturbation varies. The effect with perturbation on A's synthesis is similar to that on A's degradation, but the effect with either B's synthesis or degradation is much weaker. Figure 3.S2 (d) shows the system's stationary distribution on the n_{A}-n_{B} plane, which can be related to a potential(Graham & Haken, 1971). Clearly the system dynamic shows transition state-like behavior, with the transition state having small numbers of both A and B. That is, leaving from the state with high A and low B (persister), for the system to make a state transition it is more important to reduce the number of A than increasing the number of B. This explains why it is more sensitive to perturb the reactions involving A.

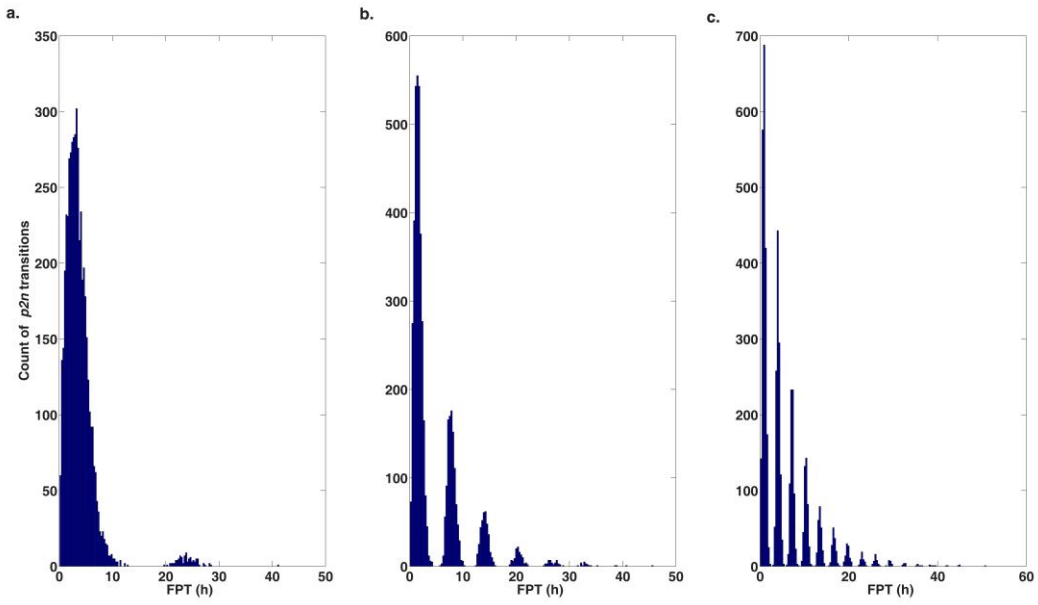

Figure 3.S1. $P(t_{p2n})$ under different signal frequency. All signals are sine-formed, as described in the main text. a. ω = 0.3 h^{-1}. b. ω = 1.0 h^{-1}. c. ω = 2.0 h^{-1}. All these three cases give values of the MFPT close to the minimum in Figure 3.2 (b) in the main text.

3.8.3 Resonant activation exists with various signal forms

In the main text, we applied a sine-formed signal to perturb the degradation rate of protein A in each generic toggle switch, and observed RA. A more practical signal form may be unidirectional on the perturbation. We tested with a step-function form. That is, the protein degradation rate k_3 was only increased from its basal rate periodically by a constant value. Again we observed that the MPFT shows a minimum at the same ω_c as with the sine function form. However, in this case some of the neighboring spikes in the FPT distribution are not fully separated, Figure 3.S3. We observed ~ 9.4% *p*2*n* transitions taking place under the growth environment, comparing to ~ 4.3% for the sine function form.

Consequently, for a system with easy population restoration (i.e., the second example discussed in the main text), the sterilization time using the periodic antibiotics treatment (K3) with the step function signal is longer than that with the sine function signal. In this case, strategy K4 under the step function signal gives a 90% quantile of the sterilization time ~39% of that with strategy K2.

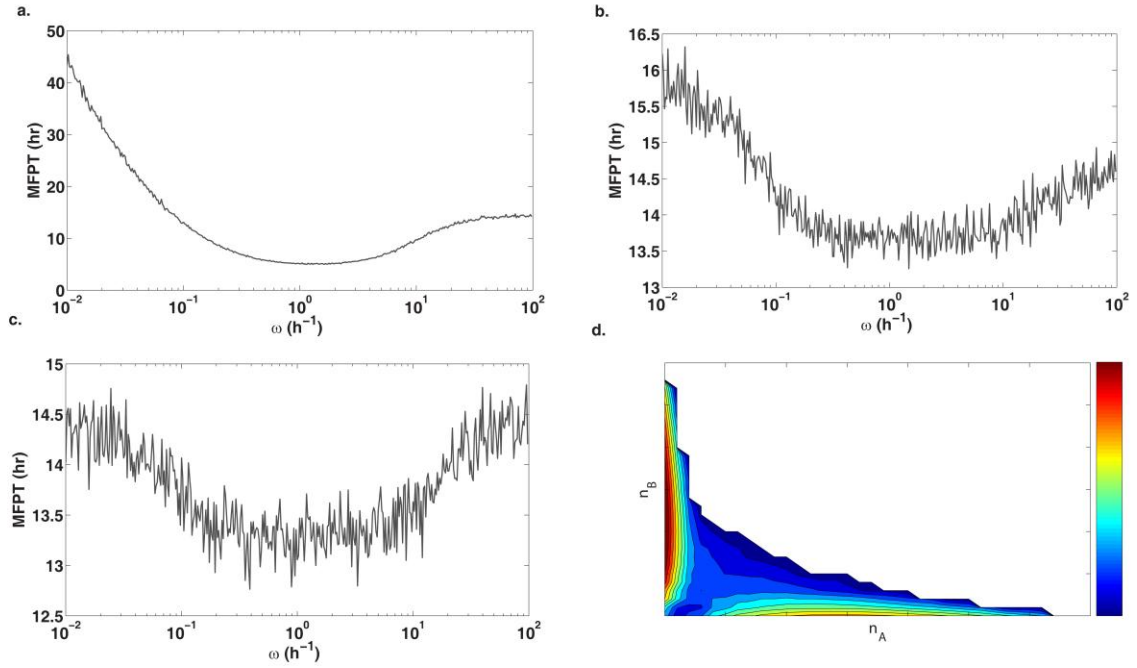

Figure 3.S2. RA with perturbation on different reactions. a) MFPT of *p*2*n* transition when A's synthesis rate k_9 is perturbed. b) MFPT of *p*2*n* transition when B's synthesis rate k_{10} is perturbed. c) MFPT of *p*2*n* transition when B's degradation rate k_4^0 is perturbed. These perturbations are implemented using sine signal with the same perturbing strength. Together with the case of perturbing A's degradation, all four cases generate local minimums around $\omega_c = 1.6\ \mathrm{h}^{-1}$, but with different fold of change in the MFPT as signal frequency varies. d) Stationary distribution on the n_A- n_B phase plane sampled with a long trajectory. Refer to the color bar for the relative probability of each (n_A, n_B), with a decreasing value from the top (red) to the bottom (blue).

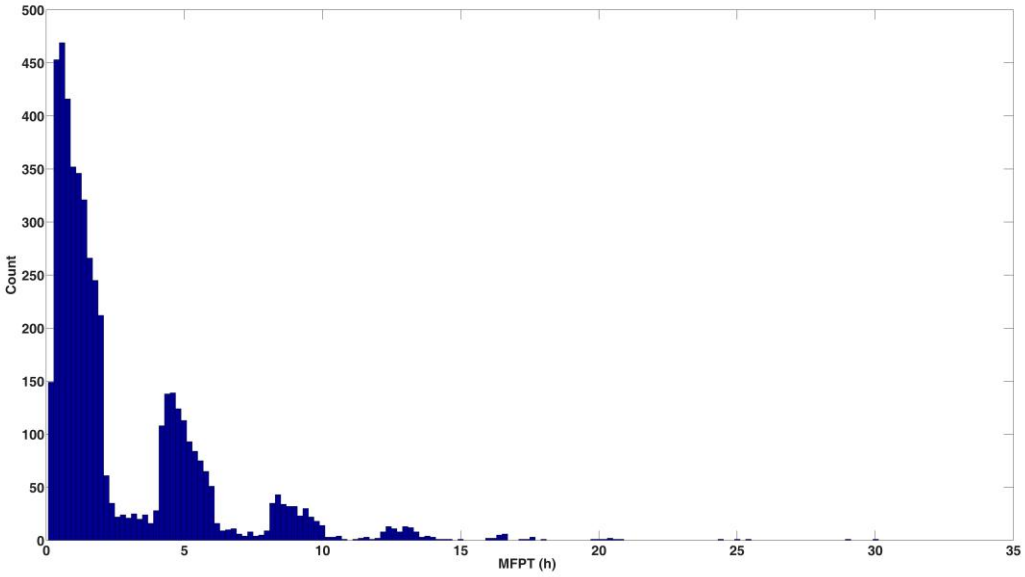

Figure 3.S3. t_{p2n} under the step-function signal. Other parameters are the same as in Table 1 of the main text.

3.8.4 The distribution of T_{kill} and the reason for using statistics *Q*

Figure 3.S4 gives the killing time distribution of the 1000 samples under strategies K1 and K3. Clearly both distributions have long tails. Therefore we suggest that the 90% quantile may be a better quantity than the mean value to compare different strategies, although the conclusions are the same.

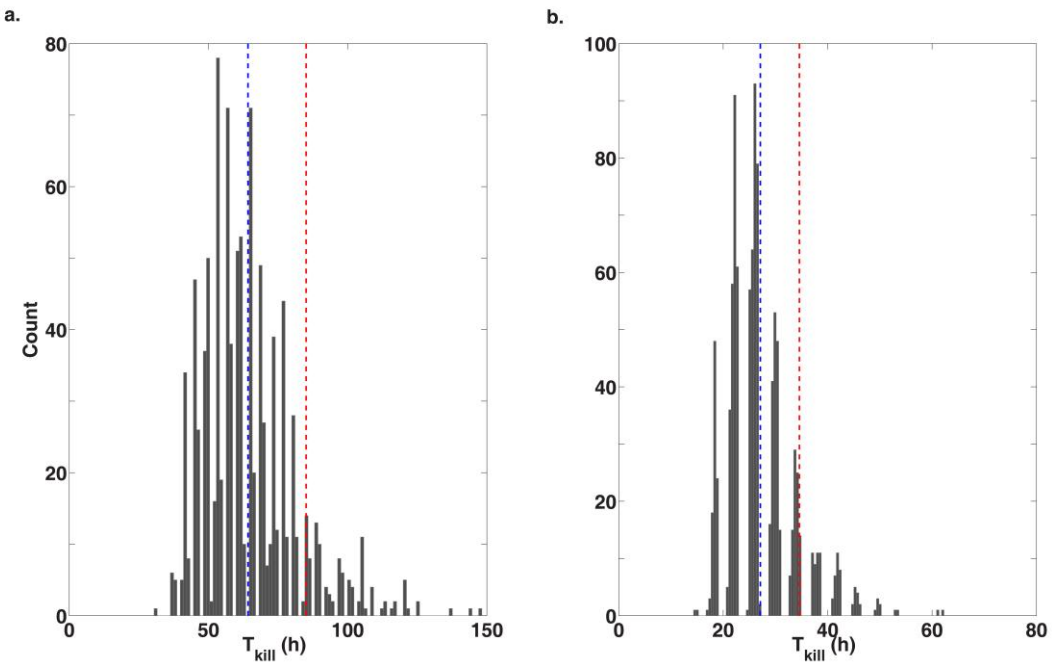

Figure 3.S4. Distribution of T_{kill}. a. Case K1. b. Case K3. Blue dash line shows the location of the mean value; red dash line shows the location of 90% quantile of the total samples (*Q*).

3.8.5 Most *p*2*n* transitions take place during antibiotic periods under killing strategy K3

By recording the population dynamics with corresponding *p*2*n* transitions under different killing strategies, Figure 3.S5 shows that most *p*2*n* transitions take place within the period of antibiotics treatment under strategy K3. Therefore, the bacterial population is difficult to re-establish when K3 is applied. On the other hand, under K1, the distribution of *p*2*n* is exponential, indicating the phenotypic transition may take place during either growth condition or antibiotic condition.

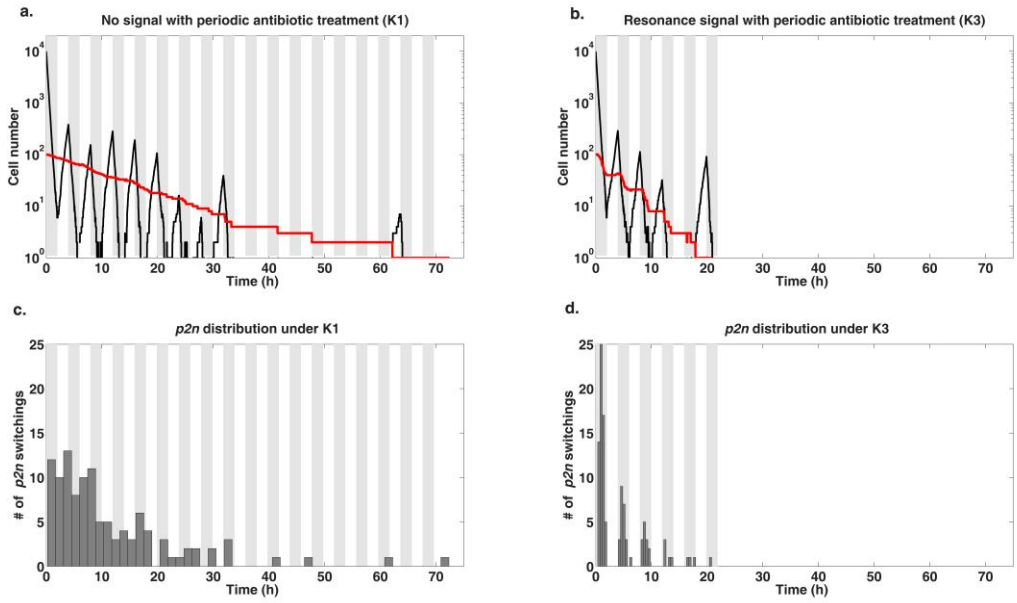

Figure 3.S5. Sample population dynamics with corresponding *p*2*n* transitions under different killing strategies. (a) K1. (b) K3, $\omega_c = 1.6\ \mathrm{h}^{-1}$, $T_{\omega_c} = 2\pi / \omega_c = 3.9\ \mathrm{h}$. (c) *p*2*n* under K1. (d) *p*2*n* under K3. Black curve shows the dynamics of normally growing population. Red curve shows the dynamics of persister population. Gray time windows in the background indicate antibiotic treatment, blank time windows represent environment good for growth.

3.8.6 Signal strength affects the sterilization time of bacteria population

As can be seen from Figure 3.S6, signals with stronger strength can reduce more time needed for sterilizing bacteria population. However, a stronger signal implies a bigger perturbation to the system, which may be unfavorable due to practical considerations and toxicity.

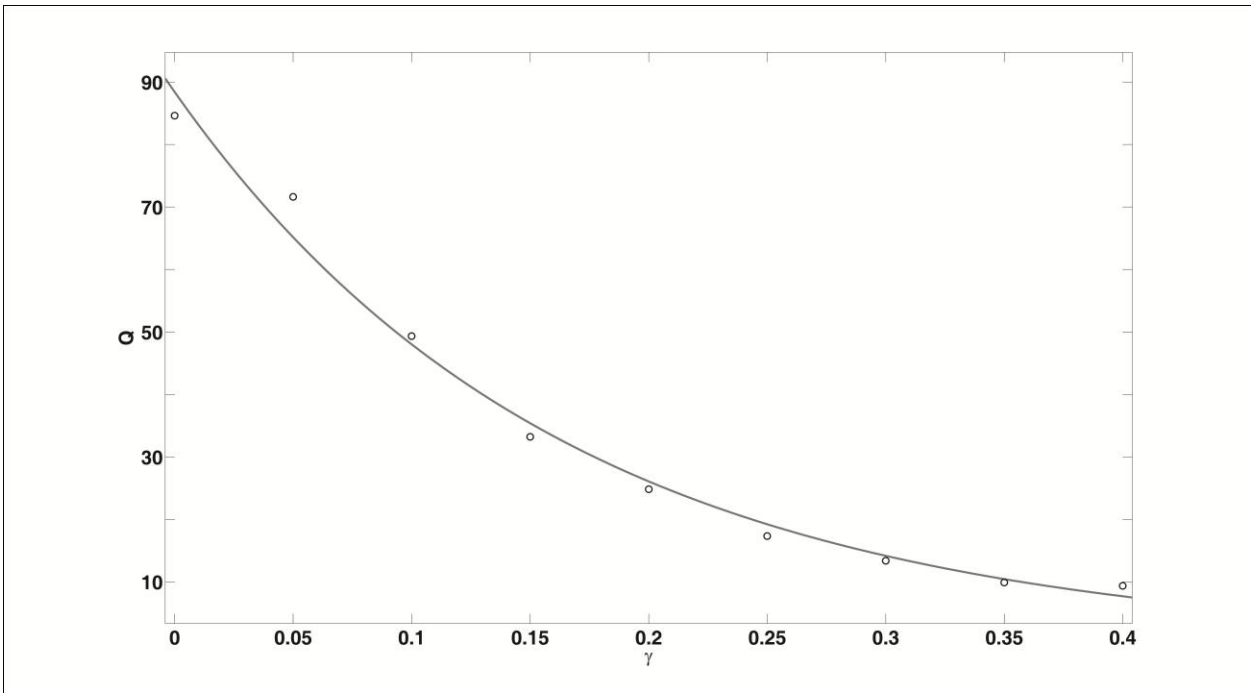

Figure 3.S6. 90% quantile of sterilization time (Q) under signal with different strength. Here we use sine-formed signal $S = \gamma \sin(\omega \cdot t)$ with strength γ. In the main text, $\gamma = 0.15$ unit. The maximal γ should be the basal degradation rate of the target protein, which in our case is 0.45 unit.

3.8.7 Duration of each session of antibiotics treatment affects sterilization time

At resonance frequency, the *p*2*n* transition distribution is multi-spike shaped. This allows discrete antibiotics treatment, as long as each session covers all or most of the *p*2*n* transition time. We performed population level simulations with different antibiotics treatment duration centered at the signal peak times. Figure 3.S7 shows the 90% quantile of the sterilization time. As expected, upon increasing the antibiotics treatment duration from zero, the sterilization time first drops sharply, and then flattens. Further increase of the antibiotic duration does not decrease the sterilization time. Therefore in this case one may further reduce the duration of each

session of the antibiotics treatment to ~ 1.3 h from the 2 h value used in in the main text, without significant increase of the sterilization time.

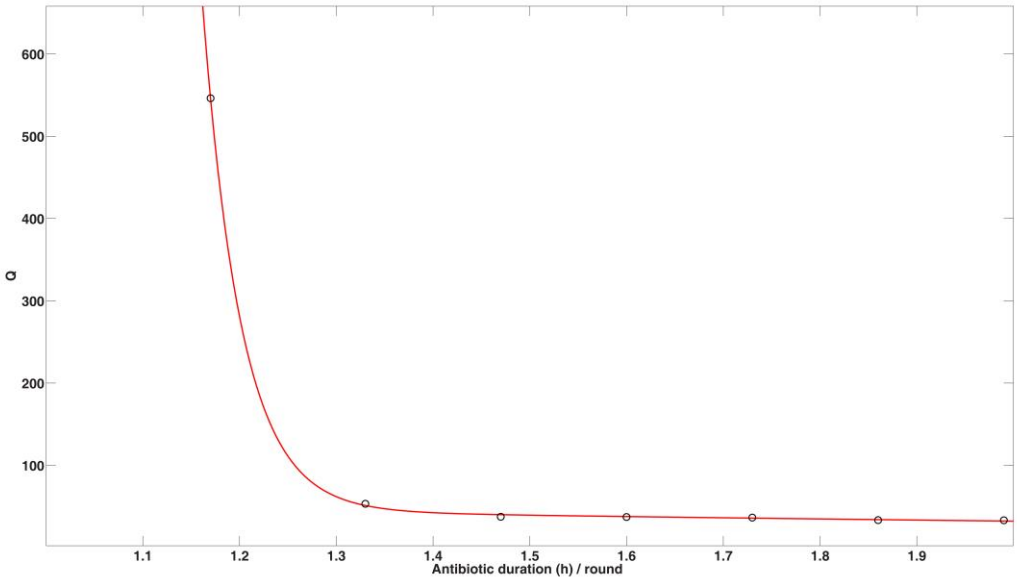

Figure 3.S7. 90% quantile of sterilization time (*Q*) under different duration of antibiotic treatment.

3.9 Supplementary Reference

Graham R, Haken H (1971) Generalized Thermodynamic Potential for Markoff Systems in Detailed Balance and Far from Thermal Equilibrium. *Z Phys* **243:** 289

Schmitt C, Dybiec B, Hanggi P, Bechinger C (2006) Stochastic resonance vs. resonant activation. *Europhys Lett* **74:** 937-943

Chapter 4. Conclusions

Systems biology has emerged and flourished at the transition of biology from a traditional experimental study into a multi-disciplinary field. As many quantitative and high-throughput experimental technique are developed, systems biology has becoming essential for us to integrate and interpret large-scale experimental data by using tools from mathematics, physics, computer science and engineering (Alon, 2007; Gardy et al, 2009; Gilchrist et al, 2006).

It remains a fundamental question to the field of systems biology how cells are able to generate not only robust but precise and specific responses to different signaling conditions. In a natural environment, cells are likely being exposed to all kinds of signaling conditions, e.g. a combination of different fluctuating signals co-stimulating or sequentially stimulating cells. As cellular behaviors are controlled by complex signaling and regulatory networks, this question is then transformed into understanding specific information processing properties emerged from signaling and regulatory networks. In this respect, the concept of "functional motifs" has been proposed to unravel a bunch intertwined static molecular interactions into several small modules with specific known information-processing functions and dynamic characteristics. Therefore, a complex network could be described as an interaction circuit composed of a number of functional motifs that could be computationally studied (Alon, 2007; Milo et al, 2002; Tyson & Novak, 2010).

In the first part of this dissertation (Chapter 2), we studied part of the above question in terms of the functional motifs and dynamics leading to adapted gene expressions under two sequential phases of LPS stimulation, known as LPS-priming and tolerance. In the study, we applied

mathematical modeling and Monte-Carlo simulations to study all possible topologies and dynamics in a generic 3-node network that can lead to a pre-defined priming and tolerance under sequential stimulations. As a result, we found over 100,000 priming motifs and over 1,000,000 tolerance motifs. A subsequent statistical and topological analysis revealed three core priming mechanisms and one tolerance mechanism out of the large number of functional motifs. Each mechanism has a unique requirement on the basic network structure and dynamics, known as backbone motif. These *in silico* found mechanisms were supported by several lines of molecular evidence from current experimental investigations. Further investigates are necessary to apply these priming and tolerance motifs in the context of specific signaling/regulatory networks to uncover candidate molecules for experimentalists to test.

In the second part of the dissertation, we theoretically studied potential ways to accelerate bacterial phenotypic transitions from persister phenotype to normally growing phenotype, as persister cells are insensitive to antibiotics while normally growing cells are sensitive (Balaban et al, 2004). We stochastically modeled the single cell dynamics based on a generic toggle switch composed of toxin and anti-toxin, with each dominating a bacterial phenotype. We then studied how the rate of phenotypic transition could be affected under a weak external signal. As a result, we discovered that with a resonance frequency, the weak external signal could induce 1) a maximum rate of phenotypic transition from persister phenotype to normally growing phenotype; 2) synchronized timing (first passage time) of phenotypic transition. The phenomenon is known as "Resonance Activation (RA)" in statistical physics (Hänggi, 2002). On integrating single cell and population level (where cells divide and die) simulations together, we found that RA could not only accelerate and synchronize timings of bacterial phenotypic

transitions, but also provide a potential way to reduce antibiotic treatment, as antibiotics are only needed at the synchronized windows where persisters cells transit into normally growing phenotype. Note in this theoretical work, we did not consider genome mutation of bacteria going through repeated antibiotic stimulations. As a matter of fact, it is highly likely that bacteria are quickly mutated. Therefore, it might be difficult to induce RA in bacteria system experimentally. However, we state that RA should be applicable to a general problem of cellular reprograming or phenotypic transition, where cellular genome is more stable.

Reference

Alon U (2007) *An introduction to systems biology: Design principles of biological circuits*, 1 edn.: Chapman and Hall/CRC.

Balaban NQ, Merrin J, Chait R, Kowalik L, Leibler S (2004) Bacterial Persistence as a Phenotypic Switch. *Science* **305:** 1622-1625

Gardy JL, Lynn DJ, Brinkman FSL, Hancock REW (2009) Enabling a systems biology approach to immunology: focus on innate immunity. *Trends Immunol* **30:** 249-262

Gilchrist M, Thorsson V, Li B, Rust AG, Korb M, Kennedy K, Hai T, Bolouri H, Aderem A (2006) Systems biology approaches identify ATF3 as a negative regulator of Toll-like receptor 4. *Nature* **441:** 173-178

Hänggi P (2002) Stochastic resonance in biology. How noise can enhance detection of weak signals and help improve biological information processing. *Chemphyschem* **3:** 6

Milo R, Shen-Orr S, Itzkovitz S, Kashtan N, Chklovskii D, Alon U (2002) Network motifs: simple building blocks of complex networks. *Science* **298:** 824-827

Tyson JJ, Novak B (2010) Functional motifs in biochemical reaction networks. *Annu Rev Phys Chem* **61:** 219-240